# Exceptional Event Demonstration for Ozone Exceedances in Clark County, Nevada – May 9, 2020

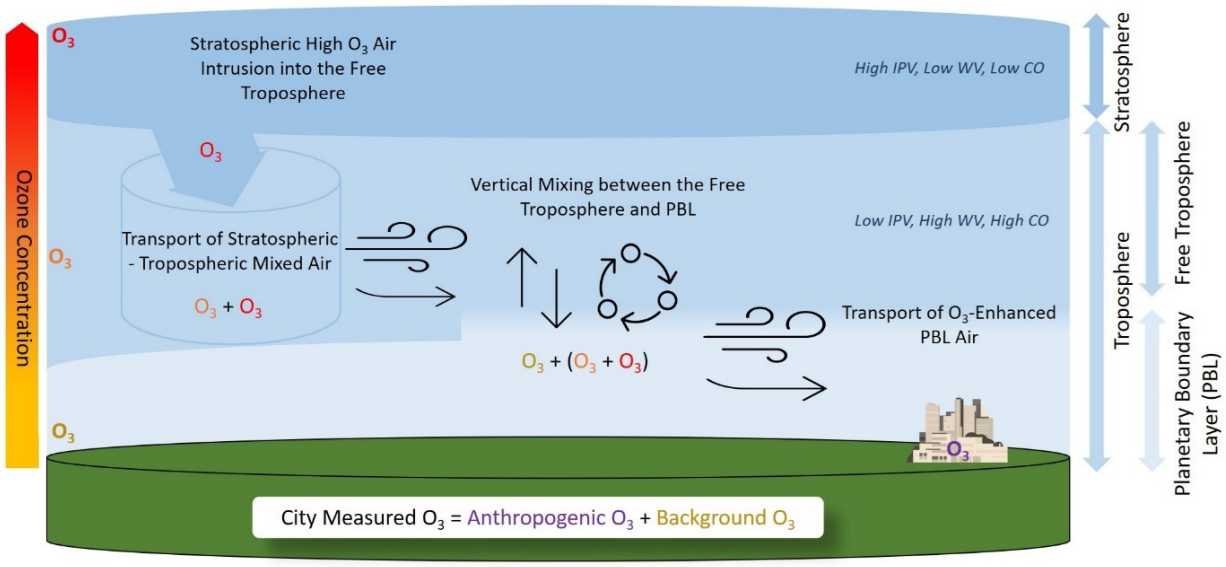


Final Report Prepared for

U.S. EPA Region 9
San Francisco, CA

July 2021

STi | Sonoma Technology

This document contains blank pages to accommodate two-sided printing.

# Exceptional Event Demonstration for Ozone Exceedances in Clark County, Nevada – May 9, 2020


## Prepared by

Steve Brown, PhD
Crystal McClure, PhD
Cari Gostic
Samantha Kramer, PhD
David Miller, PhD
Charles Scarborough
Ningxin Wang, PhD

Sonoma Technology
1450 N. McDowell Blvd., Suite 200
Petaluma, CA 94954
Ph 707.665.9900 | F 707.665.9800
sonomatech.com

## Prepared for

Mike Sword
Araceli Pruett

Clark County Department of Environment & Sustainability
Division of Air Quality
4701 W. Russell Road, Suite 200
Las Vegas, NV 89118
Ph 702.455.3206
www.clarkcountynv.gov



## Final Report

STI-920053-7477

## July 1, 2021


Cover graphic illustrates an example of stratospheric intrusion and transport. See Section 2.4 for more information.

# Contents

# Figures

# Tables

# Executive Summary

On May 9, 2020, Clark County, Nevada, experienced an atypical, area-wide episode of elevated ambient ozone; during this episode, the 2015 8-hr ozone National Ambient Air Quality Standards (NAAQS) threshold (0.070 ppm) was exceeded at the Walter Johnson and Paul Meyer monitoring sites. The exceedances at both sites could lead to an ozone nonattainment designation for the Clark County area. Air trajectory analysis and air quality modeling suggest that this ozone exceedance was influenced by a Stratospheric Ozone Intrusion (SOI) over the Pacific Ocean, west of Baja California, that transported ozone-rich air to Clark County. The EPA Exceptional Event Rule (U.S. Environmental Protection Agency, 2016) allows air agencies to omit air quality data from the design value calculation if it can be demonstrated that the measurement in question was caused by an exceptional event. This report describes analyses that help to establish a clear causal relationship between the SOI and the May 9, 2020, ozone exceedance at the Walter Johnson and Paul Meyer sites.

The analyses conducted provides evidence supportive of SOI impacts on ozone concentrations in Clark County. Analyses show that (1) prior to May 9, there was an SOI event upwind of Clark County signified by an area of stratosphere-troposphere exchange over the Pacific Ocean west of Baja California; (2) ozone-rich stratospheric air was transported from the SOI over the Los Angeles Basin—which likely enhanced ozone and contributed to the exceedance—and to the lower troposphere and surface of the Clark County area; (3) the SOI and subsequent transport of dry stratospheric air impacted the typical diurnal profiles of ground-level meteorological measurements, including relative and absolute humidity, in the Clark County area on May 9; and (4) meteorological regression modeling and similar meteorological day analysis show that ozone observations on May 9 were unusual in the historical record given the meteorological conditions. Sources of evidence used in these analyses include (1) air quality monitor data to show that supporting pollutant trends at the surface were influenced by upwind effects from the SOI; (2) air trajectory analysis to show transport from the SOI to the Clark County area; (3) satellite imagery and meteorological model results; (4) meteorological regression modeling; and (5) meteorologically similar day analysis.

The EPA "Guidance on the Preparation of Exceptional Events Demonstration for Stratospheric Ozone Intrusions" (U.S. Environmental Protection Agency, 2018) describes a two-tier approach to evaluating an SOI event and then developing evidence for the EE demonstration. Depending on the complexity of the event, increasingly involved information may be required to demonstrate a causal relationship between an SOI event and an exceedance. This report documents the results of analyses conducted to address Tier 1 and Tier 2 exceptional event demonstration requirements.

These analyses show that ozone-laden air was transported from the SOI over the Pacific Ocean west of Baja California over the days leading up to May 9 to the Clark County area. Combined with additional evidence, such as meteorological regression modeling and meteorologically similar day analysis, our results provide key evidence to support SOI impacts on ozone concentrations in Clark County on May 9, 2020.

# 1. Overview

## 1.1 Introduction

Stratospheric Ozone Intrusions (SOIs) occur when ozone-enriched, stratospheric air descends into the troposphere and injects ozone ($O_3$) at altitudes where ozone concentrations are usually lower. SOIs can directly affect surface-level ozone when a tropopause fold (carrying ozone-enriched stratospheric air) extends down to the surface. However, because tropopause folds do not typically extend below around 600 hPa (4.5 km above ground level [agl]) in the mid-latitudes, this effect usually only occurs at high altitude sites. Alternatively, a tropopause fold (or other stratospheric-tropospheric mixing) can occur at high altitudes, and then ozone can be directly transported to the surface downwind of the event. The mixing of ozone-enriched air can be enhanced where the boundary layer (i.e., the lowest well-mixed atmospheric layer that reaches the surface) is very deep (4-5 km) on hot, dry days. In desert regions such as Clark County, Nevada, an upwind SOI can efficiently be mixed down to the surface during hot spring and summer days, which can enhance ozone concentrations. Such an SOI event occurred upwind of Clark County on May 6-7, 2020, and then affected ozone concentrations on May 9. On May 9, two of the 14 ozone monitoring locations around Clark County recorded an exceedance of the 2015 National Ambient Air Quality Standard (NAAQS) for 8-hour ozone (0.070 ppm).

Typically, ozone concentrations in the stratosphere are around 5-10 parts per million (ppm). Depending on the amount of dilution after the SOI event, surface-level ozone concentrations can be significantly enhanced above background tropospheric levels (~0.040-0.050 ppm). Even in areas with urban emissions, such as Las Vegas, the addition of ozone from an upwind SOI event can enhance ozone concentrations above usual levels, potentially driving concentrations above the ozone standard. SOIs in the western U.S. typically occur in spring and are well-documented to affect ozone concentrations in Clark County, providing up to 18-22 ppb of ozone enhancement in May and June (Langford, 2014; Langford and Senff, 2019). We can identify and track the movement of air from an SOI event because stratospheric air (1) is typically depleted in both anthropogenic compounds (i.e., particulate matter [PM], carbon monoxide [CO], and nitrogen oxides [$NO_x$]) and water vapor compared with tropospheric air, and (2) has enhanced isentropic potential vorticity (IPV). According to guidance from the U.S. Environmental Protection Agency (EPA), exceptional events (EE) such as SOIs that affect ozone concentrations can be subject to exclusion from calculations of National Ambient Air Quality Standards (NAAQS) attainment if a clear causal relationship can be established between a specific event and the monitoring exceedance (U.S. Environmental Protection Agency, 2018).

For the case in Clark County on May 9, we describe the clear causal relationship between the event causing the exceedance (the SOI off the coast of Baja California) and the downwind effects on the monitoring sites in Clark County that recorded an exceedance of the maximum daily 8-hour ozone

average (MDA8). The evidence in this report provides a Tier 2 analysis required by EPA's Exceptional Event Guidance for more complex SOI events: comparison with non-event ozone concentrations, analysis of meteorological transport, satellite and model analysis of stratospheric tracers, transport analysis from the SOI to the surface, measurements of column ozone at a high-altitude site, meteorologically similar day analysis, and the effect of the SOI on surface ozone (and other tracer) concentrations. Additionally, we provide Generalized Additive Model (GAM) statistical results to help quantify the effect of the SOI on this exceptional event (EE). The SOI that affected ozone concentrations in Clark County could not be reasonably controlled or prevented because SOIs are considered natural events. Table 1-1 lists the sites affected during the May 9 event, as well as their locations and MDA8 ozone concentrations.

Concurrent with this document, Clark County is submitting documentation for other ozone EEs in 2018 and 2020 due to wildfires and stratospheric intrusions. These events are mentioned throughout this report and are referred to as "proposed 2018 and 2020 exceptional events," recognizing that EPA concurrence on these events is still pending. All proposed EEs in 2018 and 2020 for Clark County are listed in Tables 1-2 and 1-3. Wherever possible, we calculated statistics to provide context both including and excluding the proposed EEs from 2018 and 2020.

**Table 1-1.** May 9, 2020, exceptional event information. All monitoring sites in Clark County that exceeded the 2015 NAAQS standard on May 9 are listed along with AQS site codes, location information, and MDA8 ozone concentrations.

| AQS Site Code | Site Name | Latitude (degrees N) | Longitude (degrees W) | MDA8 O3 Concentration (ppb) |
|---|---|---|---|---|
| 320030043 | Paul Meyer | 36.106 | -115.253 | 74 |
| 320030071 | Walter Johnson | 36.170 | -115.263 | 71 |

**Table 1-2.** Proposed Clark County 2018 exceptional events. For each site and date combination where the 2015 NAAQS standard was exceeded, the MDA8 ozone concentration is shown in ppb. Blank cells indicate that there was no exceedance on that site/date combination.

| Date | Paul Meyer | Walter Johnson | Green Valley | Jerome Mack | Joe Neal | Palo Verde | Jean | Indian Springs | Apex | Boulder City |
|---|---|---|---|---|---|---|---|---|---|---|
| 6/19/2018 | 72 | 72 | 77 | 75 | | | | | | |
| 6/20/2018 | 71 | 74 | | | 72 | | | | | |
| 6/23/2018 | 72 | 76 | 75 | 72 | 72 | 71 | 77 | 73 | | |
| 6/27/2018 | 75 | 76 | 78 | 76 | 72 | 72 | 81 | 78 | 74 | 72 |
| 7/14/2018 | 72 | | 78 | 78 | | | | | | |
| 7/15/2018 | | 71 | 73 | 73 | 78 | | | | | |
| 7/16/2018 | 75 | 79 | 71 | 73 | 80 | 75 | | | | |
| 7/17/2018 | 74 | 77 | | | | 74 | | | | |
| 7/25/2018 | 71 | 72 | 72 | | | | | | | |
| 7/26/2018 | 72 | 75 | 77 | 77 | | | | | 71 | |
| 7/27/2018 | 72 | 74 | | | 76 | | | | | |
| 7/30/2018 | | | 73 | 72 | | | | | | |
| 7/31/2018 | | 73 | | | 73 | | | | | |
| 8/6/2018 | 79 | 77 | 74 | 71 | 76 | 72 | | | 74 | |
| 8/7/2018 | 73 | 74 | 72 | 71 | 74 | | | | 71 | |

**Table 1-3.** Proposed Clark County 2020 exceptional events. For each site and date combination where the 2015 NAAQS standard was exceeded, the MDA8 ozone concentration is shown in ppb. Blank cells indicate that there was no exceedance on that site/date combination.

| Date | Walter Johnson | Paul Meyer | Joe Neal | Jerome Mack | Green Valley | Boulder City | Jean | Indian Springs | Apex |
|---|---|---|---|---|---|---|---|---|---|
| 5/6/2020 | 78 | 77 | 76 | 73 | 72 | | 75 | | 76 |
| 5/9/2020 | 71 | 74 | | | | | | | |
| 5/28/2020 | 71 | 76 | | | | | | | |
| 6/22/2020 | 73 | 74 | 78 | | | | | | |
| 6/26/2020 | | 73 | | | | | | | |
| 8/3/2020 | 82 | 78 | 81 | | 72 | 72 | 73 | 71 | |
| 8/7/2020 | 71 | | 72 | | | | | 72 | |
| 8/18/2020 | 82 | 79 | 78 | | | | | | |
| 8/19/2020 | 74 | 74 | 73 | | 71 | | | | |
| 8/20/2020 | | | 71 | | | | | | |
| 8/21/2020 | | 71 | | | | | | | |
| 9/2/2020 | 75 | 73 | | | | | | | |
| 9/26/2020 | 71 | | 75 | | | | | | |

## 1.2 Exceptional Event Rule Summary

The EPA "Guidance on the Preparation of Exceptional Events Demonstration for Stratospheric Ozone Intrusions" (U.S. Environmental Protection Agency, 2018) describes a two-tier approach to evaluating

an SOI event and then developing evidence for the EE demonstration. A summary of event requirements for both tiers is listed in Table 1-4. From the EPA 2018 SOI Guidance:

- Tier 1 analyses can be used for events when ground ozone concentrations are much higher than typical observations, with conditions unfavorable to photochemical ozone production, and with synoptic meteorological conditions conducive to stratospheric intrusion being the cause.
- Tier 2 analyses are appropriate for cases when both local photochemical ozone production and stratospheric ozone contributions are present, or for events where the observed ozone is within range of typical seasonal values of that location. Tier 2 demonstrations involve more supporting analytical documentation than Tier 1 demonstrations.

In this demonstration, we conduct the Tier 2 analysis (which is cumulative with Tier 1) because local photochemical ozone production existed simultaneously with the SOI contribution.

**Table 1-4.** Tier 1 and 2 requirements for evaluating stratospheric intrusion impacts on ozone exceedances.

| Tier | Elements of SOI Event |
|---|---|
| 1 | • Stratospheric intrusion events that cause obvious ozone impacts during periods when:<br>– ozone concentrations are typically low, and<br>– meteorological patterns are suggestive of potential transport from the stratosphere.<br>• Meteorological analyses suggest intrusion was recent, nearby, and expansive:<br>– associated with a frontal passage, and<br>– with elevated ozone observed across a large region.<br>• Ozone concentrations are clearly distinguishable from usual conditions.<br>• Occurred outside the period in which high ozone from local and/or regional production is typically observed.<br>• Occurred when and where local photochemical production was minimal:<br>– at night,<br>– associated with cold air advection, high wind speeds, and/or<br>– strong dispersion conditions. |
| 2 | • The relationship between the stratospheric intrusion and influenced ozone concentrations is complex and not fully elucidated with Tier 1 elements.<br>• Resulted from long-distance, multi-day transport requiring detailed analyses.<br>• The event-influenced concentrations were in the range of typical exceedances (i.e., close to the area's design value).<br>• Occurred in season when ozone exceedances are historically common.<br>• Occurred in association with other processes and sources of ozone, or on days where meteorological conditions were conducive to local ozone formation. |

## 1.3 Demonstration Outline

Although each stratospheric intrusion event is likely to have unique characteristics, this demonstration shows that stratospheric air entered the free troposphere (FT), was mixed down to the surface, and subsequently caused an ozone exceedance at the surface. We use the recommended analyses listed throughout the EPA 2018 SOI guidance. Table 1-5 summarizes the required and

recommended analyses for both a Tier 1 and Tier 2 SOI analyses and shows the corresponding sections for each analysis in this report.

**Table 1-5.** Locations of Tier 1 and 2 analyses within this report.

| Type of Analysis | Tier 1 + Tier 2 | Section of This Report (Analysis Type) |
|---|---|---|
| Conceptual Model | What conditions generally lead to high ozone in the area? | Section 2.3 (Characteristics of non-event historical $O_3$ formation) |
| Historical Comparison | • ≥ 5 years of peak daily ozone data with other high event days flagged.<br>• Table with percentile ranks of days.<br>• Historical diurnal profile comparison (Tier 2). | Section 3.1 (Comparison of event with historical data) |
| Event overview | • Spatial and temporal depictions of ozone during the event.<br>• Description of surface and upper air meteorological conditions during the event.<br>• Begin to establish the complex relationship between the intrusion and eventual impact at surface (Tier 2). | Section 2.4 (Stratospheric intrusion event description) |
| Establish stratospheric intrusion | Several of following are likely needed:<br>• Water vapor imagery<br>• Total column ozone<br>• Meteorological evidence | Sections 3.2.1 (Total column ozone and water vapor); Section 3.2.2 (Model results of ozone, CO, water vapor, & meteorological conditions) |
| Establish stratospheric air reached surface | Several of following are likely needed:<br>• LIDAR, rawinsonde data<br>• Meteorological evidence<br>• Modeled parameter cross sections<br>• Trajectory models | Section 3.2.2 (Model parameter cross sections); Section 3.3.1 (HYSPLIT trajectories); Sections 3.3.2 (LIDAR measurements of the ozone vertical profile); Section 3.3.3 (Meteorological analysis) |
| Impacts at the surface | Several of following are likely needed:<br>• Coincidence between high ozone and meteorological/parameter conditions characteristic of stratospheric intrusions<br>• statistical model evidence of impacts<br>• Summary narrative | Section 3.4 (Ozone & RH, ozone & $NO_x$ diurnal patterns, surface ozone concentration time series); Section 3.5.1 (Meteorologically similar matching day analysis); Section 3.5.2 (GAM statistical analysis); Section 3.6 (Summary narrative) |

In Chapter 2 of this report, we establish a narrative conceptual model of the EE with a description of the monitoring network, the event causing the exceedance, and transport from the event that led to the exceedance at the affected monitors. Section 2.1 and 2.2 provides detailed information of the region and the existing ozone monitors. Section 2.3 summarizes the processes that led to high ozone concentrations at the monitor on non-event days and the ozone seasonality. In Section 2.4, we introduce the meteorology that caused the stratospheric ozone intrusion and provide a brief narrative for how stratospheric air was transported into the free troposphere and ultimately mixed down through the planet boundary layer (PBL) to the surface monitors.

In Section 3 of this report, we establish the clear causal relationship between the event and the monitored ozone exceedance. As a first step, we provide a comparison of the exceedance concentrations with historical data in Section 3.1. In Section 3.2, we provide evidence of Stratospheric-Tropospheric exchange using satellite imagery and meteorological model results. Section 3.3 shows evidence of stratospheric air reaching the surface using trajectory analysis, lidar ozone measurements, and meteorological observations. We then demonstrate the event impact at the surface in Section 3.4. Additionally, we developed a statistical Generalized Additive Model (GAM) to estimate the contribution of stratospheric ozone to the monitored ozone concentrations in Section 3.5.

Following the EPA's SOI event guidance, we performed both Tier 1 and Tier 2 analyses to show the clear causal relationship between the stratospheric intrusion event which occurred to the west of Baja California and the exceedance event in Clark County, Nevada, on May 9, 2020. Focusing on characterization of the meteorology, transport, and air quality on the days leading up to the event, we conducted the following specific analyses (results from these analyses are presented in both Section 2 and 3):

- Developed time series plots that show the May 9 ozone concentrations in historical context at each affected monitoring site for both 2020 and the past five years.
- Compiled maps of ozone and water vapor in the area from satellite data.
- Retrieved total column ozone from the Ozone Mapping and Profile Suite (OMPS) instrument aboard the Suomi NPP satellite
- Provided evidence of a stratospheric intrusion event over Baja California using model results of isentropic potential vorticity (IPV), relative humidity (RH), and potential vorticity (PV) at 300 hPa using the Global Forecast System (GFS).
- Provided model results and cross sections of ozone and CO concentrations using the Realtime Air Quality Modelling System (RAQMS).
- Provided model results of ozone at 500 hPa height using the NCAR Whole Atmosphere Community Climate Model (WACCM).

- Provided surface and upper-level (500 hPa) meteorological maps using the North American Surface Analysis.
- Provided boundary layer depth analysis on the EE day using North American Mesoscale (NAM) data and the UCAR Integrated Data Viewer (IDV).
- Showed the transport patterns of stratospheric ozone from the intrusion location to the Clark County region via the Hybrid Single-Particle Lagrangian Integrated Trajectory (HYSPLIT) model.
- Performed statistical analysis to compare event ozone concentrations to non-event concentrations.
- Developed plots to show diurnal patterns of ozone and supporting pollutants such as RH and nitrogen oxides ($NO_x$).
- Assessed vertical transport of stratospheric ozone using LIDAR measurements of ozone mixing ratio and temperature vertical profiles above sea level at the JPL Table Mountain Facility from the Tropospheric Ozone LIDAR Network (TOLNet).
- Created a GAM model of MDA8 ozone concentrations to assess the enhancement of ozone concentrations at the impacted monitors due to the transported stratospheric ozone.

## 1.4 Conceptual Model

The conceptual model for the exceptional event that led to the ozone exceedances at the Walter Johnson and Paul Meyer sites on May 9, 2020, is outlined in Table 1-5. We provide the analysis techniques performed and evidence for each Tier. This establishes a weight of evidence for the clear causal relationship between a stratospheric intrusion west of Baja California and the May 9 exceptional ozone event. We assert that stratospheric ozone was transported into the upper troposphere over the eastern Pacific Ocean near Baja California, and subsequently reached Clark County, where it contributed to the ozone exceedances at the two monitoring sites on May 9. In support of this assertion, the key points of evidence for the conceptual model are summarized below.

1. The May 9, ozone exceedance occurred during a typical ozone season, but event concentrations at the two exceedance sites were significantly higher than non-event concentrations. Ozone concentrations at the exceedance sites showed a high percentile rank and regional enhancements when compared with the past six years and ozone seasons.
2. Multiple atmospheric models (GFS, WACCM, and RAQMS) provide consistent evidence from isentropic potential vorticity, water vapor, and CO concentrations for a stratospheric intrusion event that injected ozone-rich stratospheric air into the upper troposphere over the Pacific

Ocean west of Baja California on May 7 at 0:00 UTC. A time series of mid-tropospheric ozone profile simulations from May 7-9 indicate a continuous stratospheric-tropospheric ozone tongue that descended in altitude as it was transported from Baja California northeastward toward Clark County.

3. Back and forward trajectories from the exceedance sites, at near-surface altitude, and the time of maximum ozone concentration show consistent transport patterns from the free troposphere (3 km altitude) coinciding with the SOI source and modeled ozone tongue to the boundary layer in Clark County on May 9. The deep mixed layer observed upwind on the preceding days and in Clark County on the event day provide evidence for sufficient vertical mixing between the mid-troposphere and the surface.
4. Back and forward trajectories originating from the location of lidar-based ozone vertical profile observations immediately downwind of the Los Angeles Basin show that enhanced free tropospheric ozone observed overnight on May 8 did not entirely originate from the daytime boundary layer in the Los Angeles Basin. This suggests that both upper-level ozone from the SOI and photochemical ozone production at the surface in the Los Angeles Basin contributed to observed free tropospheric ozone enhancements along the transport path to Clark County.
5. Meteorological conditions on May 9 did not favor enhanced local ozone production when compared with meteorologically similar ozone season days. Average MDA8 ozone across similar days was well below the ozone NAAQS and > 10 ppb lower than the May 9 exceedance.
6. GAM model predictions of MDA8 ozone on May 9 are all well below the 70 ppb ozone NAAQS for each EE-affected site. Using the GAM residuals (observed MDA8 ozone minus GAM-predicted MDA8 ozone) to estimate the effect of the SOI on Clark County, we find a contribution of 12 ppb ozone from an atypical source, in this case, likely the stratospheric intrusion. Furthermore, trajectory cluster GAM analysis demonstrates that ozone contributions from Los Angeles Basin transport are well captured by the GAM with near-zero residuals. The positive GAM residuals on May 9 represent additional discrepancies that cannot be attributed to Los Angeles Basin photochemical ozone transport alone.
7. The arrival of dry, SOI influenced air to Clark County coincided with abnormally lower daytime surface absolute humidity on May 9 in Clark County. NO and $NO_2$ concentrations were within average levels on May 9 in Clark County, suggesting that local photochemical ozone production was unlikely the only source of the high ozone exceedance event.

# 2. Historical and Non-Event Model

## 2.1 Regional Description

Clark County is located in the southern portion of Nevada and borders California and Arizona. Clark County includes the City of Las Vegas, which has a population of approximately 2 million and is one of the fastest growing metropolitan areas in the United States (U.S. Census Bureau, 2010). Las Vegas is located in a 1,600 $km^2$ desert valley basin at 500 to 900 m above sea level (Langford et al., 2015). It is surrounded by the Spring Mountains to the west (3,000 m elevation) and the Sheep Mountain Range to the north (2,500 m elevation), and three mountain ranges to the south. The valley floor slopes downward from west to east, which influences surface wind, temperature, precipitation, and runoff patterns. The Cajon Pass and I-15 corridor to the west is an important atmospheric transport pathway from the Los Angeles Basin into the Las Vegas Valley (Langford et al., 2015). **Figures 2-1 and 2-2** show the topography of the Clark County area and surrounding areas.

The Las Vegas Valley climatology features abundant sunshine and hot summertime temperatures, with average summer month high temperatures of 34-40°C. Because of the mountain barriers to moisture inflow, the region experiences dry conditions year-round (~107 mm annual precipitation, 22% of which occurs during the summer monsoon season in July through September). The urban heat island effect in Las Vegas during the summer leads to large temperature gradients within the valley, with generally cooler temperatures on the eastern side. During the summer season, monsoon moisture brings high humidity and thunderstorms to the region, typically in July and August (National Weather Service Forecast Office, 2020). Winds in the Las Vegas basin tend to be out of the southwest (from Los Angeles) during the spring and summer; winds in the fall and winter tend to be out of the northwest, with air transported between the neighboring mountain ranges and along the valley.

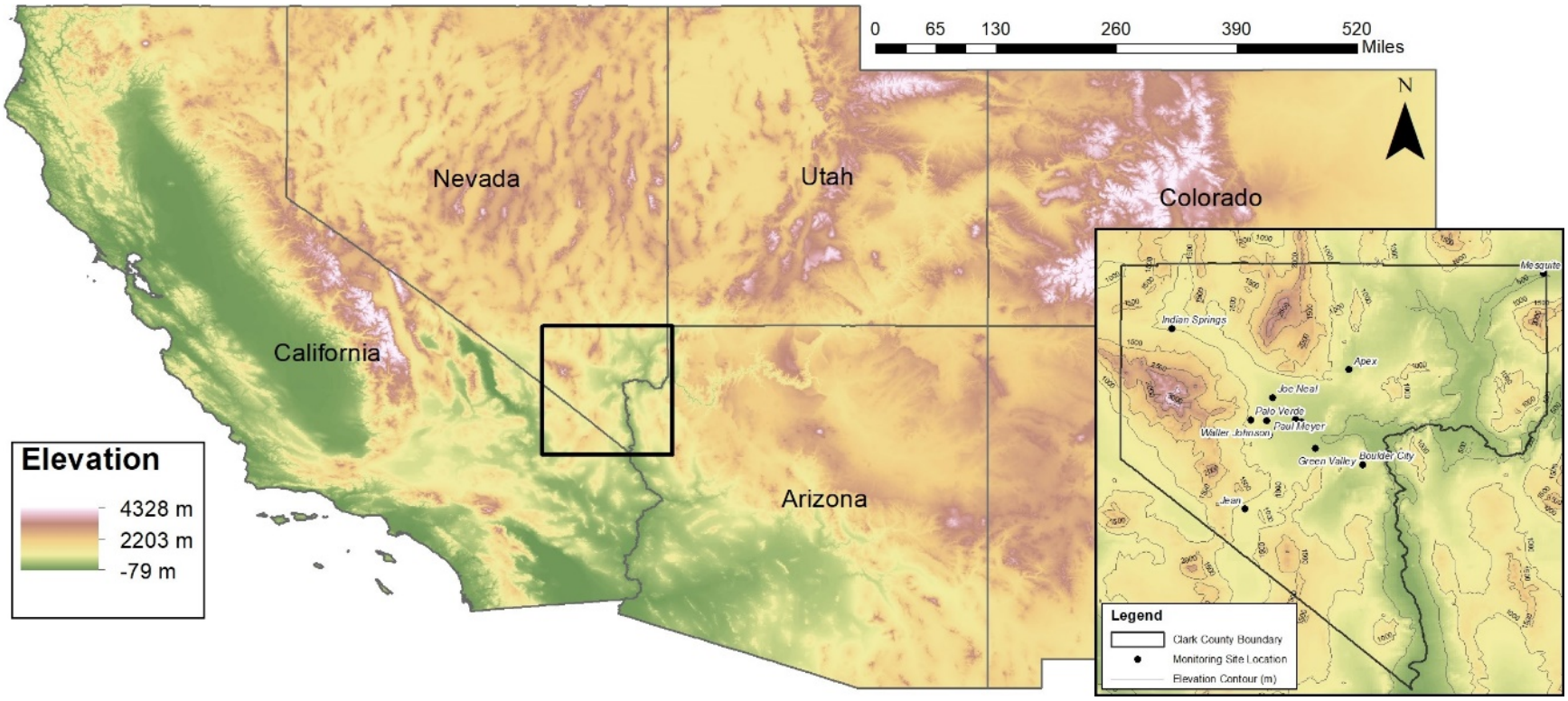


**Figure 2-1.** Regional topography around Clark County, with an inset showing the county boundaries and the air quality monitoring sites analyzed in this report.

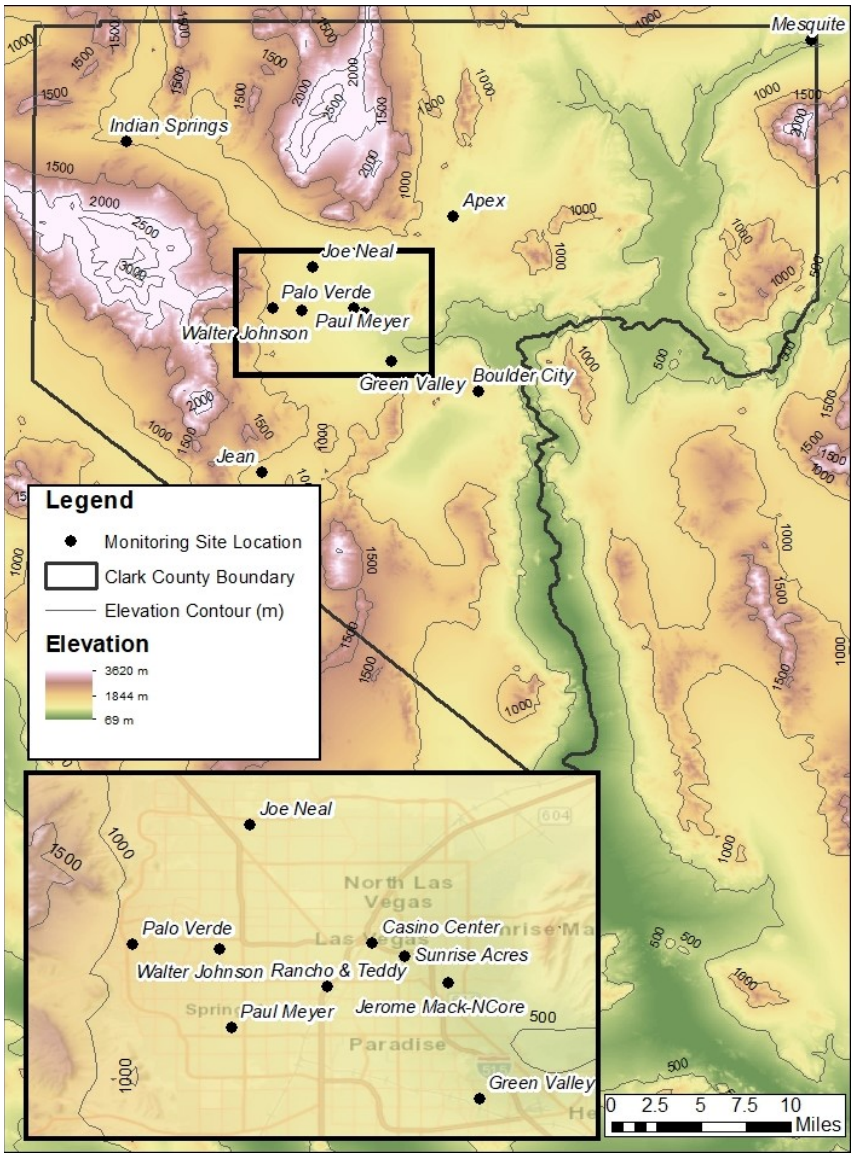


**Figure 2-2.** Clark County topography, with an inset showing air quality monitoring sites that measure ozone in the Clark County area.

## 2.2 Overview of Monitoring Network

The Clark County Department of Environment and Sustainability, Division of Air Quality (DAQ), operated 14 ambient air monitoring sites in the region during 2020 (shown in Figure 2-2). These sites measure hourly ozone, particulate matter with a diameter less than 2.5 micrometers ($PM_{2.5}$), particulate matter with a diameter less than 10 micrometers ($PM_{10}$), $NO_x$, total nonmethane organic compounds (TNMOC), and carbon monoxide (CO) concentrations along with meteorological parameters. Table 2-1 presents the monitoring data coverage for all the monitoring sites used in this report across time and space for criteria pollutants, surface meteorological parameters (barometric

pressure, temperature, wind speed, and direction), and mixing height. We examined ozone and other criteria pollutants at 11 sites around Clark County to investigate the high ozone event observed on May 9, and Table 1-1 shows the two monitoring sites (Paul Meyer and Walter Johnson) that are investigated for NAAQS ozone exceedances due to a stratospheric ozone intrusion. DAQ's ambient air monitoring network meets the monitoring requirements for criteria pollutants pursuant to Title 40, Part 58, of the Code of Federal Regulations (CFR), Appendix D (Code of Federal Regulations, 1997). Data are quality-assured in accordance with 40 CFR 58 and submitted to the EPA's Air Quality System (AQS). The spatial distribution of the monitoring sites characterizes the regional air quality in Las Vegas, as well as air quality upwind and downwind of the urban valley region (Figure 2-2). The Jean monitoring site along the I-15 corridor is generally upwind such that it captures atmospheric transport into the region and is least impacted by local sources.

**Table 2-1.** Clark County monitoring site data. The available date ranges of all parameters and monitoring sites used in this report are shown for Clark County, Nevada.

| Site | AQS Sitecode | $O_3$ | $PM_{2.5}$ | CO | NO | $NO_2$ | TNMOC | Temp. | Wind Speed | Wind Direction | Barom. Pressure | Mixing Height |
|---|---|---|---|---|---|---|---|---|---|---|---|---|
| Apex | 320030022 | 2014-2020 | | | | | | 2014-2020 | 2014-2020 | 2014-2020 | | |
| Boulder City | 320030601 | 2014-2020 | | | | | | | | | 2014-2016 | |
| Casino Center | 320031502 | | | | | | | 2014-2020 | 2016-2020 | 2016-2020 | | |
| Green Valley | 320030298 | 2015-2020 | 2014-2020 | 2020 | | | | 2016-2020 | 2014-2020 | 2014-2020 | 2014-2016 | |
| Indian Springs | 320037772 | 2014-2020 | | | | | | | | | | |
| Jean | 320031019 | 2014-2020 | 2014-2020 | | | | | 2014-2020 | 2014-2020 | 2014-2020 | 2014-2016 | |
| Jerome Mack | 320030540 | 2014-2020 | 2014-2020 | 2015-2020[1,2] | 2015-2020 | 2015-2020 | 2020 | 2014-2020 | 2014-2020 | 2014-2020 | 2014-2020 | 2020 |
| Joe Neal | 320030075 | 2020 | 2018-2020 | 2019-2020 | | 2015-2020 | | 2014-2020 | 2014-2020 | 2014-2020 | 2014-2016 | |
| Mesquite | 320030023 | 2014-2020 | | | | | | 2014-2020 | 2014-2020 | 2014-2020 | | |
| Palo Verde | 320030073 | 2014-2020 | 2020 | | | | | 2014-2020 | 2014-2020 | 2014-2020 | 2014-2016 | |
| Paul Meyer | 320030043 | 2014-2020 | 2017-2020 | | | | | 2014-2020 | 2014-2020 | 2014-2020 | 2014-2016 | |
| RT | 320031501 | | | | | | | 2015-2020 | 2015-2020 | 2015-2020 | 2014-2016 | |
| Sunrise Acres | 320030561 | | | 2020 | | | | 2014-2020 | 2014-2020 | 2014-2020 | 2014-2016 | |
| Walter Johnson | 320030071 | 2014-2020 | 2020 | | | | | 2015-2020 | 2015-2020 | 2015-2020 | 2014-2016 | |

[1] CO data invalid at Jerome Mack on Sep. 2, 2020

[2] CO data invalid at Jerome Mack Apr. 28, 2020 – May 20, 2020

## 2.3 Characteristics of Non-Event Historical $O_3$ Formation

During the ozone season (April–September) in Clark County, ozone concentrations are typically influenced by local formation, transport into the region, and on occasion by EEs such as wildfires and stratospheric intrusions. Transport from upwind source regions (e.g., the Los Angeles Basin, Mojave Desert, Asia) occurs with southwesterly winds, and southerly transport dominates the later portion of the season due to the summer monsoon (Langford et al., 2015; Zhang et al., 2020). Local precursor emissions in Clark County include mobile $NO_x$ and volatile organic compounds (VOCs) sources, natural-gas fueled power generation $NO_x$ sources, and biogenic VOC emissions. Based on 2017 Las Vegas emission inventories, on a typical ozone season weekday there are 98 tons of $NO_x$ emissions per day and 238 tons of VOC emissions per day (Clark County Department of Environment and Sustainability, 2020). On-road mobile sources comprise 40% of $NO_x$ emissions and total mobile emissions comprise 88% of total $NO_x$ emissions during the ozone season. In contrast, 52% of VOC emissions originate from biogenic sources within Clark County. Local emissions and/or precursors transported into the region contribute to ozone formation within Clark County (Langford et al., 2015; Clark County Department of Air Quality, 2019).

Stratospheric ozone intrusion events over the western U.S. have impacted Clark County when stratospheric ozone mixes with regional pollutants and local photochemical ozone leading to exceedance events (Zhang et al., 2020). The 2017 Fires, Asian, and Stratospheric Transport-Las Vegas Ozone Study (FAST-LVOS) provides evidence for April, May and June stratospheric intrusion events impacting ozone in Clark County (Zhang et al., 2020). **Figure 2-3** depicts contributions of stratospheric ozone (stratospheric $O_3$ tracer [O3Strat]) and non-anthropogenic ozone to MDA8 surface $O_3$ concentrations across the western U.S. from the NOAA GFDL AM4 model on two exemplary SOI events in April and May 2017. AM4 model results generally agree well with observations, with reduced ozone biases compared with AM3. O3Strat tracks ozone of stratospheric origin and its anomaly can be used qualitatively because it is subject to tropospheric chemical and depositional losses. Based on the FAST-LVOS study, Clark County typically experiences episodes with elevated O3Strat of 20–40 ppbv above April-June mean O3Strat ozone and larger non-anthropogenic ozone contributions (Zhang et al., 2020). The exceedance event examples in Figure 2-3 show 5 and 15 ppb O3Strat anomalies along with ~60 ppb ozone contributed from non-anthropogenic sources. Overall, stratospheric ozone intrusions can play a large role in ozone exceedances during April through June in the Clark County area.

Typical SOI events in Clark County occur under similar meteorological conditions as those on May 9, 2020. Both the May 9 exceptional event and the LVOS study ozone exceedances occurred during periods with south-southwest winds and dry air (Langford, 2014), similar to the meteorological conditions on May 9 in Clark County. These meteorological conditions are typical for late spring ozone exceedances and well-documented in the LVOS and FAST-LVOS study periods.

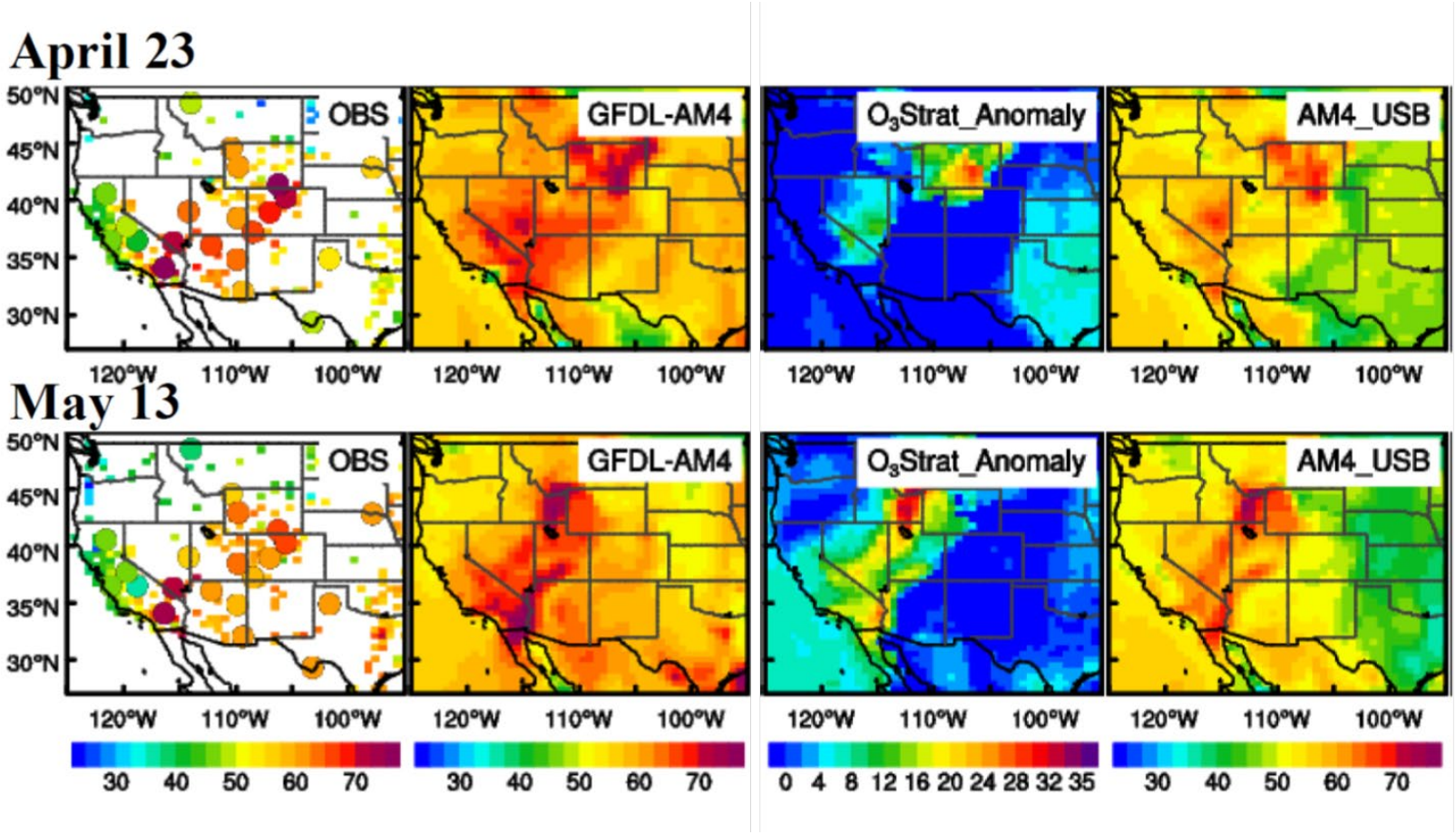


**Figure 2-3.** Observed (left) and NOAA GFDL AM4 modeled MDA8 ozone, along with stratospheric ozone tracer anomaly in AM4 relative to monthly means (O3Strat_Anomaly), and the non-anthropogenic emissions AM4 ozone simulation (AM4_USB). Two examples of stratospheric intrusion influenced days in Clark County are shown during the FASTLVOS study (April 23 and May 13, 2017) Adapted from Figure S6 in Zhang et al. (2020).

In this demonstration, we discuss the impacts of a stratospheric intrusion event on ozone concentrations in Clark County on May 9, 2020. In order to fully discern the effect of the stratospheric intrusion on ozone concentrations in Clark County on this date, we examine the historical ozone record for all affected sites (Table 1-1). *Non-event days* refer to all days other than the May 9 event. Because percentile rankings are sensitive to including the relatively large number of potential EE days during 2018 and 2020, we also provide statistics *excluding potential EE days* (i.e., without including the 2018 and 2020 potential EE days as defined in Tables 1-2 and 1-3 in Section 1). The 8-hour ozone design value (DV) is the three-year running average of the fourth-highest MDA8 ozone concentration (U.S. Environmental Protection Agency, 2015). Within Clark County, Las Vegas is classified as an EPA Region 9 marginal nonattainment region, with a 73 ppb ozone DV for 2017-2019 (U.S. Environmental Protection Agency, 2020). Ozone EE days are identified as days with significant wildfire or stratospheric intrusion influence in addition to an MDA8 concentration greater than 70 ppb. By this criterion, 15 possible EE days in 2018 and 13 possible EE days in 2020 were identified, with no EE days in 2019 identified.

The May 9, 2020, EE occurred early in the ozone season under hot, dry air conditions with a deep mixed layer and surface level trough of low pressure over Clark County. These meteorological conditions, which are often associated with a typical, non-event high ozone day, favor enhanced vertical mixing of free tropospheric air into the boundary layer. Compared with a non-event conceptual model of local precursor emissions contributing to ozone formation at ground level under similar conditions, the May 9 conditions indicate transport of free tropospheric air via upper-level west winds.

Figures 2-4 through 2-7 depict the six-year historical record and seasonality of MDA8 ozone concentrations at each EE affected monitoring site, along with the 99th percentile and NAAQS standard ozone concentrations. May 9 ranks in

- the top 1% for daily maximum ozone concentration in the six-year historical record at the Paul Meyer monitoring site.
- the top 5% for MDA8 ozone during the ozone season at the Walter Johnson monitoring site.

Figure 2-8 depicts a two-week ozone diurnal cycle of 1-hour ozone, beginning one week before the May 9 event and ending one week after. On May 9, daily maximum 1-hour ozone concentrations were the second highest at four monitoring sites during this two-week period, including the two EE affected sites (see Table 1-1). The highest concentrations during this two-week period were on May 6, which is another EE submitted concurrently with this report.

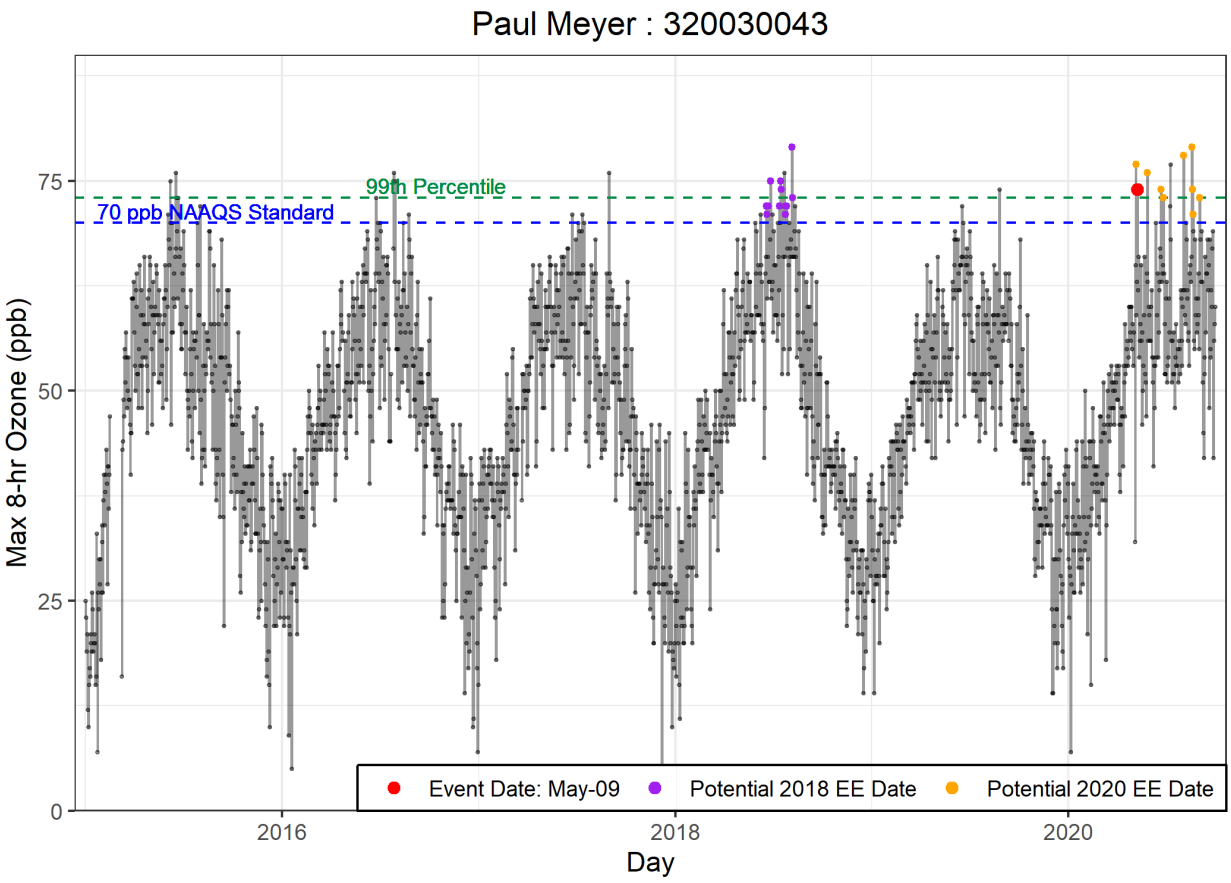


**Figure 2-4.** Time series of 2015-2020 ozone concentrations at the Paul Meyer site. May 9, 2020, is shown in red.

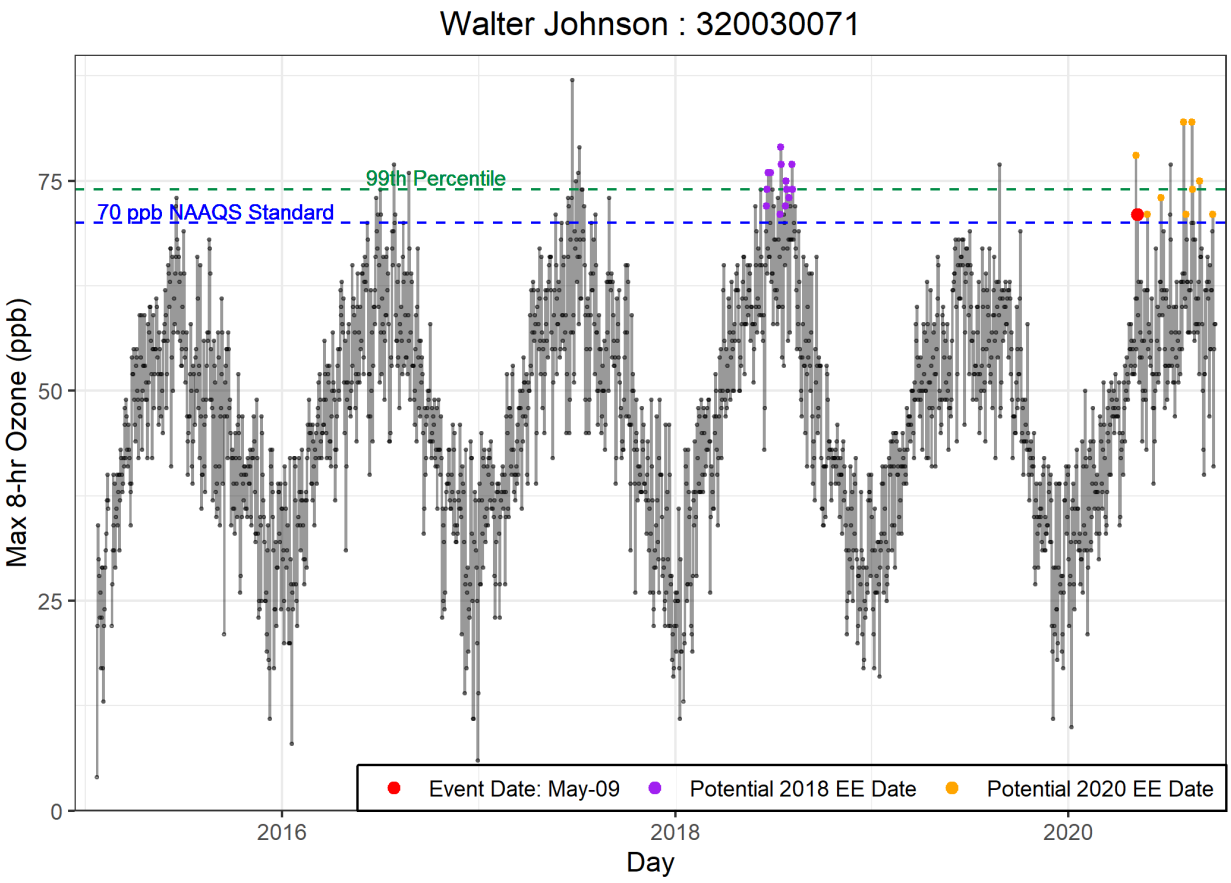


**Figure 2-5.** Time series of 2015-2020 ozone concentrations at the Walter Johnson site. May 9, 2020, is shown in red.

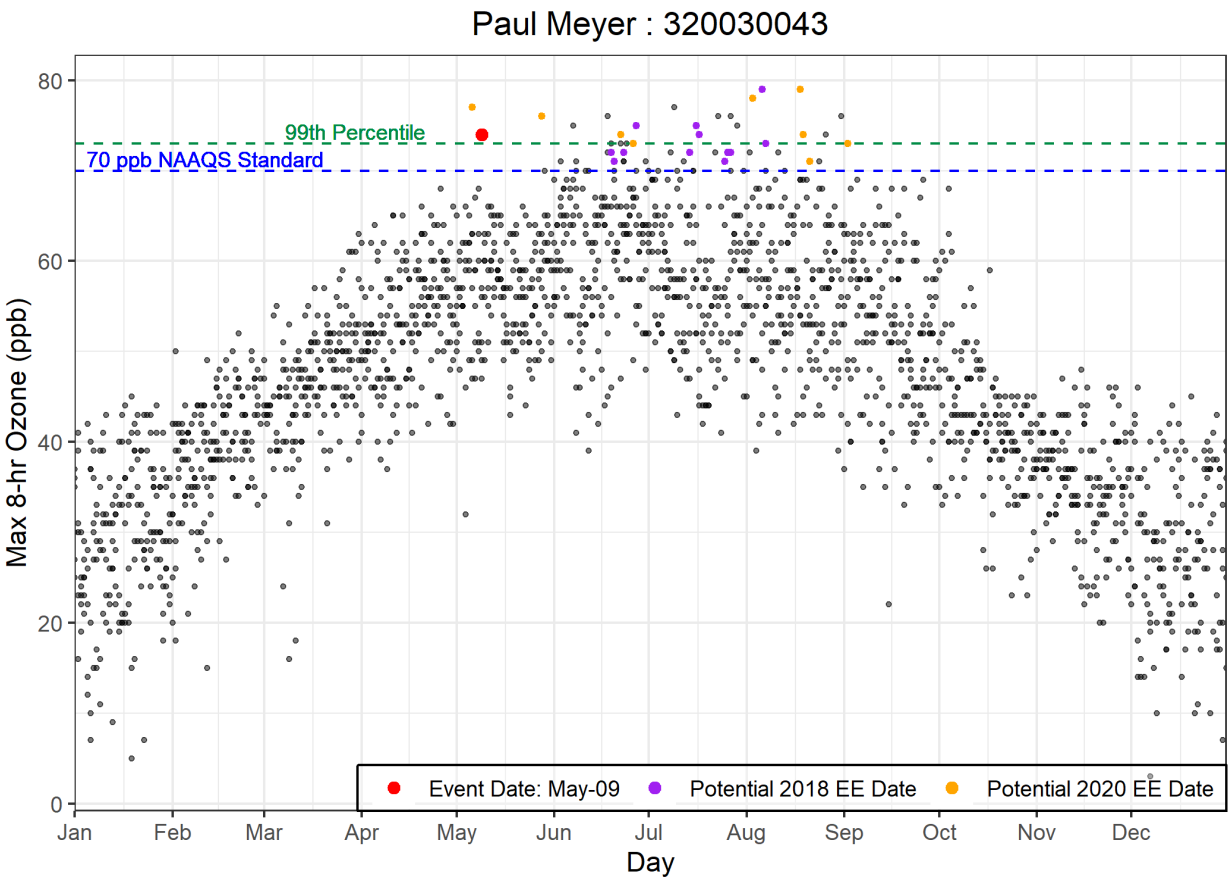


**Figure 2-6.** Seasonality of 2015-2020 ozone concentrations from the Paul Meyer site. May 9, 2020, is shown in red.

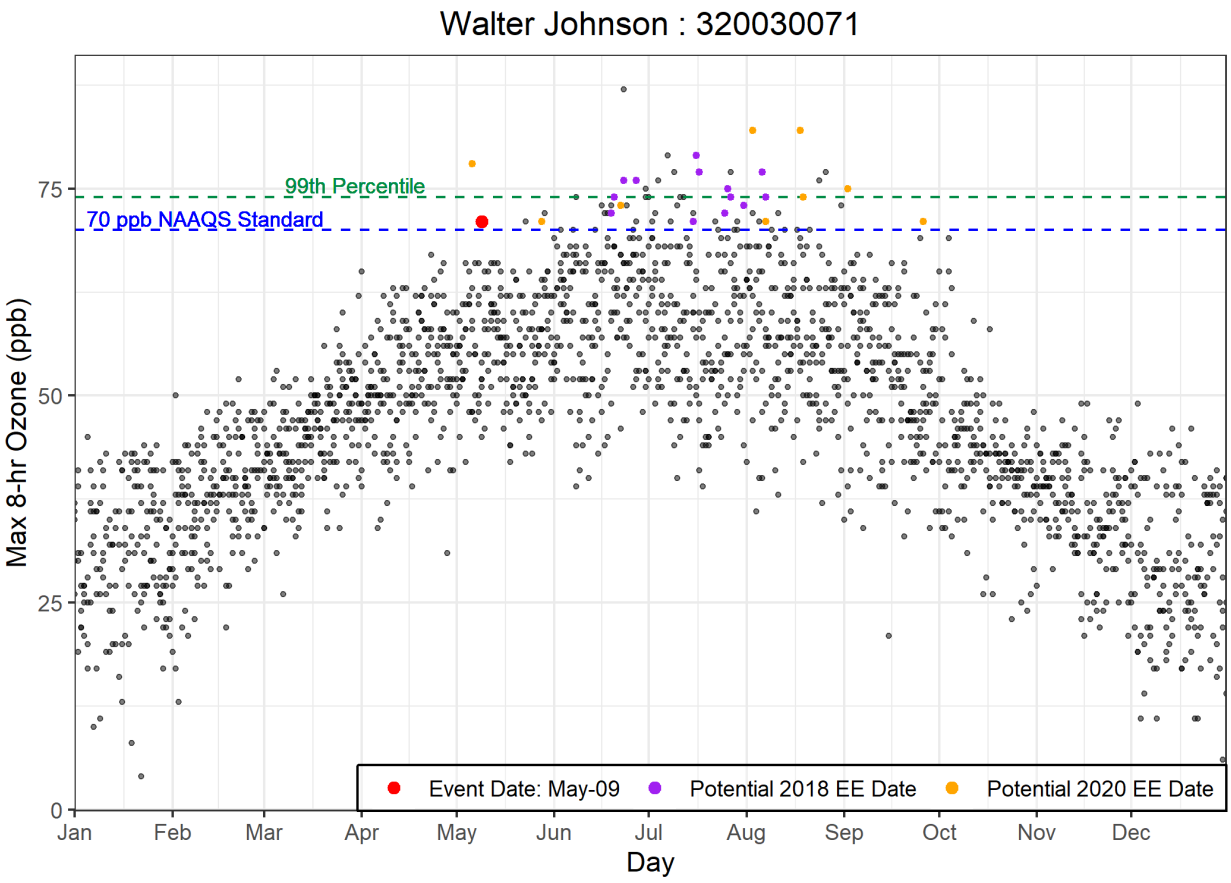


**Figure 2-7.** Seasonality of 2015-2020 ozone concentrations from the Walter Johnson site. May 9, 2020, is shown in red.

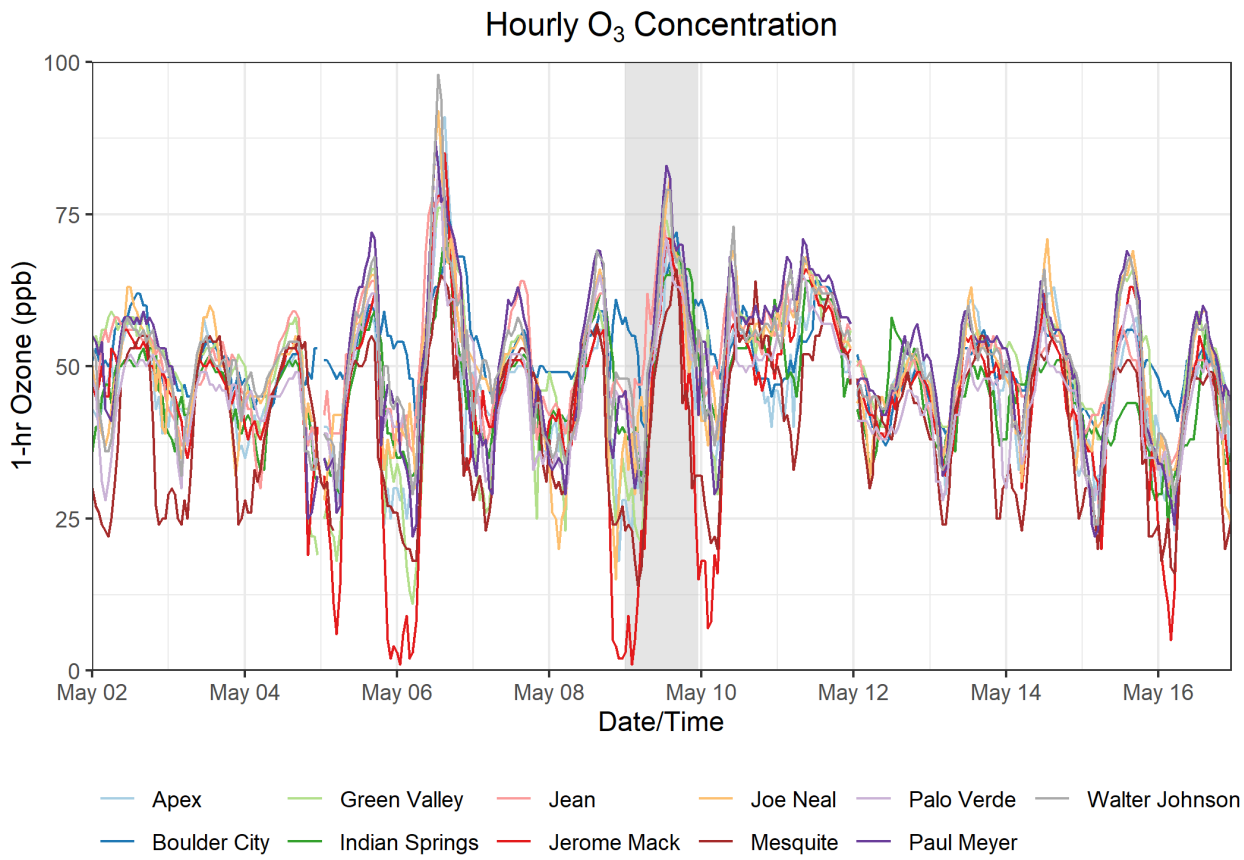


**Figure 2-8.** Time series of hourly ozone concentrations at all monitoring sites in Clark County for one week before and one week after the May 9, 2020, event. May 9 is shaded for reference.

## 2.4 Stratospheric Intrusion Event Description

Figure 2-9 shows a basic model of stratospheric-tropospheric mixing and transport of ozone-rich air downwind to an area like Clark County. The basic narrative for these events starts with a stratospheric intrusion of high ozone air into the troposphere, then transport and mixing of the stratospheric-tropospheric air into the free troposphere and PBL, which is eventually mixed to the surface. In this narrative, the city-measured ozone concentration—a combination of anthropogenic and background ozone—can thus be enhanced by the transport of stratospheric ozone into the area. On photochemically active days, the addition of even small quantities of stratospheric ozone can cause ozone concentrations to exceed the NAAQS standards. In order to trace stratospheric air, we can look for the key parameters identified in Figure 2-9. Stratospheric air usually has high ozone concentrations, high IPV, low concentrations of water vapor, and low CO concentrations, while tropospheric air has lower ozone concentrations, low IPV, higher concentrations of water vapor, and high CO concentrations. First, we identify where stratospheric intrusion occurred, as indicated by the

above parameters, then show that the stratospheric-tropospheric air mass was transported and mixed to the surface. Table 2-2 identifies the analyses needed to confirm each step of the stratospheric intrusion and transport. Each piece of evidence described in the table is shown in Section 3 and is consistent with the EPA SOI demonstration requirement shown in Table 1-5.

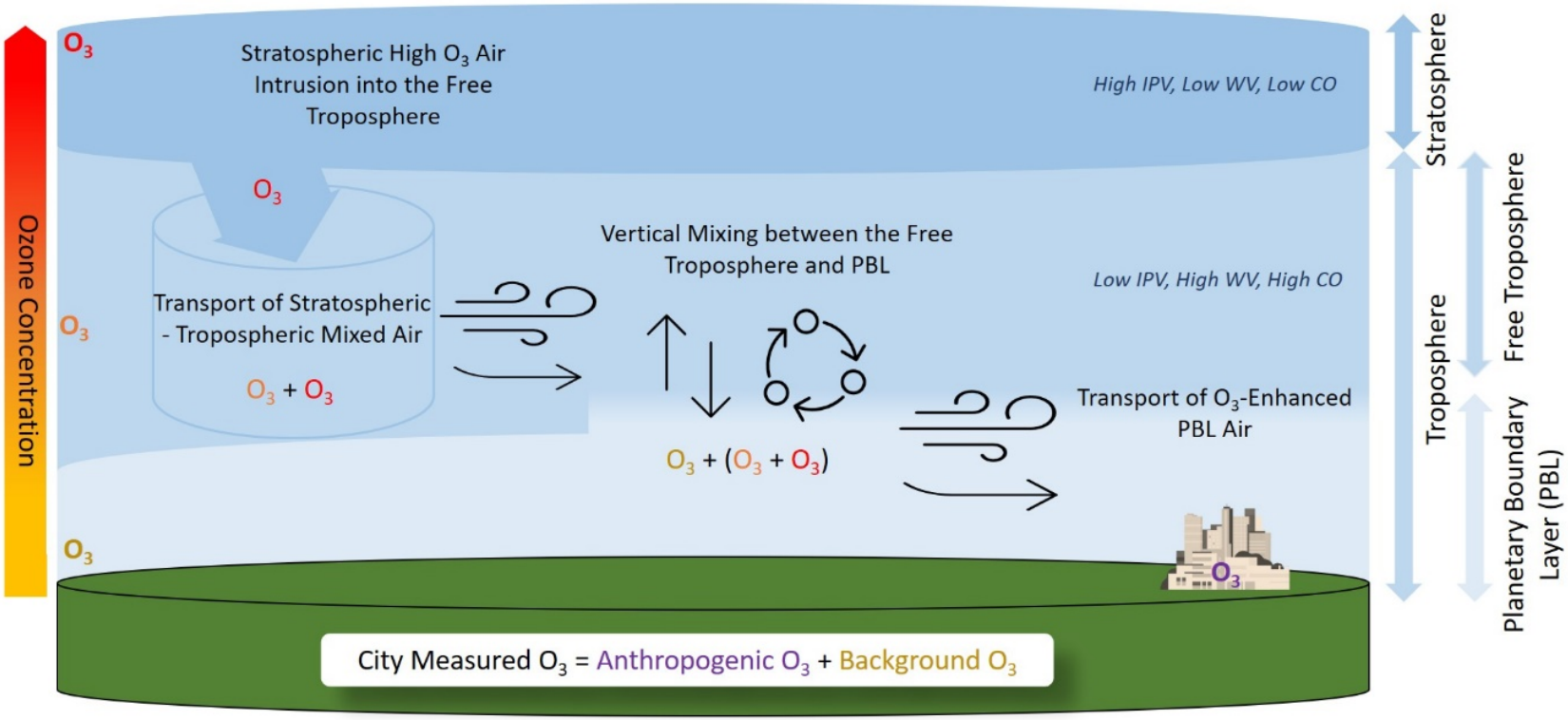


**Figure 2-9.** Stratospheric intrusion and transport example. Ozone concentration with height is shown on the left, and ozone is colored by each source region to illustrate transport. Tracers for stratospheric and tropospheric air are shown on the right, as well as labels for the different atmospheric layers.

**Table 2-2.** Transport mechanisms during a stratospheric ozone intrusion (as displayed in Figure 2-9) and evidence needed to determine transport.

| Transport of Stratospheric Air | Evidence of Transport |
|---|---|
| Stratospheric High Ozone Air Intrusion into the Free Troposphere | Potential Vorticity Plots, High Ozone, Low Carbon Monoxide, Low Water Vapor |
| Transport of Stratospheric – Tropospheric Mixed Air | Upper-Level Meteorology Maps, HYSPLIT Modeling |
| Vertical Mixing between the Free Troposphere and PBL | Meteorology Maps, Skew-T Diagrams, PBL Height Maps |
| Transport of Ozone-Enhanced PBL Air | Surface-Level Meteorology Maps, HYSPLIT Modeling, Measured of Ozone, Water Vapor, and $NO_X$ |

In this report, we describe evidence of a stratospheric intrusion upwind of Clark County influencing already high ozone levels expected under the non-event conceptual model for May 9, 2020. We detail evidence for (1) stratospheric intrusion into the free troposphere, (2) transport of ozone-rich air in the free troposphere, (3) vertical mixing between the free troposphere and PBL, and (4) mixing into the PBL and surface in Clark County. The meteorological conditions on May 9 (explained in Sections 2.3 and 3.3.3) suggest that local and regional ozone production from surface pollutant precursors should be relatively high. Any additional free tropospheric ozone entrained into the PBL could increase surface concentrations over the 70 ppb NAAQS standard. The key differences between the observed SOI event-related concentration(s) and a typical non-SOI event ozone exceedance are detailed in Section 3.1.

Back trajectories from Clark County (Section 3.3.1) demonstrate that air was transported from the free troposphere (above 1 km marine boundary layer) over the Pacific Ocean west of Baja California. We identified this source region for a possible stratospheric intrusion based on evidence for the exchange of stratospheric and tropospheric air. Specifically, there is evidence for this exchange based on IPV, water vapor mass mixing ratio at 250 hPa pressure level, enhanced ozone, and depleted CO levels in the upper troposphere. Values of water vapor below 0.1 g/kg, CO at or below 100 ppb, and ozone concentrations greater than 40-60 ppb in the mid-troposphere, can be indicative of stratospheric influence. IPV is a proxy for atmospheric rotation and is a critical indicator for detecting stratospheric intrusion events. Stratospheric air has values of greater than 1 potential vorticity unit (PVU), which are much greater than the IPV of tropospheric air; values remain above 1 even after stratospheric air enters the troposphere. In the source region on May 7 at 00 UTC, we see stratospheric air in the upper troposphere with modeled IPV greater than 1 and water vapor mixing ratio less than 0.1 g/kg (Section 3.2.2). High modeled ozone and low modeled CO concentrations are seen in the source region near the tropopause at this same time and location (Section 3.2.2). The

combination of high IPV and ozone concentrations, as well as low water vapor and CO concentrations, provides evidence for a stratospheric intrusion off the coast of Baja California (~30 °N and -120 °W) at ~200-300 hPa level on May 6-7.

Ozone vertical profiles and surface observations provide spatial and temporal depictions of ozone immediately preceding and during the May 9 exceedance event. Specifically, ozone vertical profile observations within the path of air transported to Clark County upwind at the JPL Table Mountain site (Section 3.3.2) show enhanced free tropospheric ozone that reached Clark County on May 9, as well as multiple surface monitors in the region that showed elevated ozone concentrations on May 9 (Section 3.4). These observations provide evidence for the free tropospheric transport of ozone enhancements towards the surface at Clark County on May 9.

Meteorological conditions promoted transport from the source region through the free troposphere to the mixed layer and surface at Clark County. Upper level (500 hPa) and surface weather maps at 7:00 PST on May 9 (Section 3.3.3) indicate surface low-pressure trough and upper-level west winds over Clark County were associated with enhanced vertical boundary layer mixing and free troposphere transport from the west of Clark County. The skew-T diagram on May 9 at 16:00 PST shows the air temperature profile follows the dry adiabatic lapse rate, indicating a well-mixed, dry layer from the surface up to 500 hPa, corresponding to a mixing height of ~4.5 km. The skew-T diagram also indicates strong winds from the southwest at the surface and from the west at 600-700 hPa (Section 3.3.2). Additionally, the modeled PBL height on May 9 was ~4.5 km. This deep, well mixed layer over Clark County with strong westerly winds indicates the potential transport and mixing of ozone to the surface (Section 3.3.3).

The combination of a stratospheric intrusion source region—based on IPV, water vapor, ozone, and CO data—along with trajectories, upper-level and surface weather maps, radiosonde temperature profiles, and modeled mixing height, provide evidence that the air mass over Clark County on May 9, 2020, originated from a region of enhanced upper tropospheric ozone, with contributions from ozone-rich stratospheric air. Further detailed meteorology, satellite imagery, and model simulation-based evidence are presented in detail in Section 3.

## 2.5 Analysis of COVID Restrictions on Ozone

Mobile emission sources decreased throughout the U.S. during the mobility restrictions for the COVID-19 pandemic went into place in mid-March 2020. Because decreases in $NO_x$ emissions from mobile sources could result in higher ozone concentrations, we evaluated the potential contribution and sensitivity of the COVID shutdown effects on ozone concentrations and MDA8 ozone on EE days. Ozone production has non-linear dependence on precursor emissions of $NO_x$ and VOCs and meteorological conditions. Changes in precursors also shift photochemical regimes. Thus, the effects of COVID-induced $NO_x$ emission changes on ozone are complex and uncertain (Kroll et al., 2020). Recent studies have found variable ozone responses during lockdowns across countries ranging from

−2 to +10% (Venter et al., 2020). (Parker et al., 2020) found spatially disparate effects of higher ozone concentrations downwind of Los Angeles and lower concentrations in the western LA basin. To evaluate the potential influence of COVID-19 shutdown precursor emission decreases on increases in MDA8 ozone, we compared ozone concentrations in May 2020 to the historical climatology and compared the GAM residuals from May 2020 with those for the same historical record.

Based on 2017 emission inventories in Las Vegas, on-road mobile sources comprise 40% of $NO_x$ emissions and total mobile (vehicle + aviation) emissions comprise 88% of total $NO_x$ emissions for typical ozone season weekday (Clark County Department of Environment and Sustainability, 2020). In contrast, only 11% of VOC emissions originate from on-road mobile sources. The effects of decreased mobility due to COVID restrictions has a significant effect on total $NO_x$ emissions, but minimal effect on VOC emissions. To determine the time period for these effects, we compared 2020 daily traffic count data from the Nevada Department of Transportation with that from 2019 across 10 monitoring sites (two examples in **Figure 2-10**). On-road traffic activity was significantly reduced from mid-March through early-June 2020 in Clark County compared with 2019. Although aviation activity remained lower than pre-pandemic levels for a longer duration of 2020, commercial aviation represents only 12% of $NO_x$ emissions in Clark County. Thus, the reduced aviation activity had a minimal influence on the precursors available for ozone formation from mid-June 2020 onwards. In this section, we focus on May 2020, the first month of 2020 with EE days.

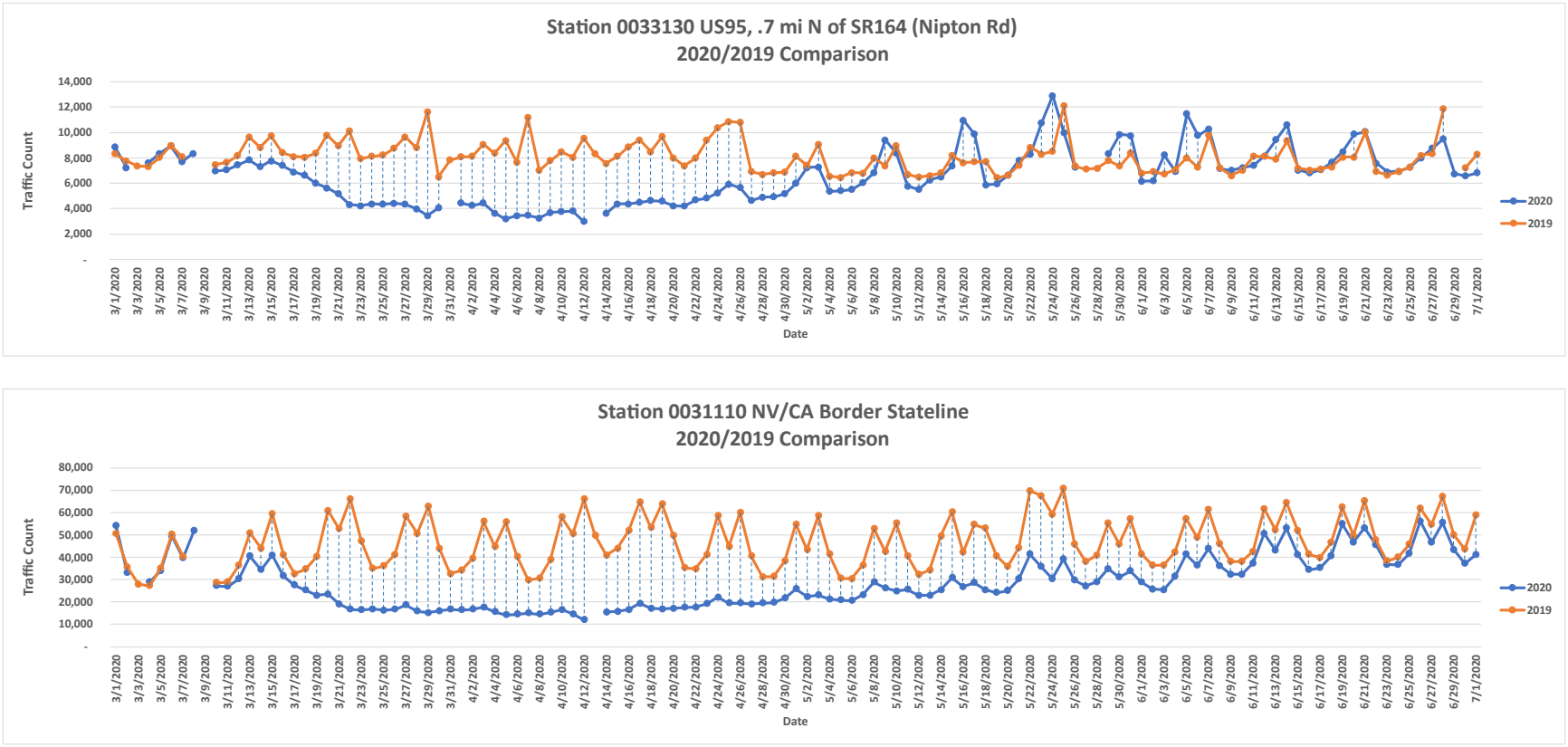


**Figure 2-10.** Time series of 2020 and 2019 traffic counts at two stations: (top) along US95 south of Las Vegas, and (bottom) at the Nevada-California border west of Las Vegas. Data were provided by the Nevada Department of Transportation.

We performed two sub-analyses for comparing ozone concentrations to historical climatology were performed. First, we compared the distribution of daily MDA8 ozone during May 2020 with those during May in each of the previous 5 years. Across all EE sites, we found median 2020 MDA8 ozone was not statistically different than any of the previous 5 years, which was illustrated by the overlap in the 95$^{th}$ confidence intervals of the monthly medians in previous years with that for 2020 (see **Figure 2-11**). Furthermore, monthly median MDA8 ozone during May 2020 was not particularly high (much less than 65 ppb) at all sites despite the exceptional event days. This indicates that the EE day exceedances were extreme episodes that did not affect the monthly median. Thus, the observations do not suggest a month-long high ozone effect due to COVID-19 emission precursor changes. Second, we compared the historical distribution of daily MDA8 ozone during May with the observations during May 2020 (**Figure 2-12**). Across all EE sites, MDA8 ozone on the exceedance days for a given site rank above the confidence interval of the historical daily median MDA8 ozone. Based on these sub-analyses, we conclude that although precursor $NO_x$ emissions decreased during May 2020 due to COVID restrictions, MDA8 ozone concentrations were not statistically higher than previous years and the EE days cannot be attributed to a consistent month-long increase in ozone concentrations due to the COVID shutdown.

To evaluate the GAM model residuals during the COVID shutdown period, Figure 3-65 in Section 3.5.2 provides a more in-depth look at the most heavily affected months of April-May 2020. The 95$^{th}$ confidence interval of the median GAM MDA8 residuals (shown by the notches in the box plots) overlap between 2020 and most other years (except 2015 and 2016). The May 2020 median residual with EE days (1.5 ppb) is lower than the typical GAM model uncertainty given by the range of confidence intervals for median residuals at comparable ozone concentrations (+2.9 to 5.3 ppb, see Table 3-12 in Section 3.5.2). The median GAM residuals during May 2020 were within the typical GAM model error during the previous 5 years.

In summary, although mobile source precursor emissions of $NO_x$ decreased during April and May 2020 due to COVID shutdown restrictions, we did not observe statistically higher ozone, nor a higher residual in the GAM model, during May 2020. We find consistent evidence across analyses that the EE day ozone concentrations cannot be attributed to an increase in ozone concentrations associated with COVID shutdown periods.

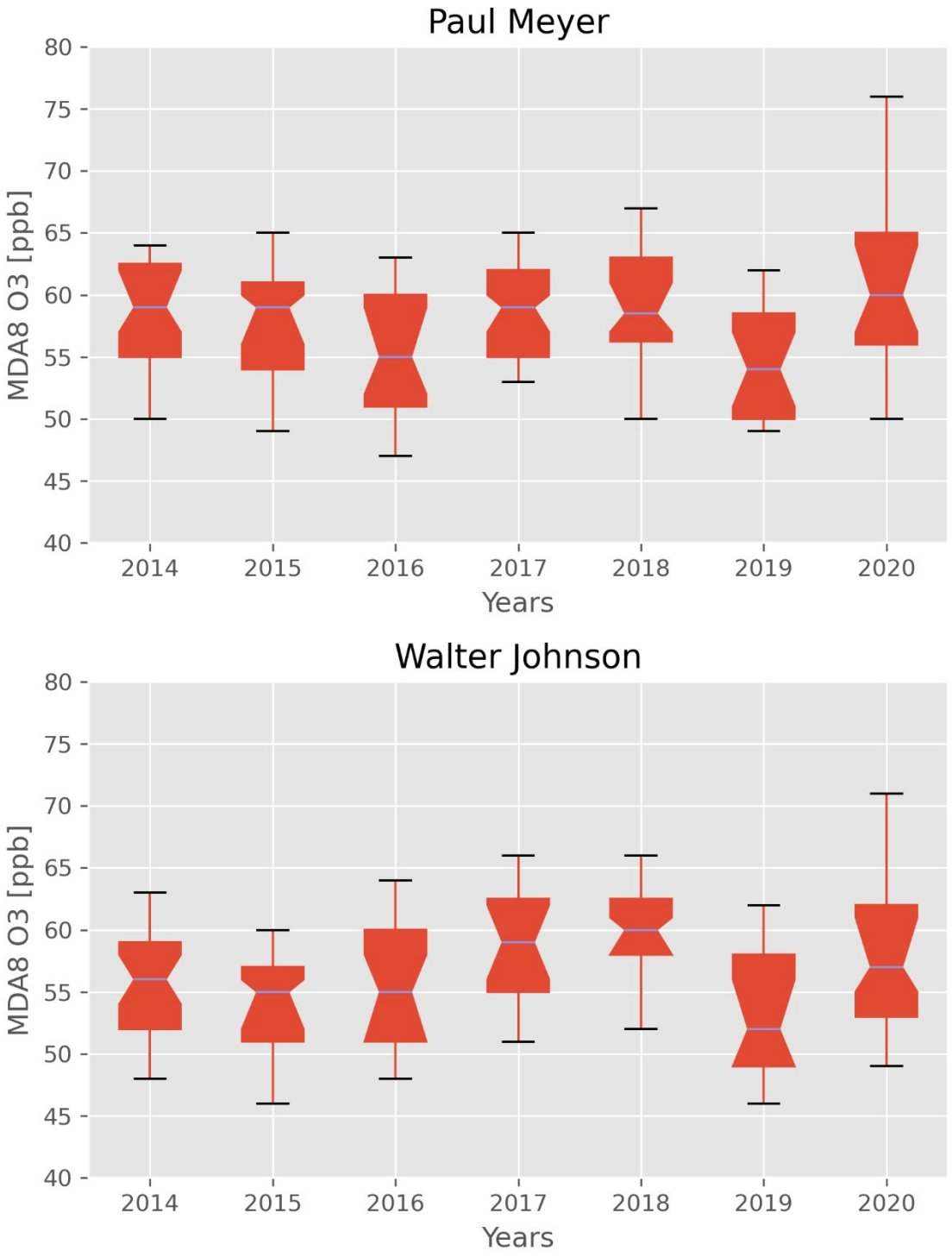


**Figure 2-11.** Annual May distributions of MDA8 ozone at sites with exceptional events during May 2020. Notches denote 95$^{th}$ confidence interval of the median, boxes are 25$^{th}$, 50$^{th}$ and 75$^{th}$ percentiles, and whiskers are 5$^{th}$ and 95$^{th}$ percentiles.

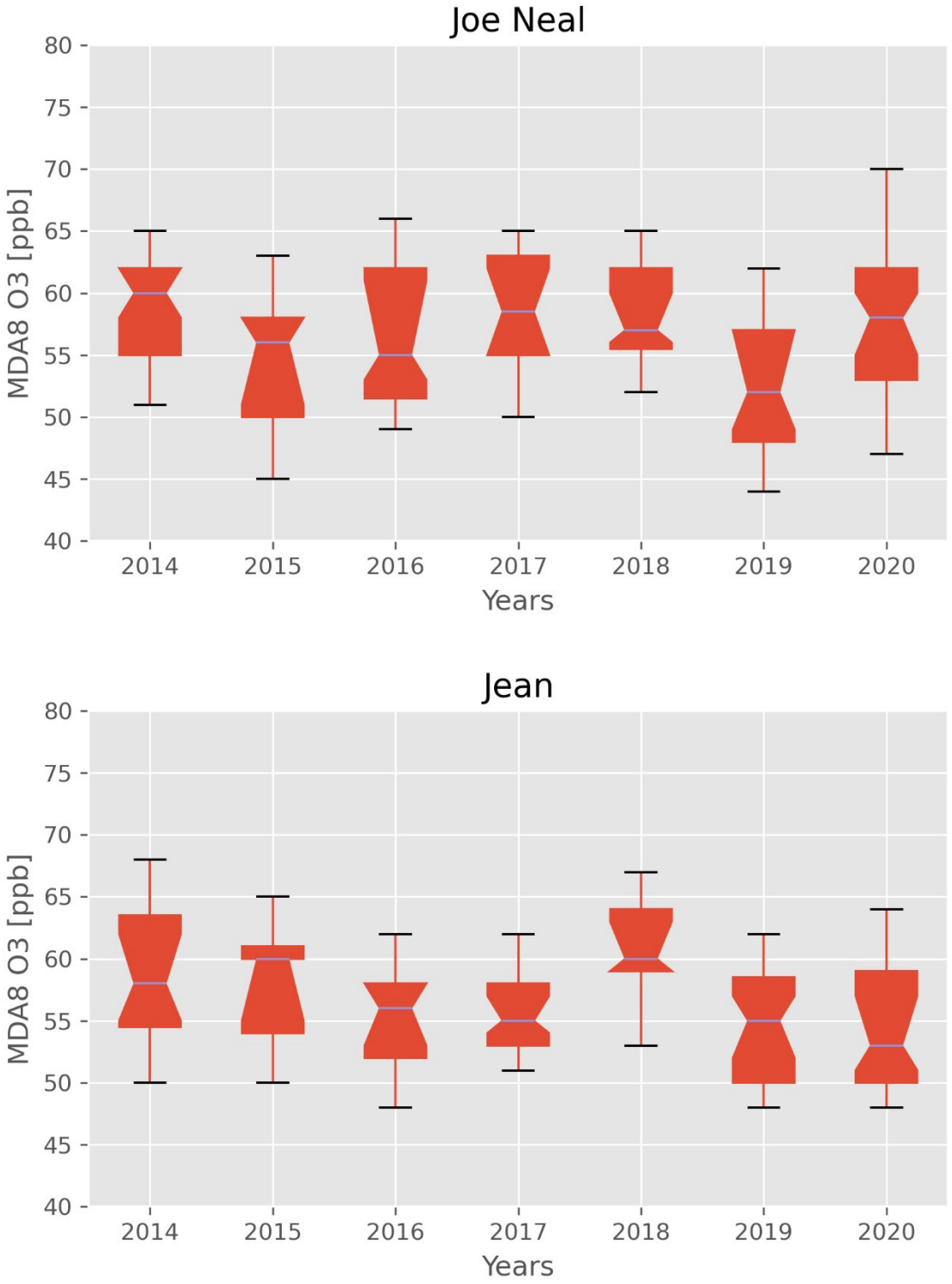


**Figure 2-11 (Cont.).** Annual May distributions of MDA8 ozone at sites with exceptional events during May 2020. Notches denote 95th confidence interval of the median, boxes are 25th, 50th and 75th percentiles, and whiskers are 5th and 95th percentiles.

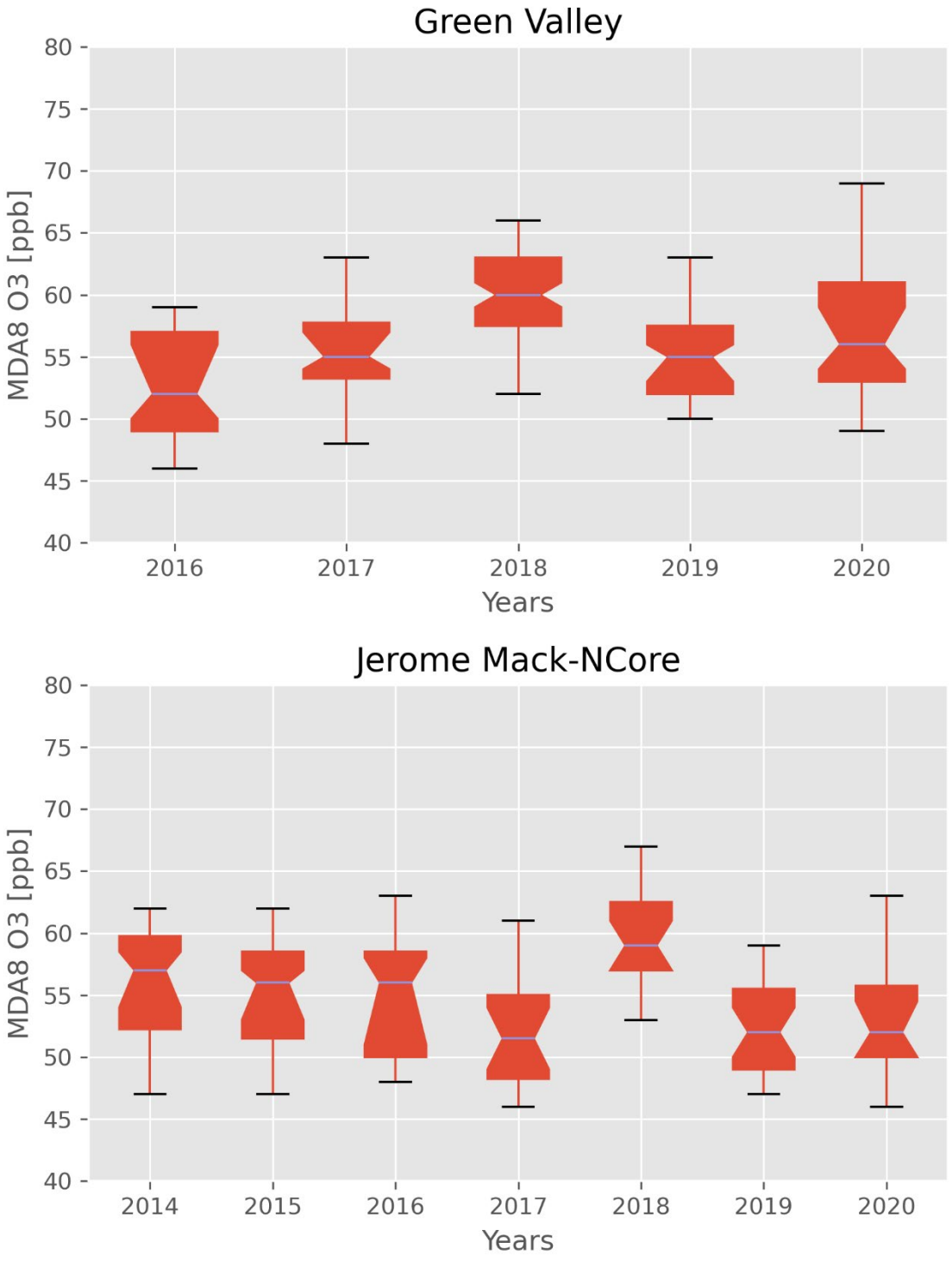


**Figure 2-11 (Cont.).** Annual May distributions of MDA8 ozone at sites with exceptional events during May 2020. Notches denote 95$^{th}$ confidence interval of the median, boxes are 25$^{th}$, 50$^{th}$ and 75$^{th}$ percentiles, and whiskers are 5$^{th}$ and 95$^{th}$ percentiles.

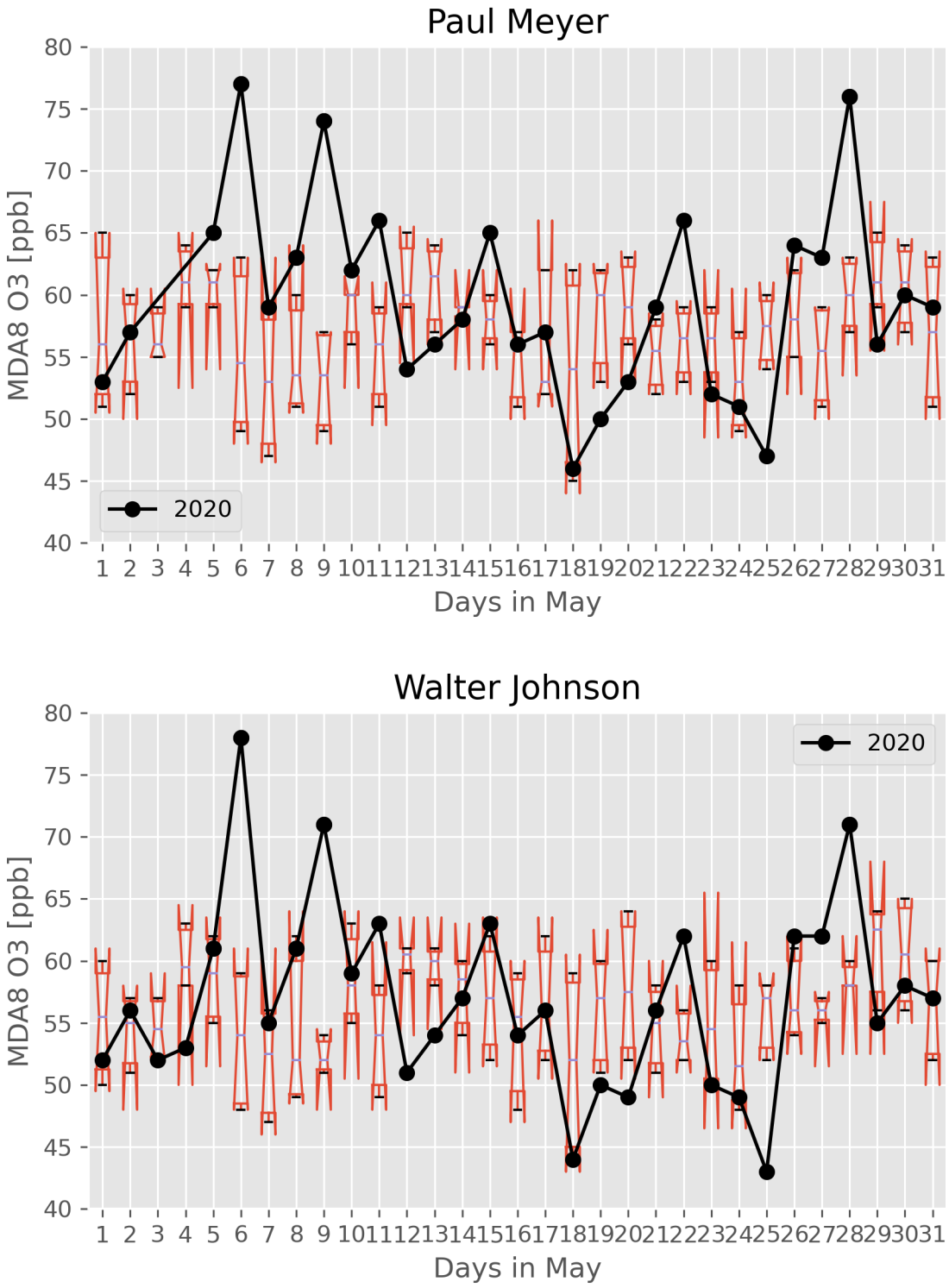


**Figure 2-12.** Daily time series of 2014-2019 MDA8 ozone distributions and 2020 MDA8 ozone at each site with proposed exceptional event during May 2020. Notches denote 95$^{th}$ confidence interval of the median, boxes are 25$^{th}$, 50$^{th}$ and 75$^{th}$ percentiles, and whiskers are 5$^{th}$ and 95$^{th}$ percentiles.

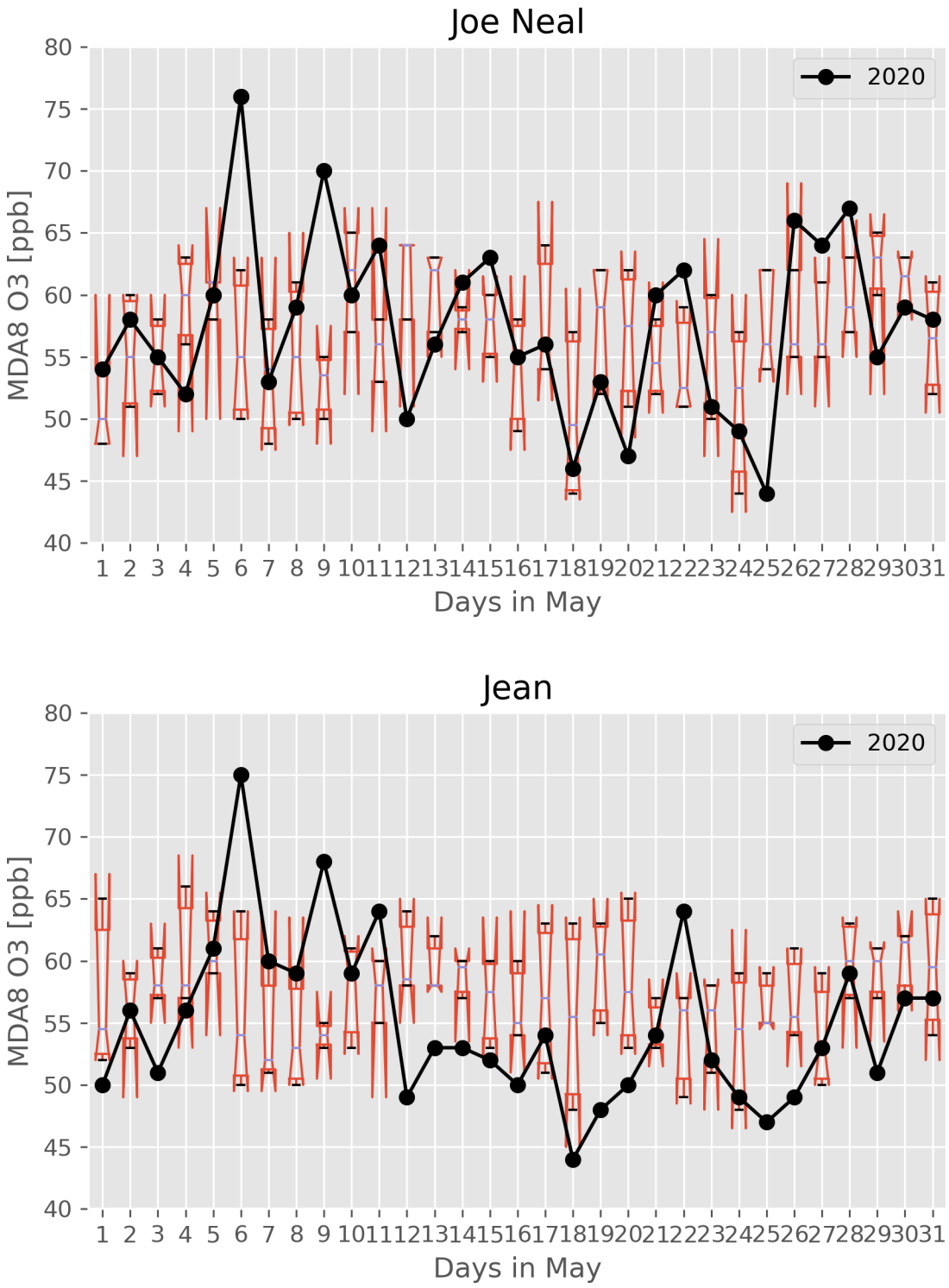


**Figure 2-12 (Cont.)**. Daily time series of 2014-2019 MDA8 ozone distributions and 2020 MDA8 ozone at each site with proposed exceptional event during May 2020. Notches denote 95$^{th}$ confidence interval of the median, boxes are 25$^{th}$, 50$^{th}$ and 75$^{th}$ percentiles, and whiskers are 5$^{th}$ and 95$^{th}$ percentiles.

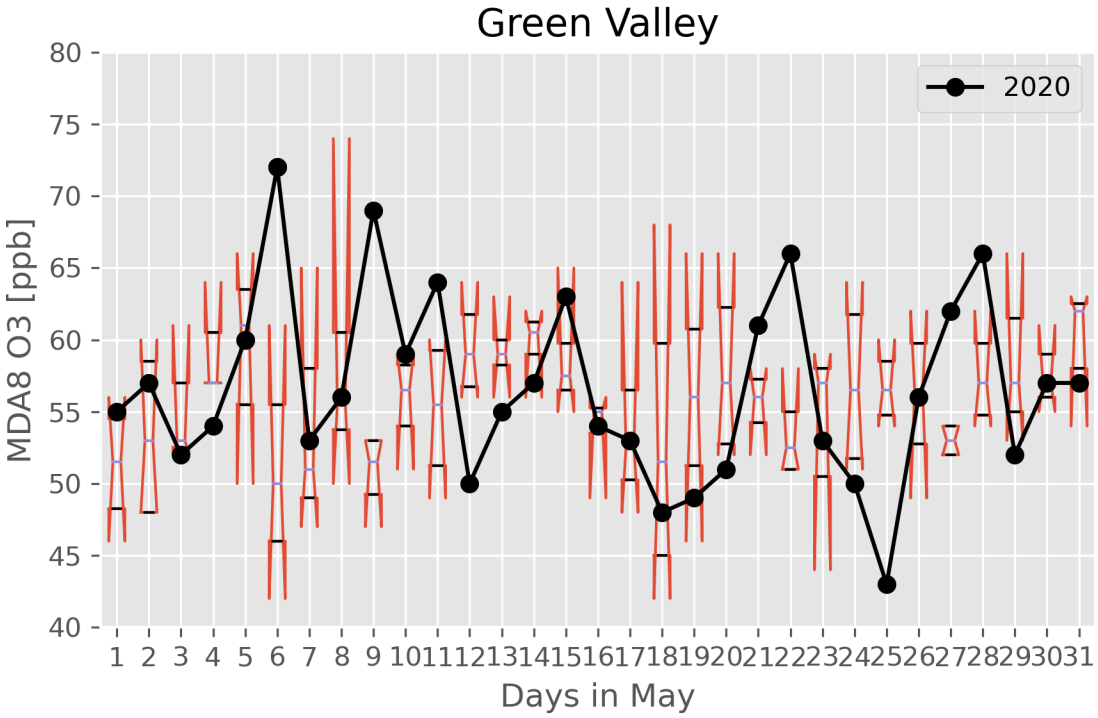


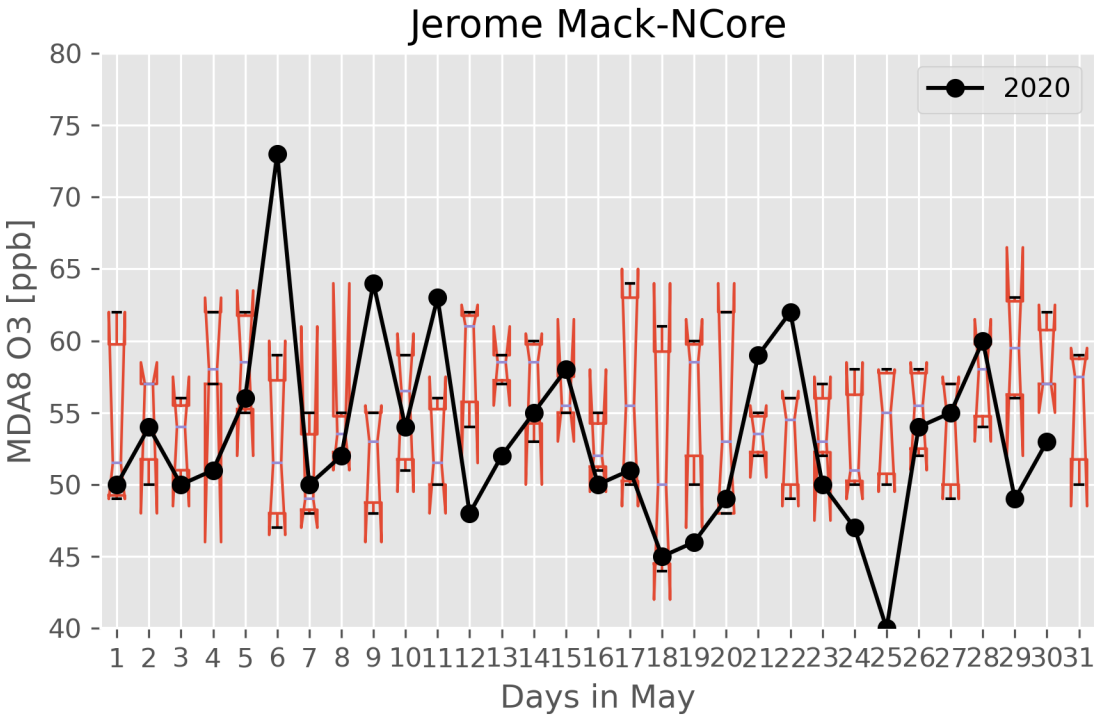


**Figure 2-12 (Cont.).** Daily time series of 2014-2019 MDA8 ozone distributions and 2020 MDA8 ozone at each site with proposed exceptional event during May 2020. Notches denote 95$^{th}$ confidence interval of the median, boxes are 25$^{th}$, 50$^{th}$ and 75$^{th}$ percentiles, and whiskers are 5$^{th}$ and 95$^{th}$ percentiles.

# 3. Clear Causal Relationship Analyses

## 3.1 Comparison of Event Concentrations with Historical Concentrations

To address the Tier 1 EE criterion of comparison with historical ozone concentrations, we compared the May 9 EE ozone concentrations at each site with the 2020 ozone record, focusing mainly on the ozone season when highest ozone concentrations occur. **Figures 3-1 and 3-2** depict the 2020 daily maximum ozone record at each monitoring site, along with the 99th percentile over the past six years, and NAAQS criteria ozone concentrations. During 2020, May 9 ranks in the top 1% for daily maximum ozone concentration in the past five years at the Paul Meyer monitoring site. For the Las Vegas Valley sites that were affected by the EE (the Paul Meyer and Walter Johnson sites), the May 9 EE was in the top 5% of MDA8 ozone concentrations in the past five years (**Table 3-1**). When compared with daily ozone rankings on May 9 over the six-year ozone record, the 2020 rankings indicate that May 9, 2020, was an extreme ozone event.

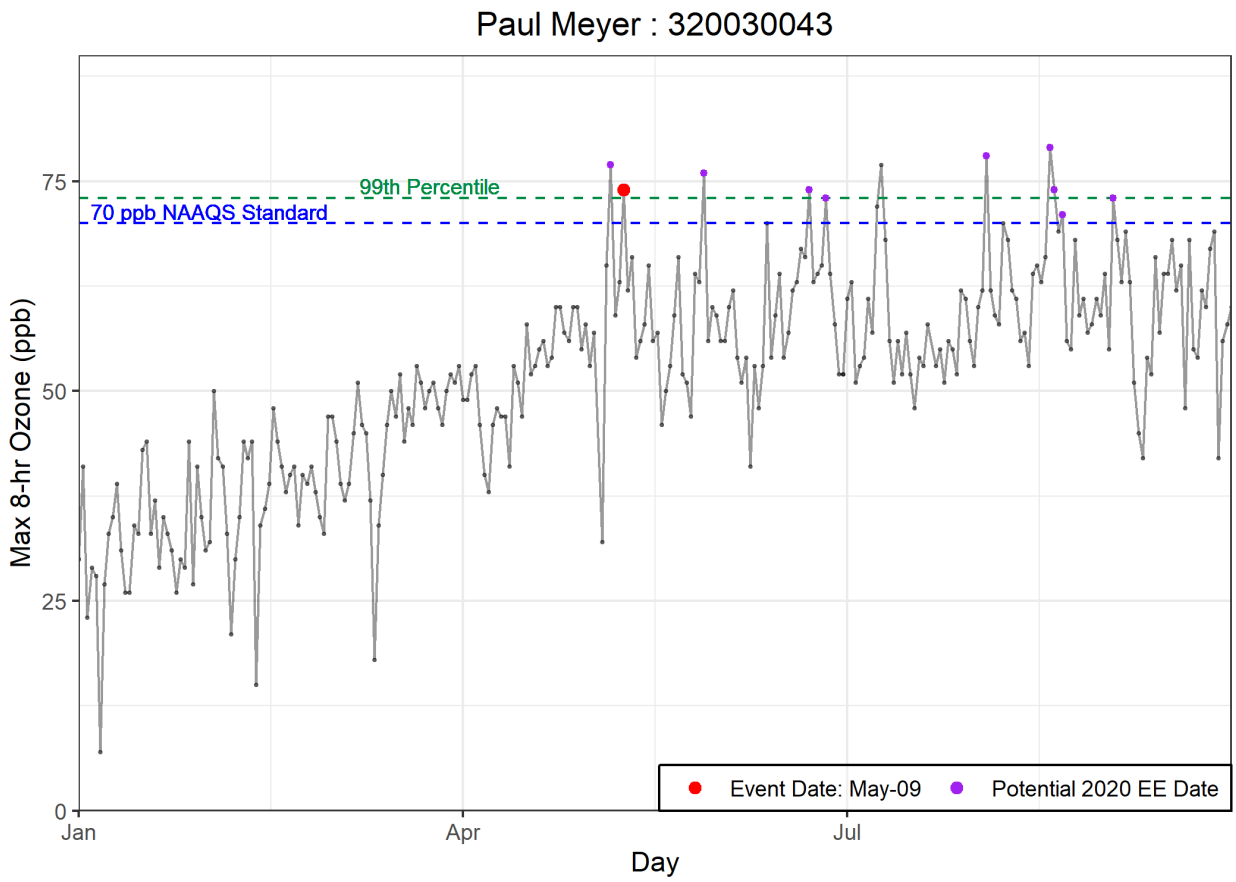


**Figure 3-1.** Time series of 2020 MDA8 ozone concentrations from the Paul Meyer site. May 9, 2020, is shown in red.

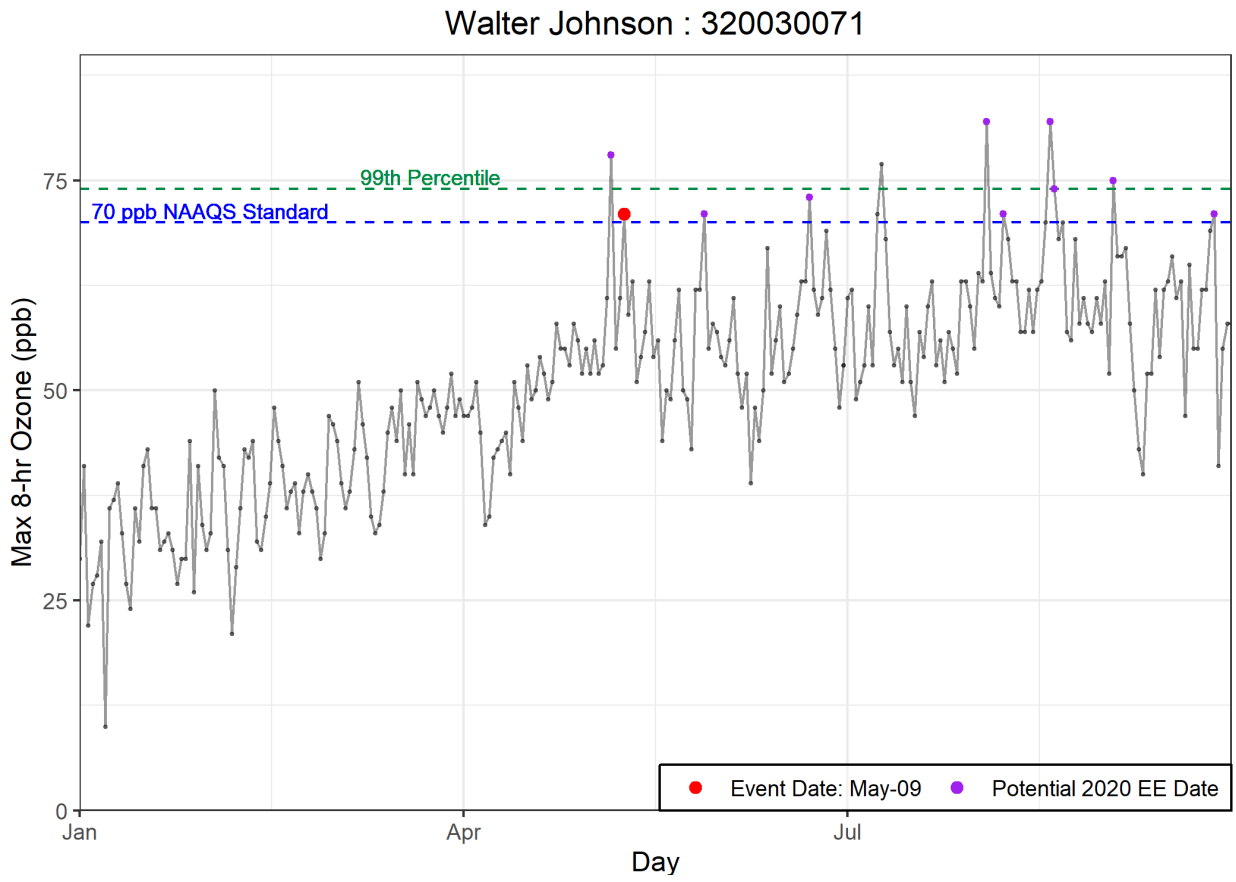


**Figure 3-2.** Time series of 2020 MDA8 ozone concentrations from the Walter Johnson site. May 9, 2020, is shown in red.

**Table 3-1.** Six-year percentile ozone. The May 9 exceptional event ozone concentration at each site is calculated as a percentile of the last six years with and without other 2018 and 2020 exceptional events included in the historical record.

| AQS Site Code | Site Name | 6-Year Percentile | 6-Year Percentile w/o EE Dates |
|---|---|---|---|
| 320030071 | Walter Johnson | 97.9 | *98.7* |
| 320030043 | Paul Meyer | 99.3 | *99.7* |

The May 9, 2020, ozone exceedance occurred during the typical ozone season, but MDA8 ozone concentrations on May 9 were the second highest in 2020 compared with daily ozone concentrations excluding potential EE days (Figures 3-1 and 3-2). Table 3-2 provides historical monitoring site statistics for each affected site on May 9. The statistics shown are for May through September from 2015-2019; we do not exclude the dates with proposed 2018 EE ozone concentrations. The MDA8

ozone concentrations on May 9 were more than 10 ppb above the mean and median ozone concentrations for the historical ozone season at all EE affected sites. In contrast, MDA8 ozone concentrations were less than 5 ppb above the 95th percentile of non-event day historical ozone concentrations at EE affected sites. Because May 9 is during the normal ozone season and MDA8 ozone concentrations at the two EE affected sites could not be clearly distinguished from the 95th percentile ozone concentration during the non-event historical ozone season, further analysis (Tier 2) is required.

**Table 3-2.** Ozone season non-event comparison. MDA8 ozone concentrations at each affected site on May 9, 2020, are shown in the top row. Five-year (2015-2019) average MDA8 ozone statistics for the May through September ozone season are shown for each affected site around Clark County to compare with the event ozone concentrations.

| | Paul Meyer 320030043 | Walter Johnson 320030071 |
|---|---|---|
| May. 9 | 74 | 71 |
| Mean | 57 | 57 |
| Median | 58 | 57 |
| Mode | 58 | 57 |
| St. Dev | 8 | 9 |
| Minimum | 22 | 21 |
| 95 %ile | 70 | 71 |
| 99 %ile | 76 | 77 |
| Maximum | 79 | 87 |
| Range | 57 | 66 |
| Count | 911 | 917 |

To address the Tier 2 EE criterion to determine whether the May 9, 2020, exceedance event is exceptional, we compare event ozone concentrations with non-event concentrations via percentile and rank-order analysis. Table 3-1 shows May 9 concentrations as a percentile in comparison with the last six years of data (with and without the other proposed 2018 and 2020 EE days). For the two monitoring sites (Paul Meyer and Walter Johnson) that show a NAAQS standard exceedance on May 9, all of the exceedances are greater than the 97th percentile when compared to the last six years of data, even with all other proposed 2018 and 2020 EE days included. Without the other EE days included, the percentiles are slightly higher (>98th percentile). To confirm that the calculated percentiles are not biased by non-ozone season data, Table 3-3 shows the May 9 percentile ranks for all monitoring sites around Clark County in comparison with the last six years of ozone season

(May to September) data. The May 9 ozone concentration percentile over the last six ozone seasons (with all proposed 2018 and 2020 EE days included) ranks above the 98th percentile at the Paul Meyer monitoring site, and above the 95th percentile at the Walter Johnson monitoring site. When the other possible EE days are excluded, the percentile rank of ozone season concentrations at the Paul Meyer site increases to the 97th percentile, and the Walter Johnson site increases to the 99th percentile. Although not all of the sites ranked above the 99th percentile of ozone season concentrations on May 9, this analysis confirms that the May 9 EE included unusually high concentrations of ozone when compared with ozone concentrations across both the last six years and the last six ozone seasons.

**Table 3-3.** Six-year ozone-season percentile ozone. The May 9, 2020, exceptional event ozone concentration at each site is calculated as a percentile of concentrations over the last six years of the ozone season (May-September) with and without other 2018 and 2020 exceptional events included in the historical record.

| AQS Site Code | Site Name | 6-Year Percentile | 6-Year Percentile w/o EE Dates |
|---|---|---|---|
| 320030071 | Walter Johnson | 95.2 | *97.1* |
| 320030043 | Paul Meyer | 98.5 | *99.2* |

We also compared the rank-ordered concentrations at each site for 2020. As shown in Figures 2-4 and 2-5, ozone concentrations across 2020 were not atypically low, which might bias our rank-ordered analysis for May 9. Tables 3-4 and 3-5 show the rank-ordered ozone concentrations for 2018 through 2020 and the design values for 2020, with the proposed 2018 and 2020 EEs included. Based on the concentration rankings, May 9 is not in the top five ozone concentrations of 2020 when including all other proposed EE events. Without other proposed EE events in 2020 included, all EE affected sites show May 9 ranked as the second highest ozone event in 2020.

**Table 3-4.** Site-specific ozone design values for the Paul Meyer monitoring site. The top five highest ozone concentrations for 2018-2020 at Paul Meyer are shown, and proposed exceptional event days in 2018 and 2020 are included.

| Paul Meyer Rank | 2018 | 2019 | 2020 |
|---|---|---|---|
| Highest | 79 | 74 | 79 |
| Second Highest | 76 | 72 | 78 |
| Third Highest | 75 | 70 | 77 |
| Fourth Highest | 75 | 69 | 77 |
| Fifth Highest | 74 | 69 | 76 |
| Design Value | | 73 | |

**Table 3-5.** Site-specific ozone design values for the Walter Johnson monitoring site. The top five highest ozone concentrations for 2018-2020 at Walter Johnson are shown, and proposed exceptional event days in 2018 and 2020 are included.

| Walter Johnson Rank | 2018 | 2019 | 2020 |
|---|---|---|---|
| Highest | 79 | 77 | 82 |
| Second Highest | 77 | 69 | 82 |
| Third Highest | 77 | 69 | 78 |
| Fourth Highest | 76 | 68 | 77 |
| Fifth Highest | 76 | 68 | 75 |
| Design Value | | 73 | |

For further comparison with non-event ozone concentrations, Table 3-6 shows five-year (2015-2019, proposed 2018 EE events included) MDA8 ozone statistics for one week before and after May 9, 2020. This two-week window analysis shows that each affected monitoring site exhibited MDA8 ozone concentrations on May 9 that were greater than 10 ppb above the mean or median, and greater than or equal to 5 ppb above the 95th percentile of ozone concentrations over the two-week window in the last five years.

**Table 3-6.** Two-week non-event comparison. May 9, 2020, MDA8 ozone concentrations for each affected site are shown in the top row. Five-year (2015-2019) average MDA8 ozone statistics for May 2 through May 16 are shown for each affected site around Clark County to compare with the event ozone concentrations.

| | Paul Meyer 320030043 | Walter Johnson 320030071 |
|---|---|---|
| May. 9 | 74 | 71 |
| Mean | 58 | 57 |
| Median | 58 | 57 |
| Mode | 59 | 61 |
| St. Dev | 6 | 6 |
| Minimum | 32 | 42 |
| 95 %ile | 66 | 66 |
| 99 %ile | 74 | 71 |
| Maximum | 77 | 78 |
| Range | 45 | 36 |
| Count | 94 | 96 |

The percentile, rank-ordered analyses, and the two-week window analysis indicate that all affected monitoring sites on May 9 showed atypically high ozone concentrations compared with non-event concentrations. This conclusion supports Tier 1 and 2 criteria, suggesting that May 9 was an EE in Clark County.

## 3.2 Evidence of Stratospheric-Tropospheric Exchange

### 3.2.1 Satellite Imagery

Satellite retrievals can help identify signatures of a stratospheric intrusion event, such as ozone-rich and extremely dry air. We examined maps of true color visible imagery from the Moderate Resolution Imaging Spectroradiometer (MODIS) instruments onboard the Aqua and Terra satellites, water vapor imagery from Geostationary Operational Environmental Satellite (GOES)-East, and total column ozone from the Ozone Mapping and Profile Suite (OMPS) instrument aboard the Suomi NPP satellite. These maps provide evidence to support the transport of dry, ozone-rich stratospheric air from an area to the west of Baja California around May 7 at 00:00 UTC, over the eastern Pacific Ocean, and into Clark County, Nevada on May 9.

True color visible satellite imagery can be used to identify areas of very dry and cloudless air that may be indicative of the effects from a stratospheric intrusion. True color visible satellite imagery from the MODIS instruments onboard the Aqua and Terra satellites show a lack of extensive cloud cover over southern California and Nevada (**Figures 3-3 through 3-5**). From May 8 to May 9, the Clark County area was almost entirely devoid of cloud cover, which can be a characteristic of dry stratospheric air.

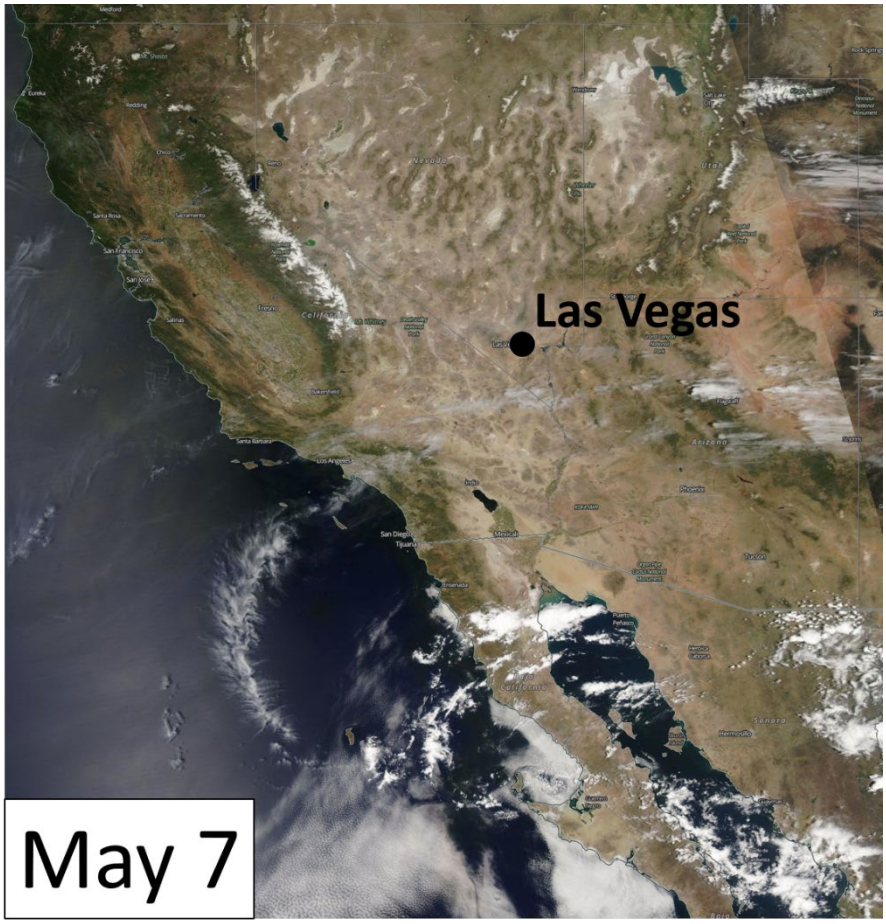


**Figure 3-3.** Visible satellite imagery from over Baja California and southern California and Nevada on May 7, 2020. Source: NASA Worldview

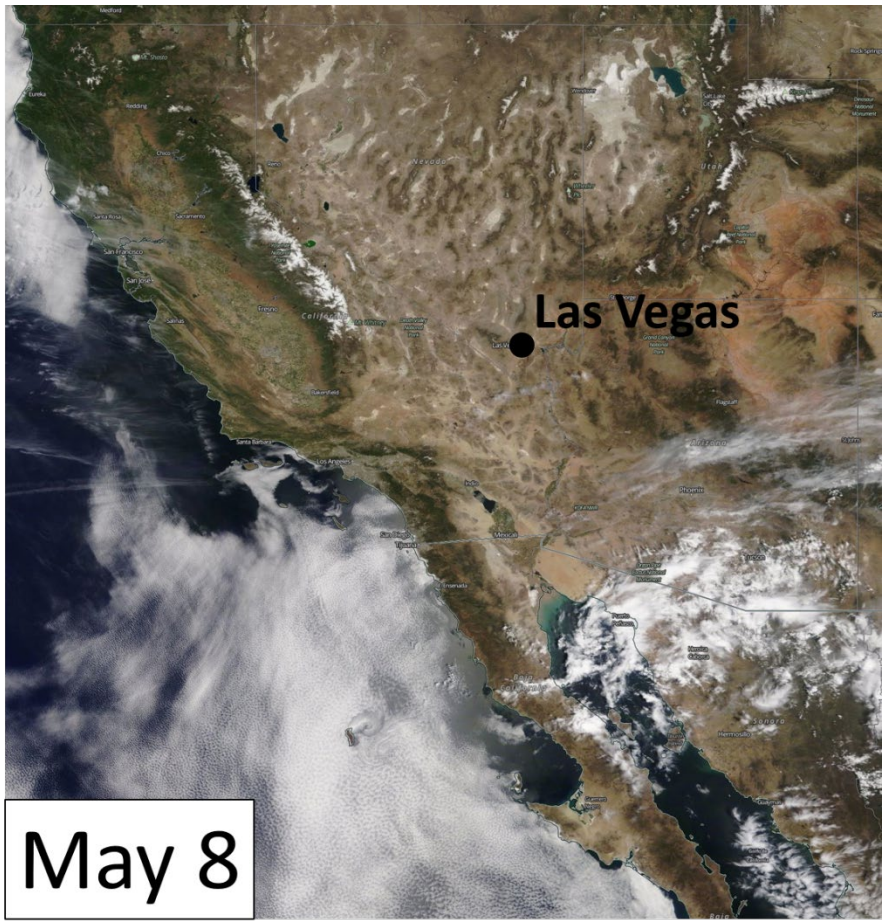


**Figure 3-4.** Visible satellite imagery from over Baja California and southern California and Nevada on May 8, 2020. Source: NASA Worldview

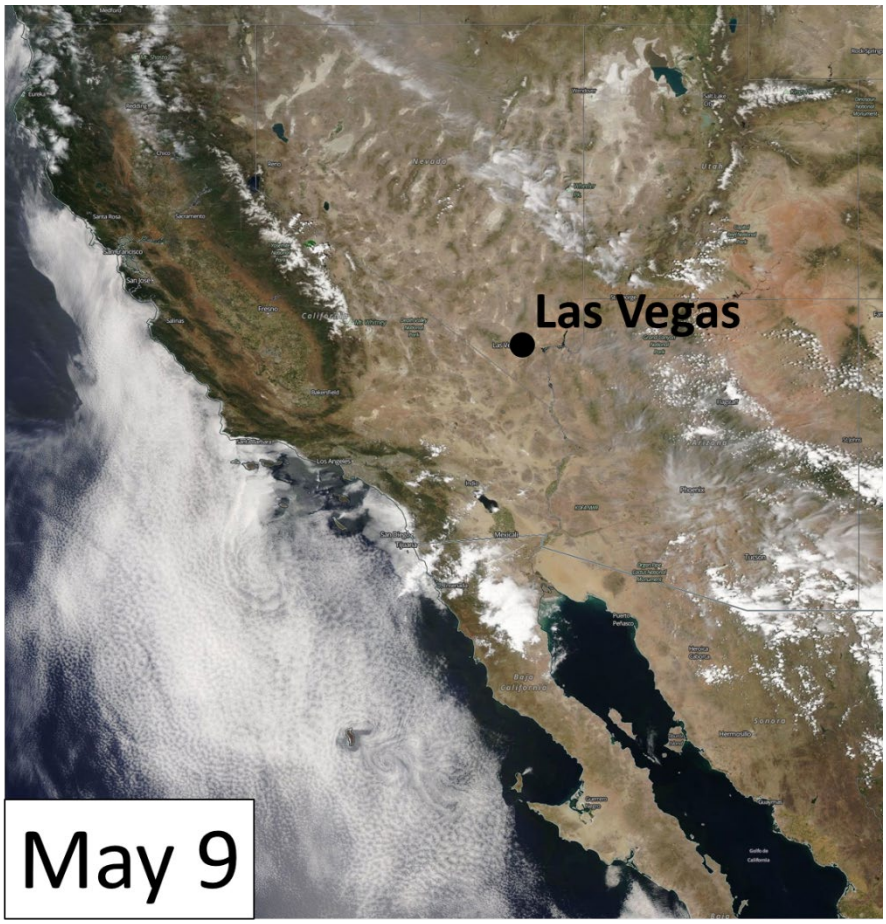


**Figure 3-5.** Visible satellite imagery from over Baja California and southern California and Nevada on May 9, 2020. Source: NASA Worldview

The stratosphere's lack of water vapor relative to that of the troposphere is a key characteristic when tracing stratospheric air. Because stratospheric intrusion events will lead to the drying of tropospheric air, satellite imagery of total column water vapor can be used to highlight areas of dry and potentially stratospheric air. Water vapor imagery from the GOES-East satellite shows an extensive area of dry air—as indicated by increasingly darker shades of brown—from Baja California to southern California along the eastern Pacific Ocean coast (**Figures 3-6 through 3-9**). From May 7 at 00:20 UTC to May 10 at 00:20 UTC, a volume of extremely dry air was located to the west of Baja California over the eastern Pacific Ocean, which is the approximate area of the stratospheric intrusion (Section 3.2.2 details the SOI source region). The maps are consistent with Figures 3-3 through 3-5, which also show an extensive area of dry air, relatively little cloud cover, and clear atmosphere over Baja California.

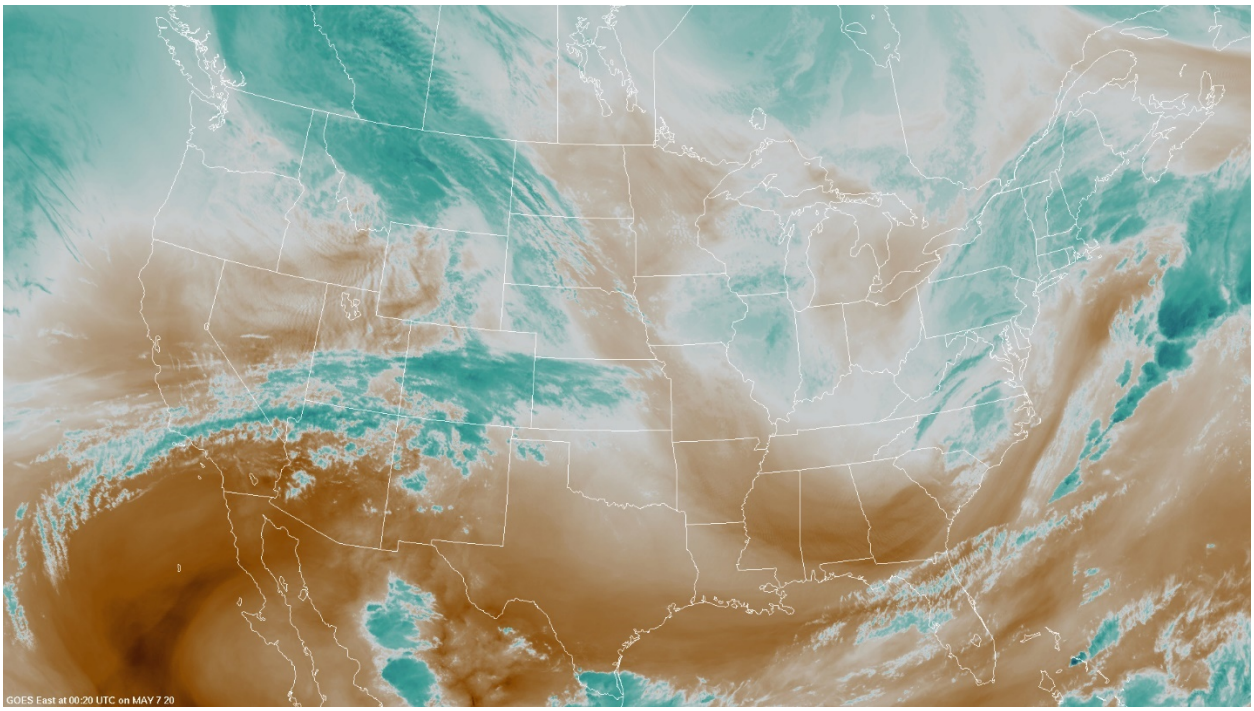


**Figure 3-6.** Water vapor imagery from the GOES-East Satellite on May 7, 2020, at 00:20 UTC. Bright blue and white areas indicate the presence of high water vapor or moisture content, whereas dark orange and brown areas indicate little or no moisture present.

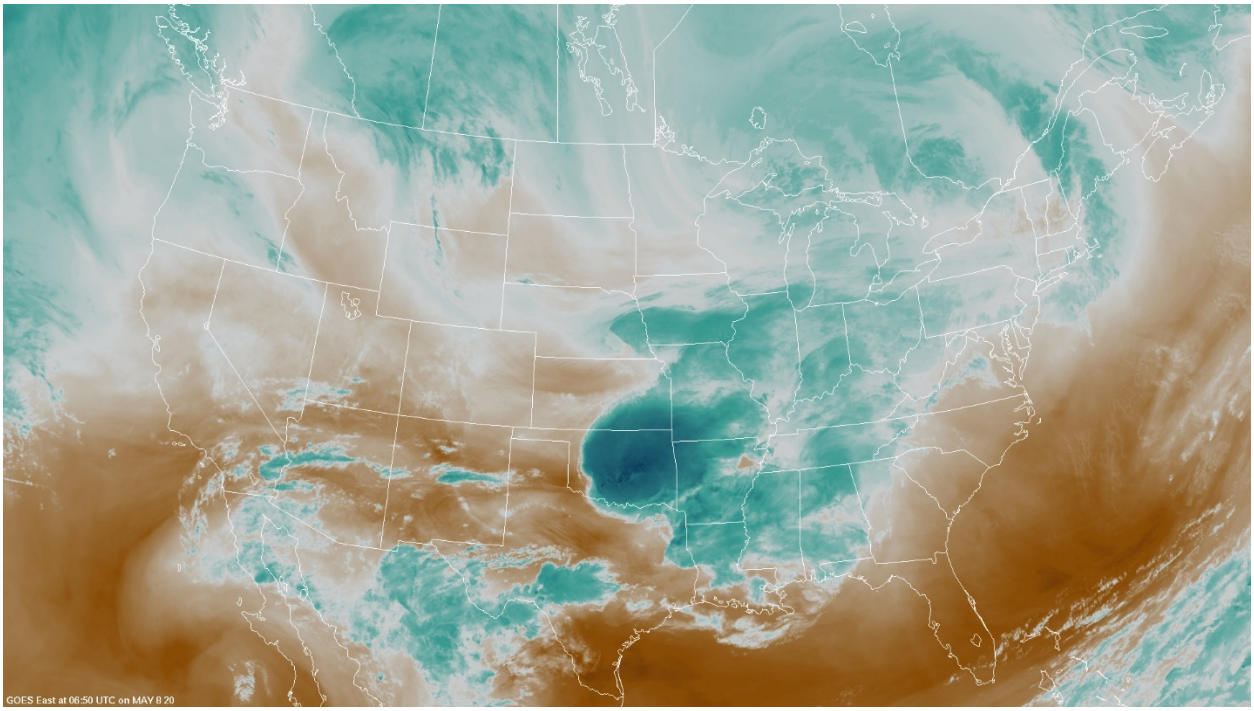


**Figure 3-7.** Water vapor imagery from the GOES-East Satellite on May 8, 2020, at 06:50 UTC. Bright blue and white areas indicate the presence of high water vapor or moisture content, whereas dark orange and brown areas indicate little or no moisture present.

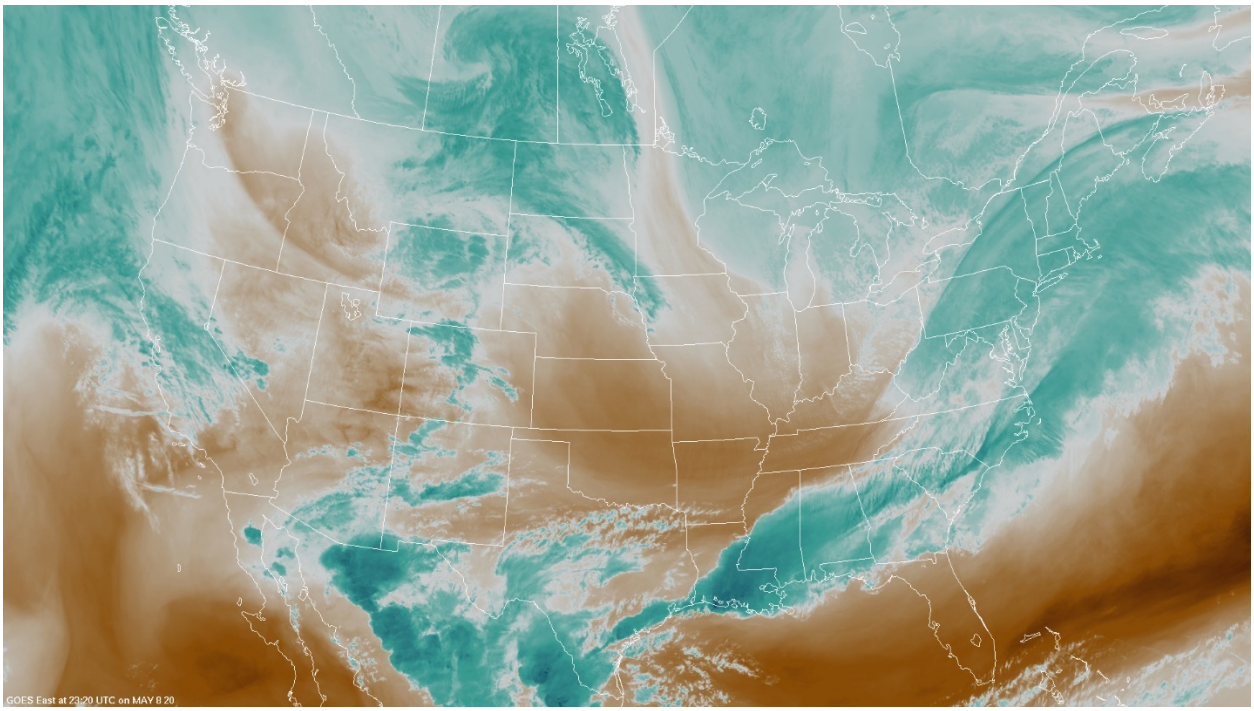


**Figure 3-8.** Water vapor imagery from the GOES-East Satellite on May 8, 2020, at 23:20 UTC. Bright blue and white areas indicate the presence of high water vapor or moisture content, whereas dark orange and brown areas indicate little or no moisture present.

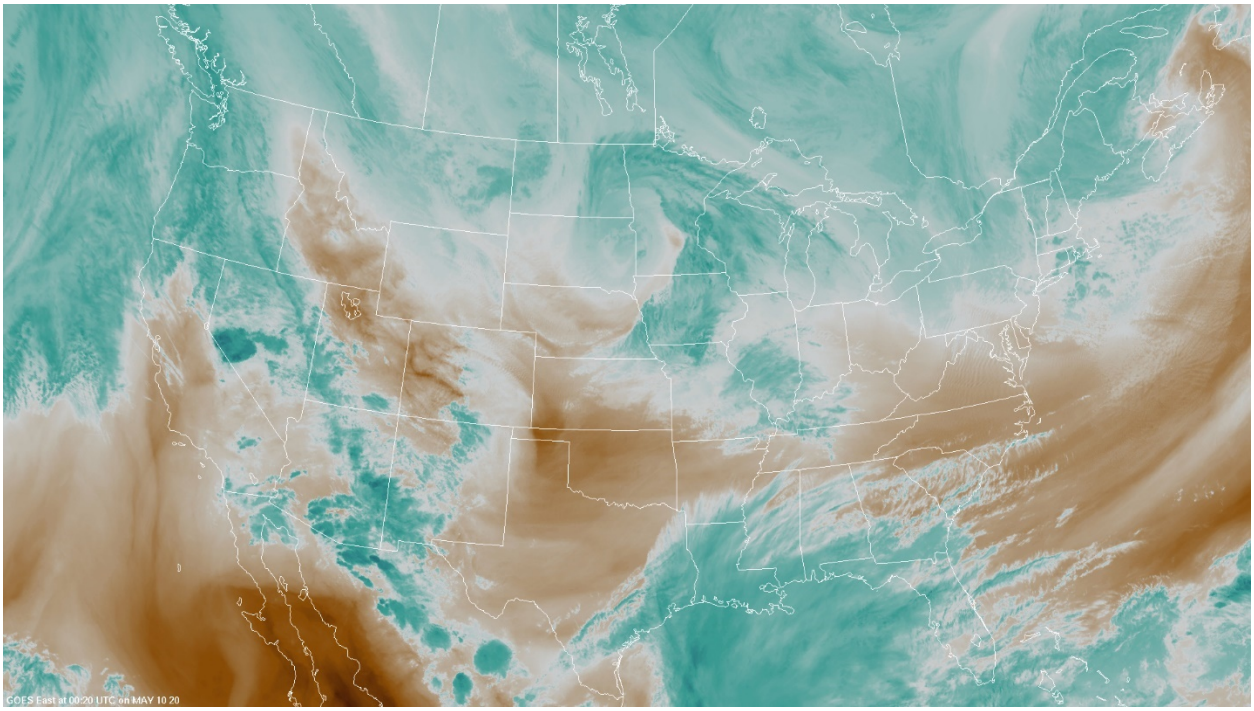


**Figure 3-9.** Water vapor imagery from the GOES-East Satellite on May 10, 2020, at 00:20 UTC. Bright blue and white areas indicate the presence of high water vapor or moisture content, whereas dark orange and brown areas indicate little or no moisture present.

Satellite retrievals of total column ozone are useful in identifying areas with high ozone concentrations that may be associated with stratospheric intrusion events. Maps of total column ozone on May 7, 8, and 9 from the OMPS instrument aboard the Suomi NPP satellite are shown in Figure 3-10. On May 7, total column ozone was slightly enhanced compared to the surrounding areas—as shown by shades of yellow and orange—off the coast of Baja to levels between approximately 315 and 340 Dobson Units (DU). Typical May total column ozone in this area is < 300 DU. Between May 7 and 9, the area of enhanced total column ozone moved northward, toward southern California and Nevada (this track is consistent with the trajectories shown in Section 3.3.1). By May 9, total column ozone concentrations were up to approximately 315 DU over the Clark County area. These maps provide evidence that total column ozone was enhanced compared with typical concentrations in the stratospheric intrusion source region and over the Clark County area relative to portions of central Mexico and the southwestern United States. Together, the visible, water vapor, and ozone satellite imagery provide evidence of a large-scale ozone event consistent with the intrusion and transport of stratospheric ozone.

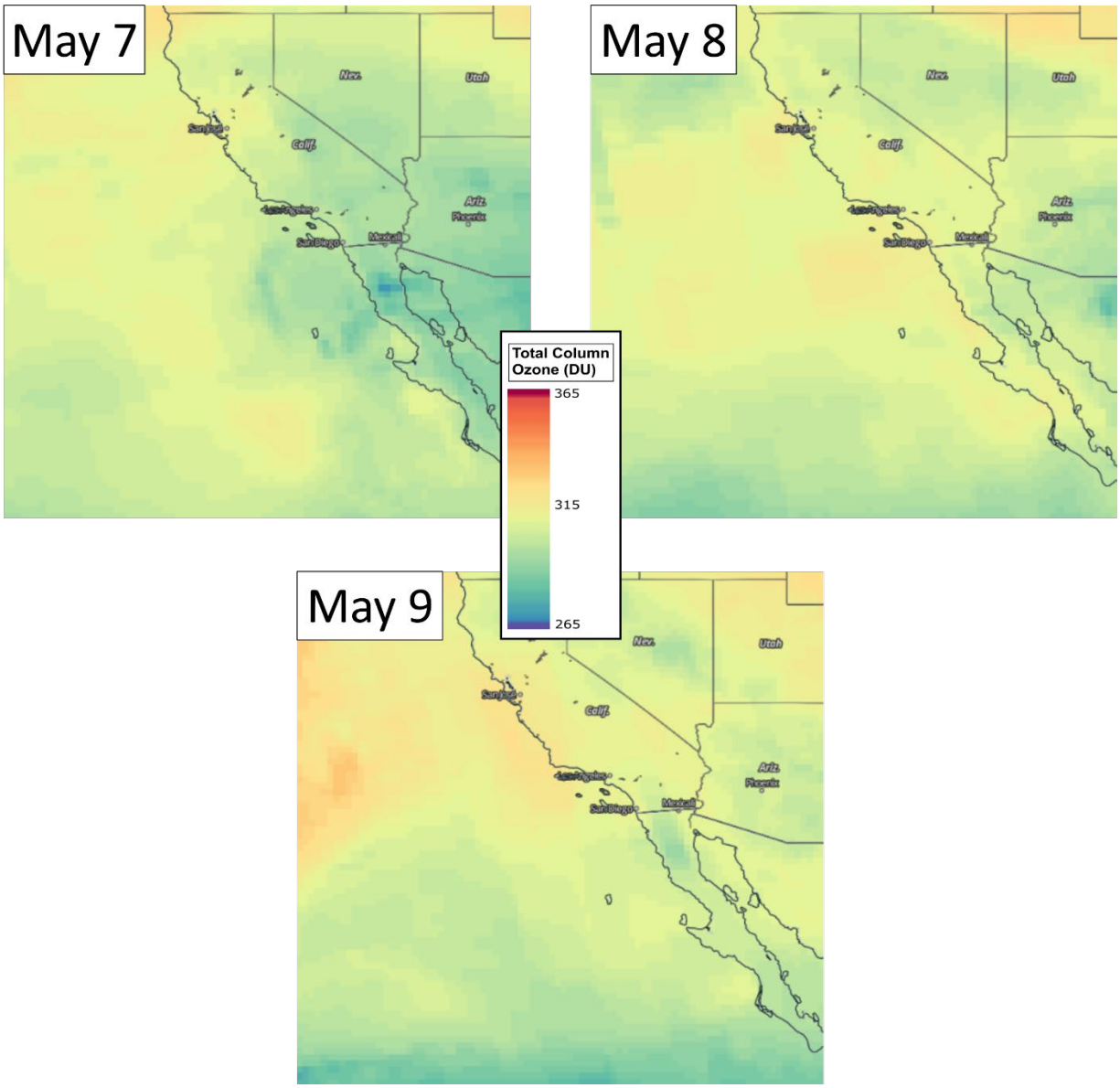


**Figure 3-10.** Maps of satellite-estimated total column ozone from May 7-9, 2020, from the OMPS instrument on the Suomi NPP satellite. Data source: NASA Worldview.

## 3.2.2 Model Results

The stratospheric-tropospheric mixing that occurred off the coast of the Baja California peninsula and likely contributed to the ozone exceedance in Clark County on May 9 was identified through the modeled analysis of IPV and ozone and CO concentrations over the affected region. Stratospheric air is characterized by high IPV, low moisture, high concentrations of ozone, and low concentrations of CO compared to tropospheric air. Therefore, these measurements can act as tracers for the penetration of stratospheric air into the troposphere. The Real-time Air Quality Modeling System

(RAQMS), Global Forecast System (GFS), Whole Atmosphere Community Climate Model (WACCM), and Modern-Era Retrospective analysis for Research and Applications, Version 2 (MERRA-2) models are utilized in this section to provide evidence of stratosphere-to-troposphere mixing through the examination of IPV, ozone, and CO levels. Animations and stratospheric ozone tracer figures to accompany the images in this section are provided in **Appendix A**.

Based on the HYSPLIT trajectories shown in Section 3.3.1, the air mass over Clark County on May 9 originated from a source region off the coast of Mexico on May 7. **Figure 3-11** shows the GFS model analysis of IPV at the 300 mb level at 00:00 UTC on May 7. Stratospheric IPV values are typically much higher than those observed in the troposphere, so a region where a stratospheric-tropospheric mixing occurs is marked by high levels of IPV. A region of high IPV off the Baja California peninsula, circled in red in Figure 3-11, provides supporting evidence of stratospheric-tropospheric mixing in this area.

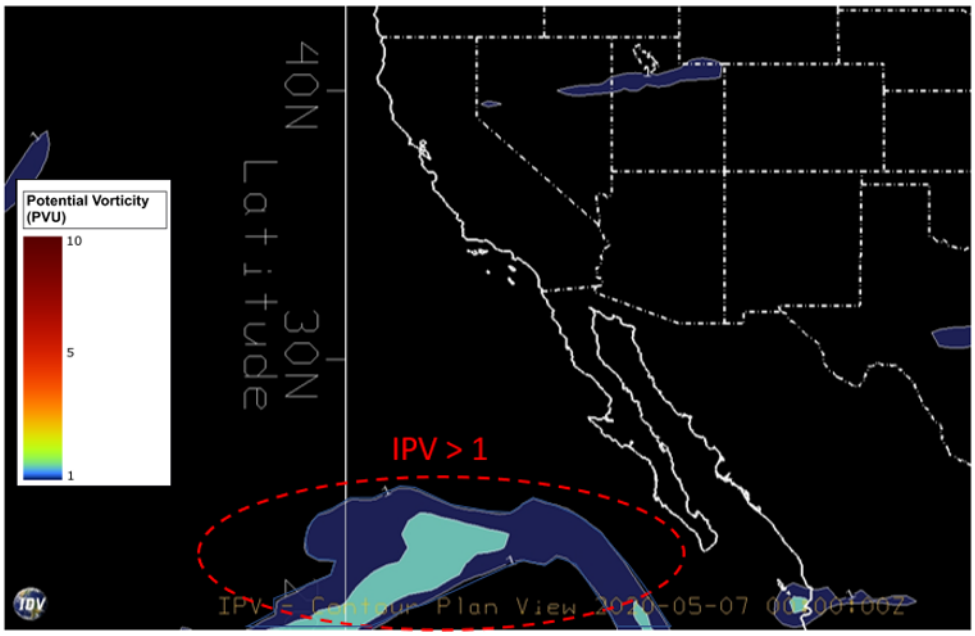


**Figure 3-11.** GFS-modeled isentropic potential vorticity (IPV) at 0:00 UTC on May 7, 2020, at 300 hPa geopotential height. Figure plotted using Unidata's Integrated Data Viewer (IDV). The region of elevated IPV, where a tropopause fold is suspected, is circled in red.

Figure 3-12 shows the GFS model analysis of water vapor mixing ratio at 300 mb at 00:00 UTC on May 7. Stratospheric air is typically quite dry, so regions near a tropospheric fold are often marked by low measurements of water vapor in the troposphere. The modeled water vapor mixing ratios off the coast of Baja California are relatively low (<0.1 g $kg^{-1}$) compared with surrounding regions, and are collocated with the region of elevated IPV (circled in red), indicating the presence of stratospheric air.

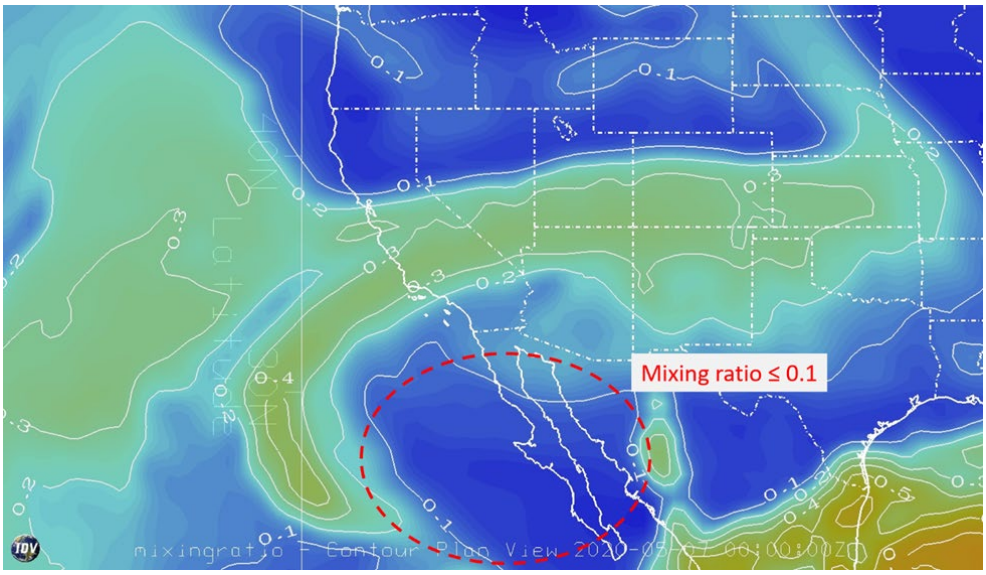


**Figure 3-12.** Mixing ratio contour map at 300 hPa geopotential height, based on GFS model simulations for 0:00 UTC on May 7 (May 6 at 16:00 PST). Each contour above 0.1 g/kg represents 0.1 g/kg increments. An area of reduced water vapor (below 0.1 g/kg) is circled in red. This region aligns with the region of elevated IPV shown in Figure 3-11.

Stratospheric air is characterized by high ozone concentrations, as ozone is produced naturally and efficiently in the stratosphere. The mid-troposphere, on the other hand, typically has much lower ozone concentrations. Figure 3-13 shows the modeled ozone concentration from RAQMS on the source region date (May 7 00:00 UTC). A region of elevated ozone can be seen off the western coast of Mexico, near the suspected stratosphere-to-troposphere exchange (circled in gray).

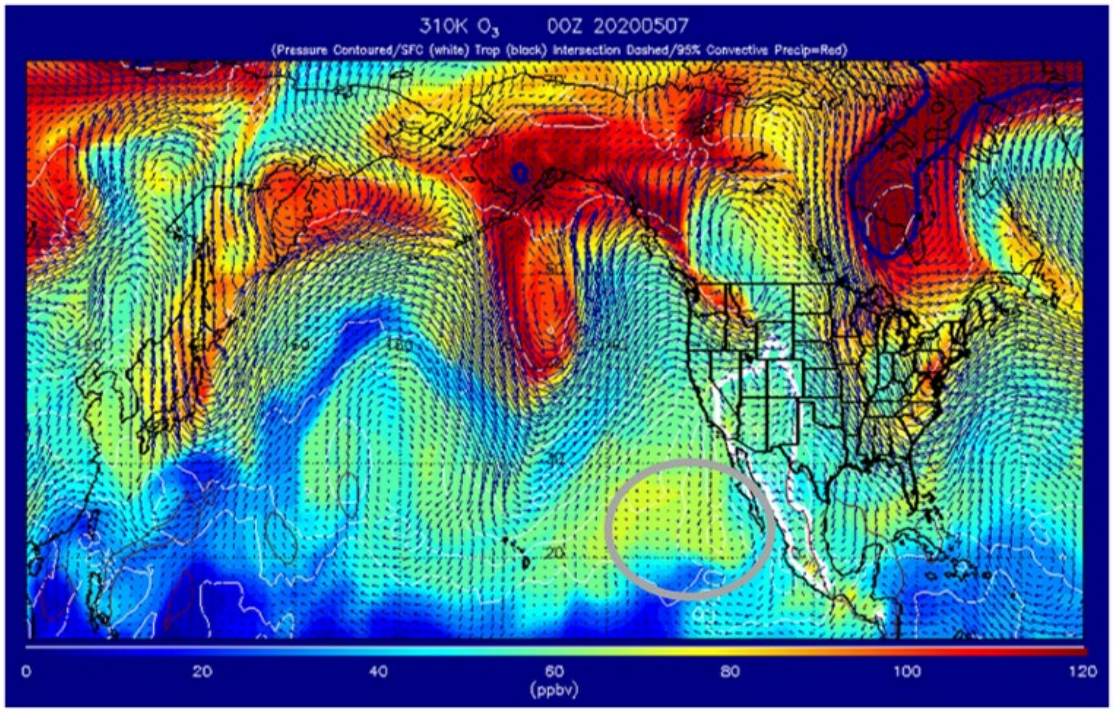


**Figure 3-13.** RAQMS-modeled ozone at the 310 K isentrope level at 00:00 UTC on May 7. The model was initialized at 12:00 UTC on May 6. The region with suspected stratosphere-to-troposphere mixing, and corresponding elevated ozone levels, is circled in gray.

Figure 3-14 shows a vertical cross section from RAQMS for 00:00 UTC on May 7 along the 120 degrees west longitude line, which passes just west of the suspected stratospheric intrusion near the Baja California Peninsula. The penetration of high ozone concentrations from the stratosphere into the troposphere (circled in gray) between 20- and 30-degrees north provides evidence that ozone-rich stratospheric air was injected into the troposphere, where high concentrations of ozone extended down to around 800 mb.

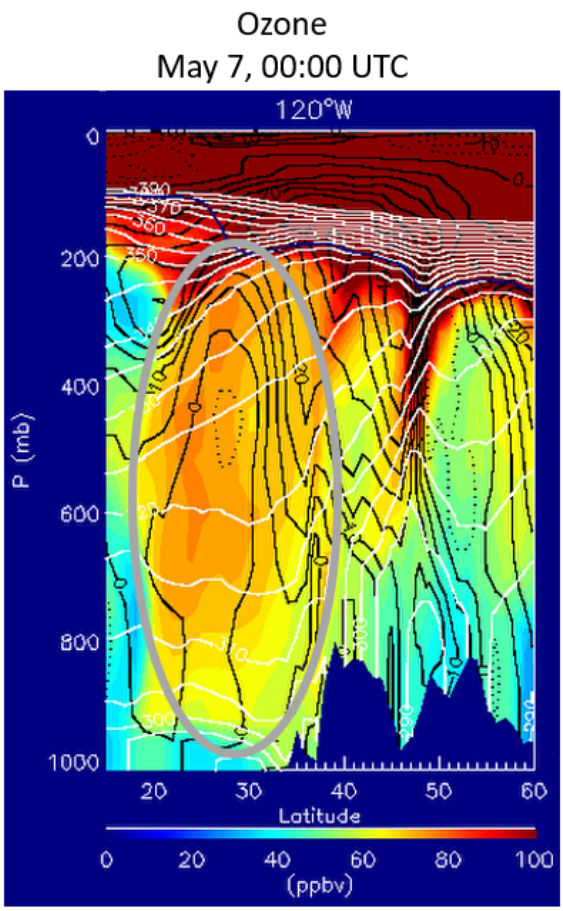


**Figure 3-14.** RAQMS-modeled cross-section of ozone along the 120 degrees west longitude line on May 7 at 0:00 UTC. The model was initialized at 12:00 UTC on May 6. The "tongue" of elevated ozone extending from the stratosphere into the mid-to-lower troposphere is circled in gray.

The WACCM model analysis of ozone on May 7 at 00:00 UTC also provides supporting evidence for stratosphere-to-troposphere mixing near the Baja California peninsula. Figure 3-15 shows modeled ozone in the mid-troposphere at the 500 mb level on the source region date. At this height, a similar area of elevated ozone, circled in red, is visible near 120 degrees west longitude. Figure 3-16 shows a vertical cross section of WACCM-modeled ozone concentrations in this region and confirms that an ozone "tongue" extending from the stratosphere (boxed in gray) exists in the suspected source region between 20- and 25-degrees north latitude. This injection of ozone-rich air extends from the stratosphere down to 800 mb. These results from WACCM agree with the RAQMS vertical cross section of ozone at 120 degrees west longitude. The modeled ozone concentrations between 80 and 120 ppb are high in magnitude for the mid-troposphere.

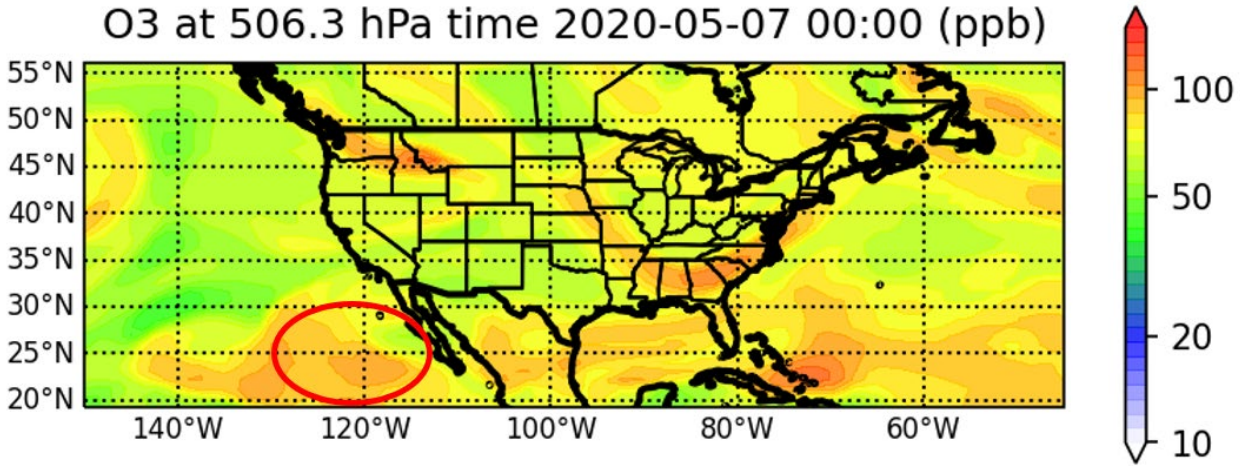


**Figure 3-15.** WACCM-modeled ozone at the 500 mb level on May 7 at 0:00 UTC. The region of elevated ozone off the coast of the Baja California peninsula is circled in red.

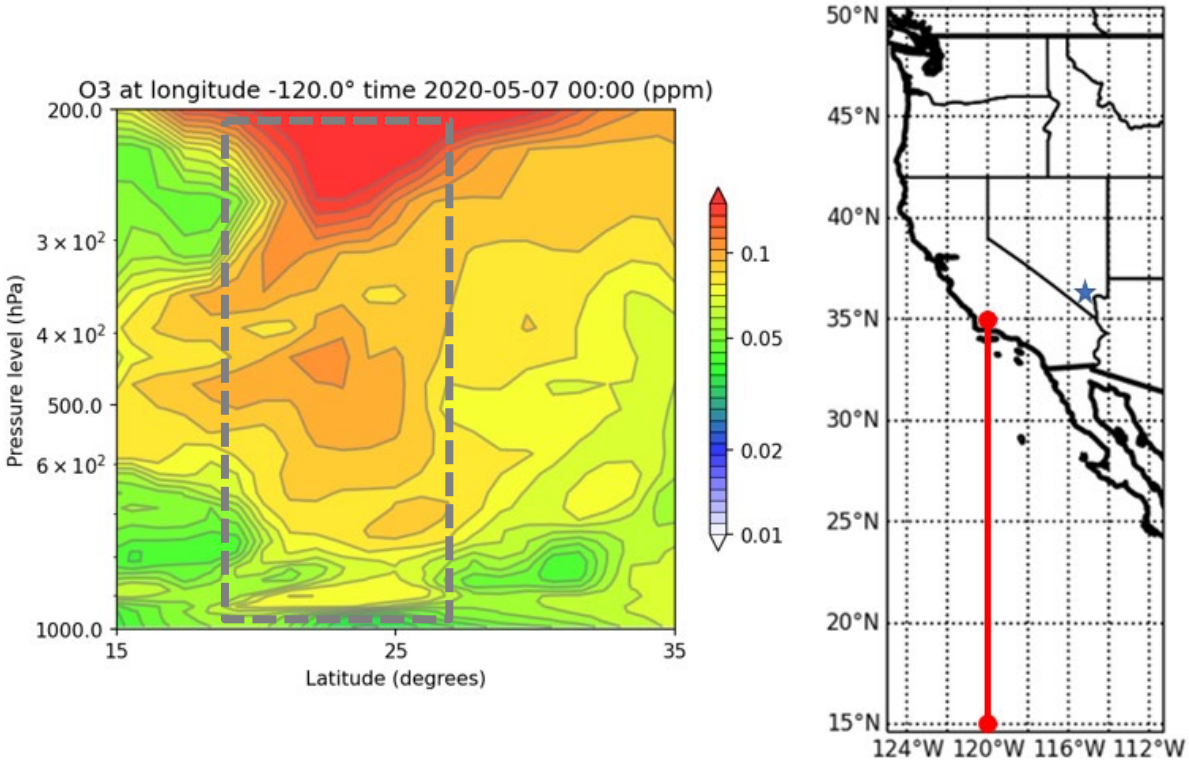


**Figure 3-16.** WACCM-modeled cross-section of ozone along the 120 degrees west longitude line on May 7 at 0:00 UTC. The "tongue" of elevated ozone extending from the stratosphere into the mid-to-lower troposphere is boxed in gray. The map to the right shows the extent of the cross section. Las Vegas is marked with a blue star.

Figure 3-17 shows the modeled ozone concentration from RAQMS on the date of the ozone exceedance in Clark County (0:00 UTC on May 10/16:00 PST on May 9). By this time, the region of elevated ozone originating off the Baja California peninsula had expanded northward across southern California and into Nevada (circled in red). This path of transport from the source region towards Clark County is supported by the HYSPLIT trajectories discussed in Section 3.3.1. This modeled analysis supports the theory that ozone-rich stratospheric air transported from off the coast of Mexico may have contributed to high surface-level ozone concentrations in Clark County on May 9.

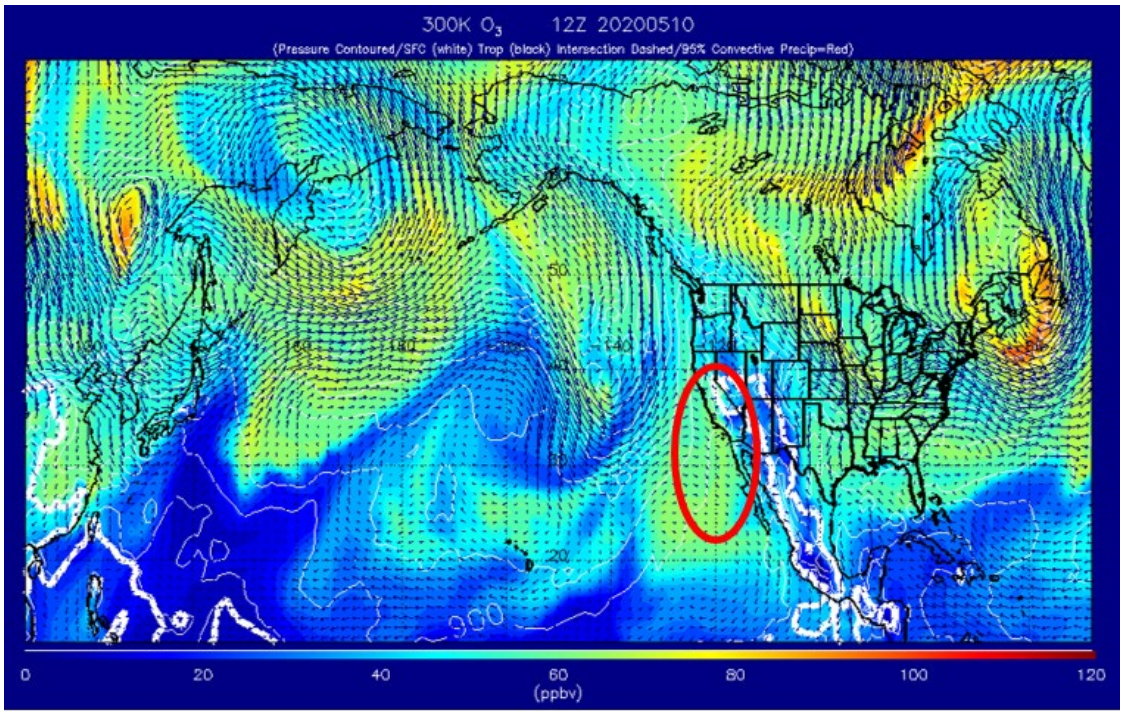


**Figure 3-17.** RAQMS-modeled ozone at the 300 K isentrope-level on the event date of May 10 at 00:00 UTC. The model was initialized at 12:00 UTC on May 9. The suspected path northward of ozone-rich air to southern Nevada from the Baja California peninsula is circled in red.

Figure 3-18 shows the modeled ozone cross-section concentration from RAQMS at 00:00 UTC on May 10 (16:00 PST on May 9), the date of the ozone exceedance. This modeled analysis shows that elevated ozone concentrations throughout the mid-troposphere, presumably originating from the stratospheric injection, have extended to at least 37 degrees north. In this modeled cross section, a secondary region of stratospheric injection is shown further north near 58-degrees N latitude, although HYSPLIT trajectories do not suggest that ozone from this secondary source contributed to surface-level concentrations in Clark County. Although this cross-section is only provided for 120-degrees W longitude, it shows that ozone-rich air moved northward, and Figure 3-17 establishes the east-west extent of ozone-rich air parcels.

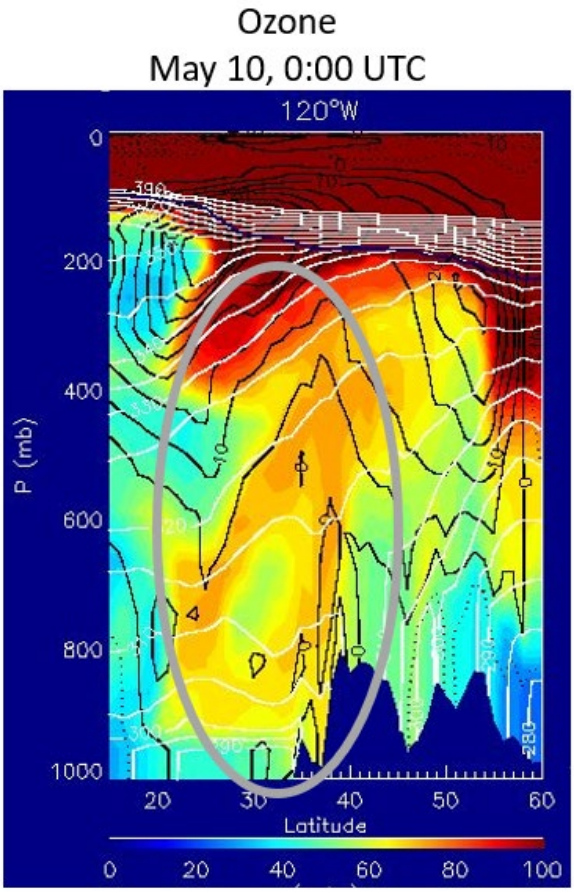


**Figure 3-18.** RAQMS-modeled cross-section of ozone along the 120 degrees west longitude line on the event date, 0:00 UTC on May 10 (16:00 PST on May 9). The model was initialized at 12:00 UTC on May 6. The "tongue" of elevated ozone extending from the stratosphere into the mid-to-lower troposphere is circled in gray.

A more detailed view of northward transport of ozone rich air is shown in Figure 3-19, which includes a cross section of WACCM-modelled ozone along the 117.5-degree W longitude line on May 7 at 12:00 UTC, May 8 at 00:00 UTC and 12:00 UTC, and May 9 at 00:00 UTC. The 117.5-degree W

longitude line approximates HYSPLIT trajectories of air transport from the source region towards Clark County during this time period (see Section 3.3.1). The large stratospheric ozone source highlighted in Figure 3-16 appears to split at its origin near 25-degrees north latitude into two distinct ozone-rich "tongues" extending from the stratosphere. One of these ozone "tongues" moves northward towards Las Vegas over the course of these two days and reaches to about 35-degrees N latitude by May 9 at 00:00 UTC. The progression of the northward-moving ozone "tongue" is highlighted in Figure 3-19 by black circles. Local ozone production from Los Angeles is visible at the surface on both May 8 and 9 at 34-degrees N latitude. **Figure 3-20** shows WACCM-modeled ozone following the northeastward transport path on the event date shown in HYSPLIT trajectories. Cross sections are shown at the 117.5-, 116.2-, and 115-degrees west longitude lines between May 9 at 12:00 UTC (May 9 at 4:00 PST) and May 10 at 0:00 UTC (May 9 at 16:00 PST). The 115-degrees W longitude line passes through Las Vegas. Each of these cross sections show enhanced ozone concentrations in the mid-troposphere extending from the ozone tongue highlighted in Figure 3-19. In the final cross section (5), which show model results on the afternoon of the exceedance event, a deep layer of elevated ozone (~70 ppb) is shown from the surface to 500 mb. The black arrows in this plot highlight the extent of the mixed layer that existed over Las Vegas, up to 550 mb, at this time (see Section 3.3.2). This indicates that vertical mixing of air likely occurred within a large boundary layer, and that ozone-rich air extending from the stratosphere into the mid-troposphere could have been transported to the surface. The WACCM-modeled progression of ozone transport between May 7-9 indicates that there was a pathway for stratospheric ozone to impact surface observations in Clark County on the event date.

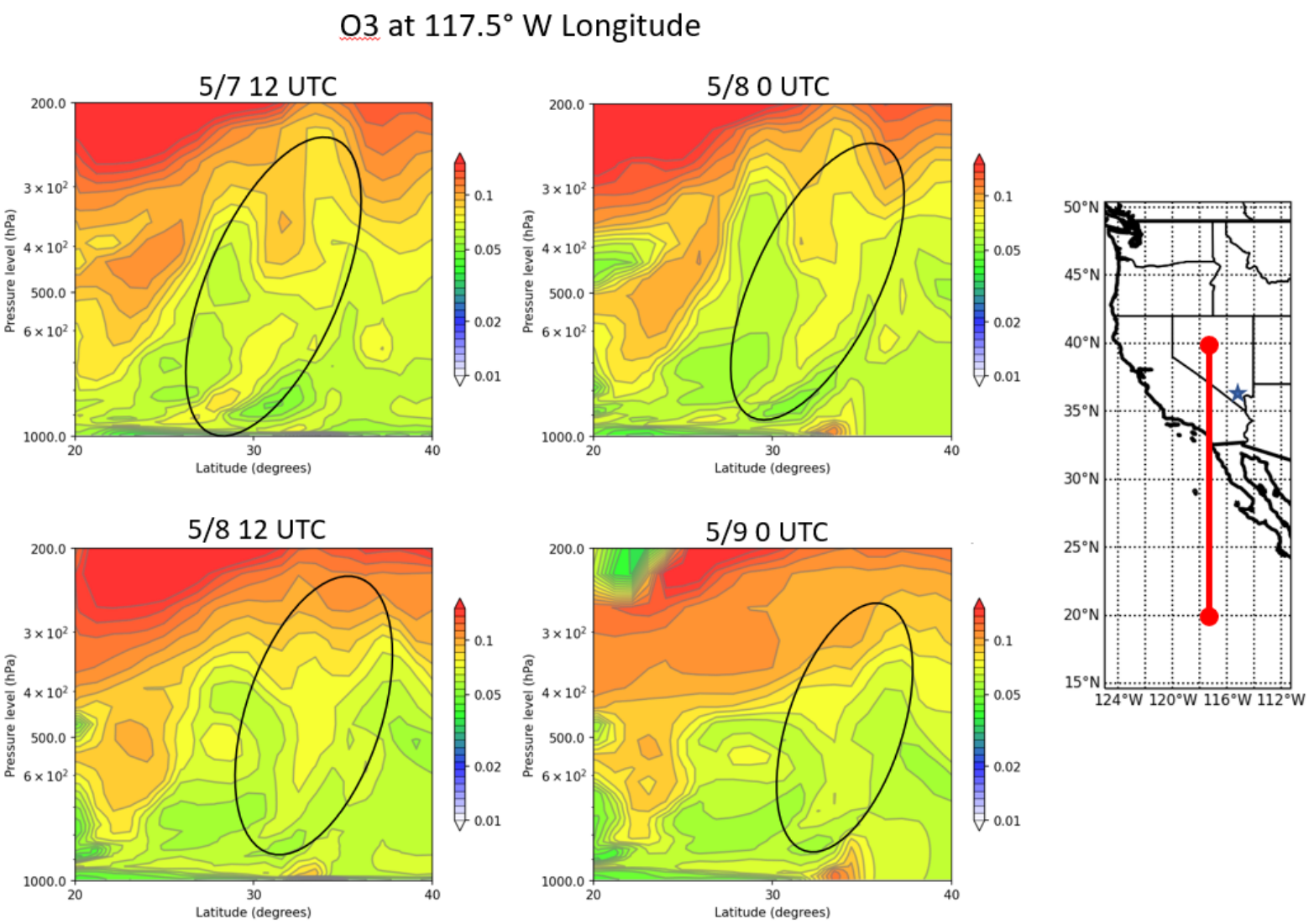


**Figure 3-19.** Progression of WACCM-modeled cross-sections of ozone along the 117.5-degrees west longitude line between May 7 at 12:00 UTC and May 9 at 0:00 UTC. The map to the right shows the extent of the cross section. Las Vegas is marked with a blue star.

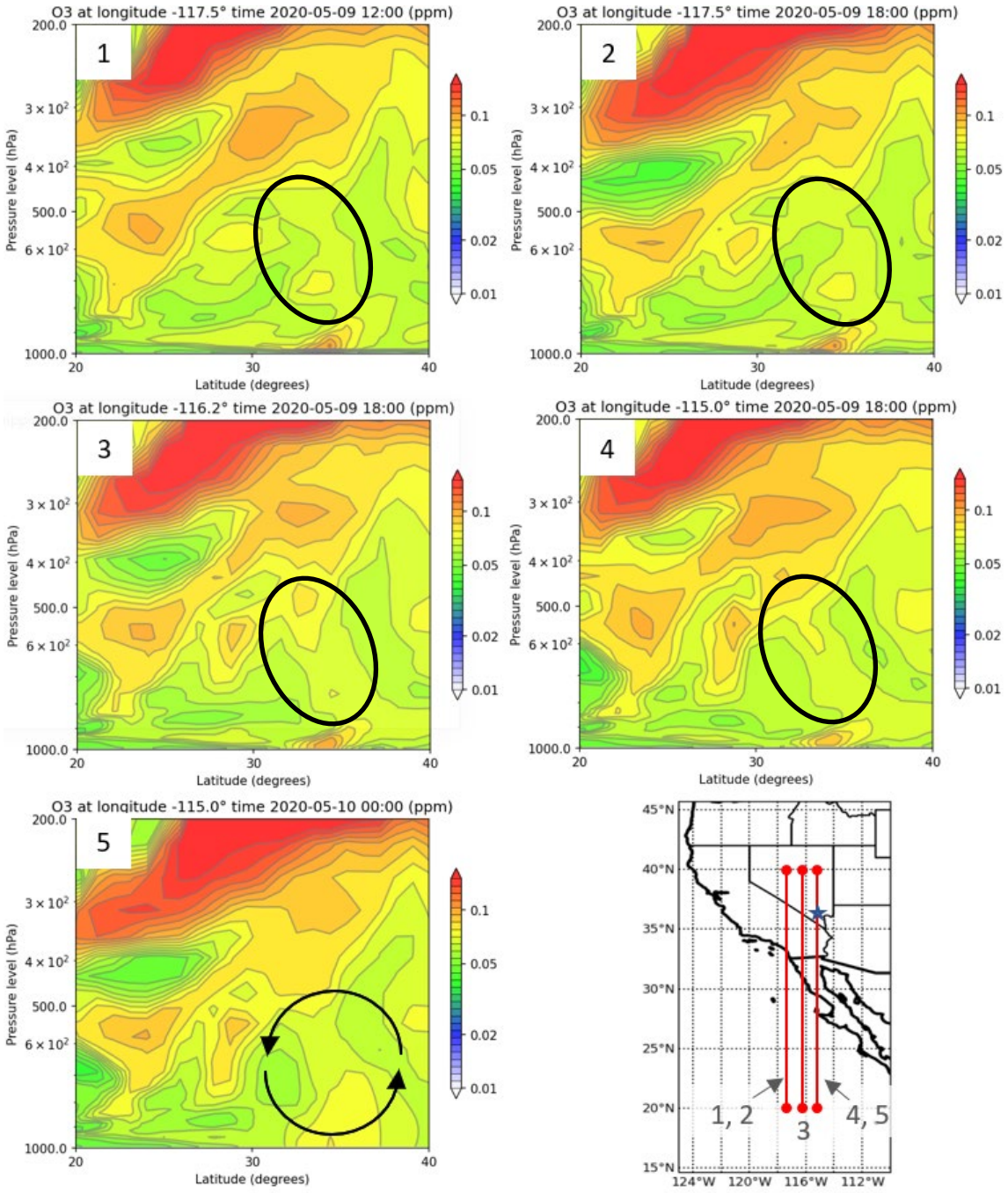


**Figure 3-20.** WACCM-modeled cross-sections of ozone on the event date, between 12:00 UTC (04:00 PST) on May 9 and 0:00 UTC on May 10 (16:00 PST on May 10). Cross sections along the 117.5-, 116.2- and 115.0-degrees west longitude lines are shown, and the number at the top left of each plot aligns with the labeled cross-section extents shown on the map. Vertical mixing in the mid-to-lower troposphere is indicated by the black arrows. Las Vegas is marked with a blue star on the map.

Figure 3-21 shows the MERRA-2 modeled mean ozone concentration west of Baja California at 488 hPa for the month of May across 2014 through 2020, compared to the modeled ozone concentration at 00:00 UTC on May 7 at the same location. Figure 3-22 shows modeled mean ozone concentration for the same parameters, but at 288 hPa. During the hours of the stratospheric intrusion that led to the May 9 ozone exceedance in Las Vegas, ozone concentrations over the Pacific Ocean west of Baja California in the upper troposphere were above the May average. On May 7 at 00:00 UTC at 488 and 288 hPa, ozone concentrations were higher than the mean May ozone concentrations over the same area. Figures 3-21 and 3-22 are consistent with Figures 3-13 and 3-15, which also show elevated ozone in the upper troposphere over the area of stratospheric intrusion.

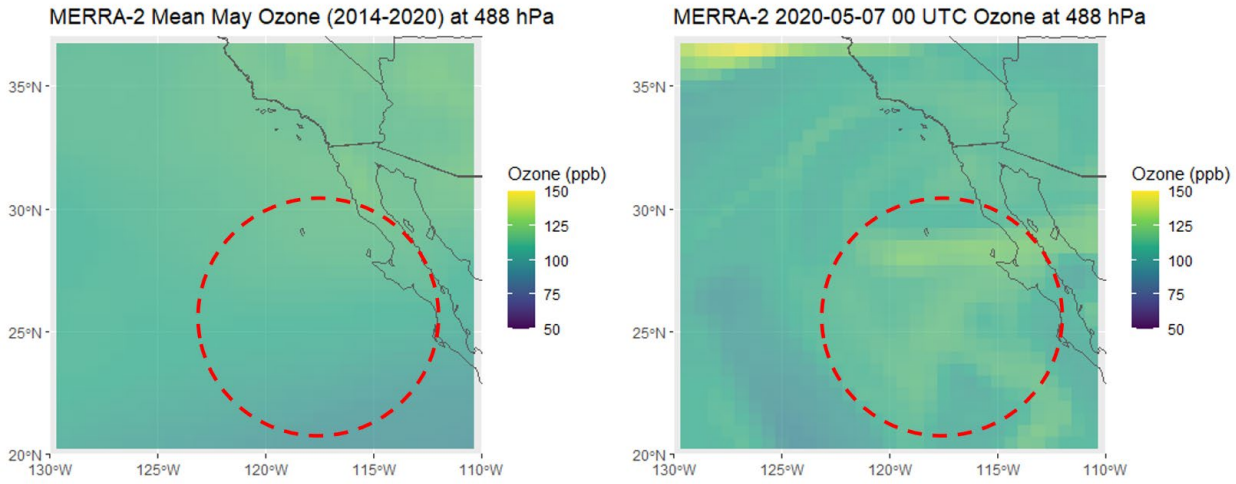


**Figure 3-21.** MERRA-2 mean ozone concentrations at the 488 hPa level for the month of May from 2014 – 2020 (left), compared to MERRA-2 ozone concentrations at the 488 hPa level on May 7, 2020, at 00:00 UTC (right). The red oval represents the approximate area of stratospheric intrusion.

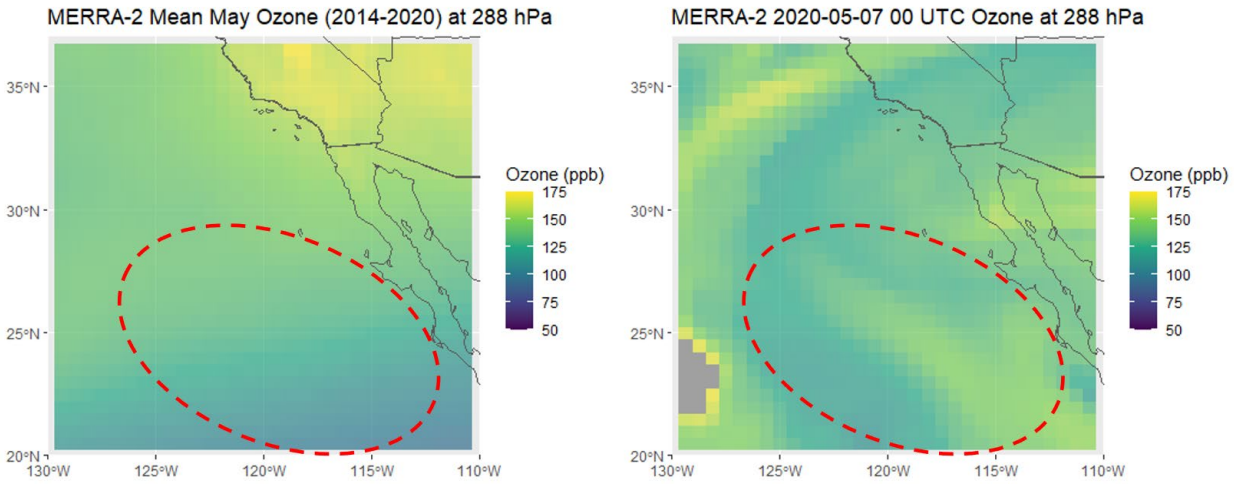


**Figure 3-22.** MERRA-2 mean ozone concentrations at the 288 hPa level for the month of May from 2014 – 2020 (left), compared to MERRA-2 ozone concentrations at the 288 hPa level on May 7, 2020, at 00:00 UTC (right). The red oval represents the approximate area of stratospheric intrusion.

Stratospheric air is characterized by low CO concentrations. Therefore, an instance of stratosphere-to-troposphere mixing may be indicated by the presence of low concentrations of CO in the troposphere. Figure 3-23 shows the modeled CO concentration from RAQMS on May 7 at 00:00 UTC. A region of low CO concentrations can be seen near the Baja California peninsula, near the suspected stratosphere-to-troposphere mixing (circled in red), aligning with the region of elevated ozone at the same time shown in Figure 3-13.

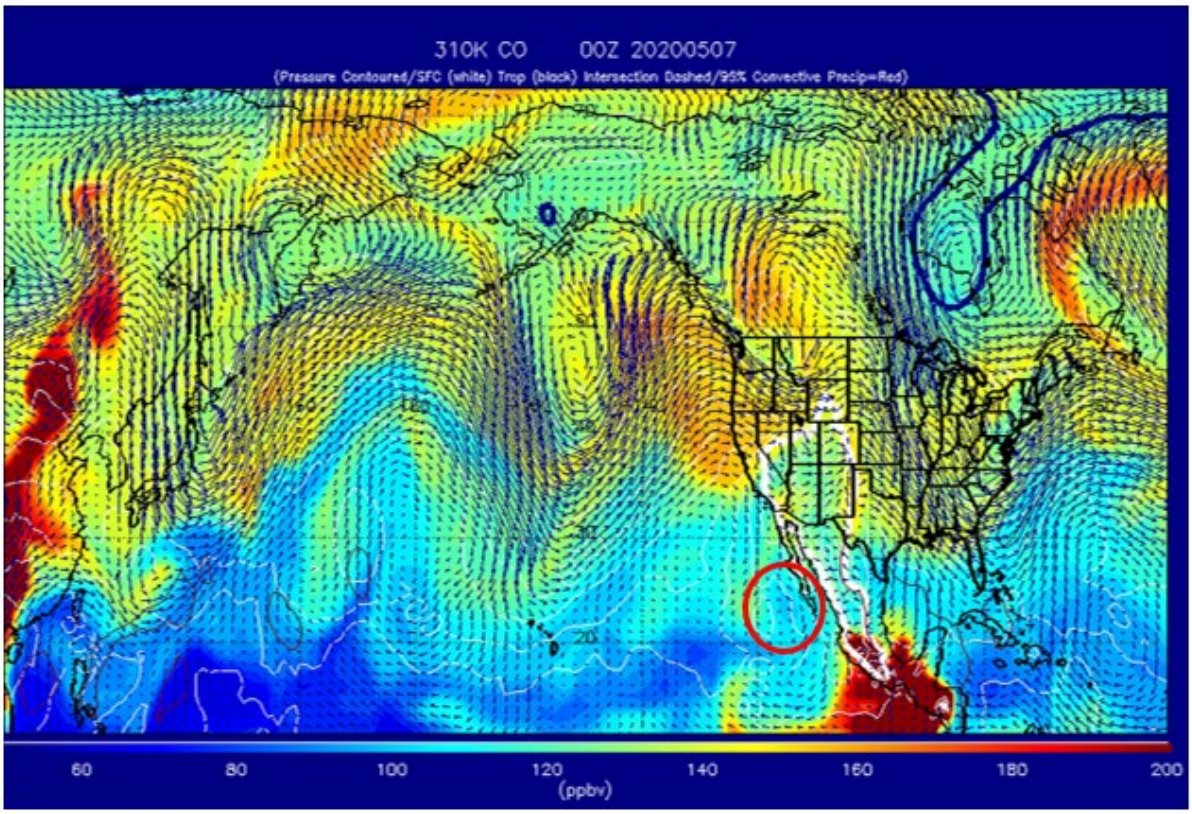


**Figure 3-23.** RAQMS-modeled CO concentrations at the 310 K isentrope-level on May 7 at 00:00 UTC. The model was initialized at 12:00 UTC on May 6. Circled in red is a depression in CO concentrations off the Baja California peninsula which aligns with elevated ozone levels at the same time.

Figure 3-24 shows a vertical cross section from RAQMS along the 120 degrees west longitude line on May 7 at 00:00 UTC. The penetration of low CO concentrations from the stratosphere into the troposphere (circled in gray) from 20 to 30 degrees latitude provides evidence that CO-poor stratospheric air mixed into the troposphere due to an SOI event.

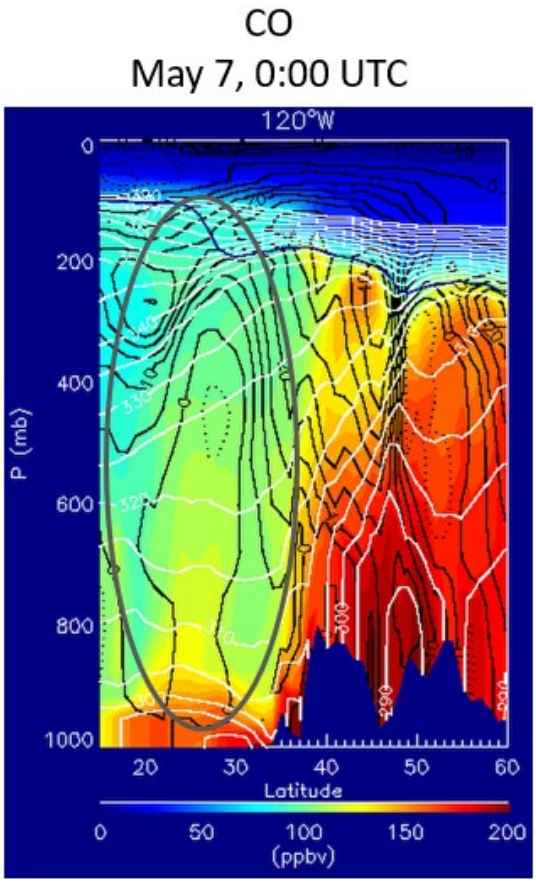


**Figure 3-24.** RAQMS-modeled cross-section of CO along the 120 degrees west longitude line at 00:00 UTC on May 7. The model was initialized at 12:00 UTC on May 6. The "tongue" of reduced CO extending from the stratosphere into the mid-to-lower troposphere is circled in gray.

Figures 3-25 through 3-27 show the RAQMS modeled CO at 00:00 UTC/16:00 PST on May 8, May 9, and May 10 (the event date), respectively. During this period leading up to the exceedance event in Clark County, the region of low CO concentrations originating near Mexico was transported northward across southern California, and eventually, into southern Nevada. The regions of relatively depleted CO that were transported to the Clark County area are circled in red on each plot.

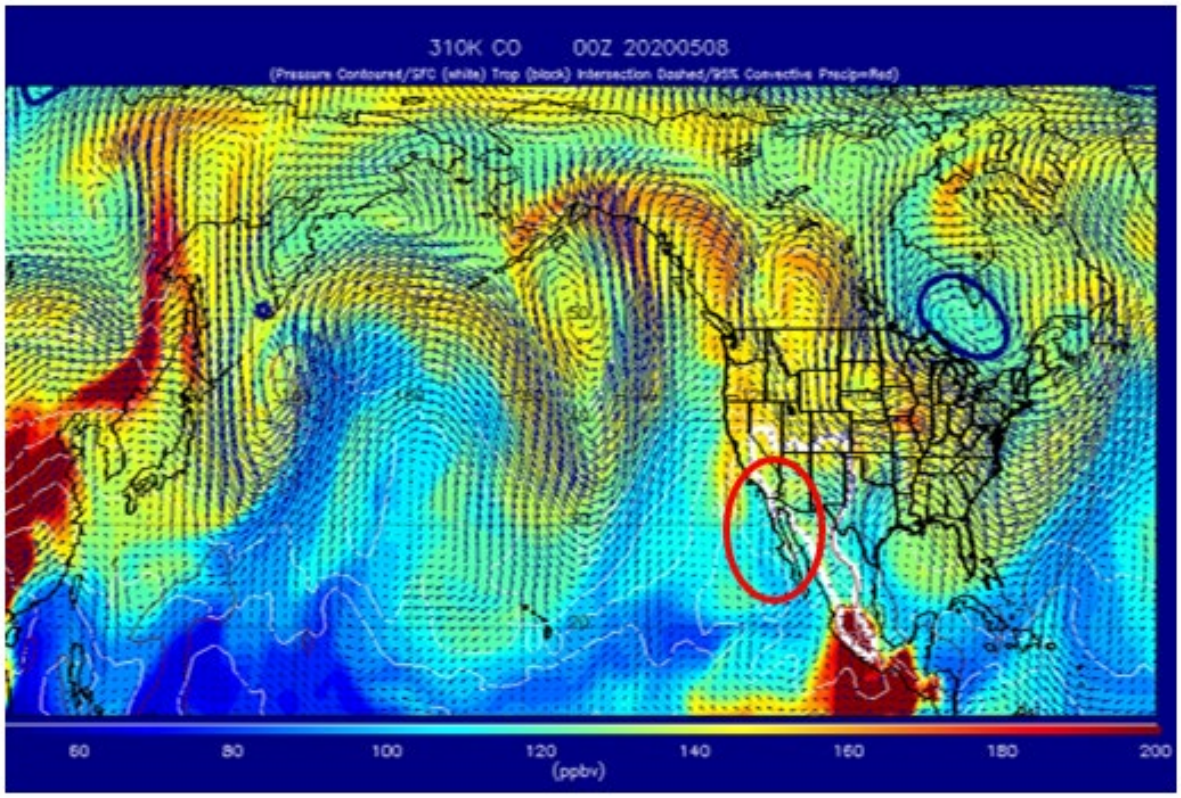


**Figure 3-25.** RAQMS-modeled CO concentrations at the 310 K isentrope-level on May 8 at 00:00 UTC. The model was initialized at 12:00 UTC on May 6. Circled in red is the extent of the reduced CO-region originating off the Baja California peninsula on May 7 (see Figure 3-18).

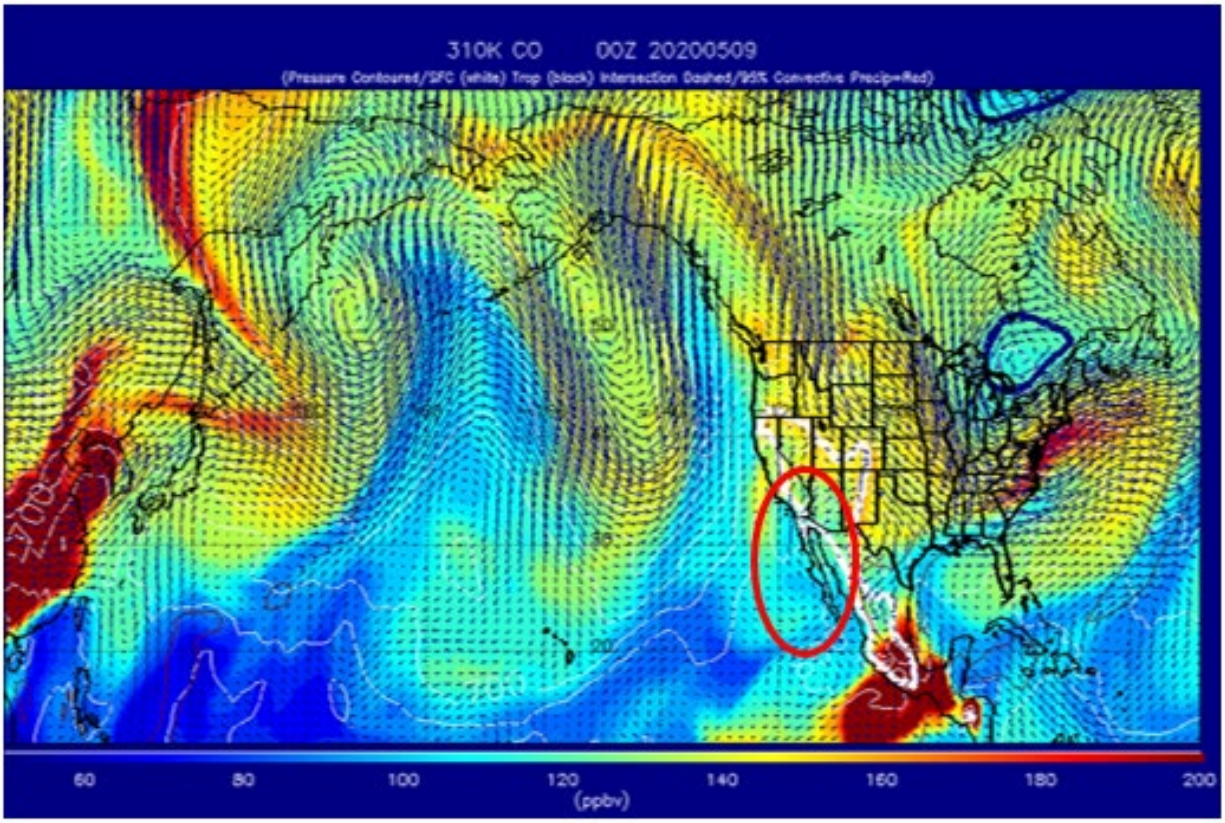


**Figure 3-26.** RAQMS-modeled CO concentrations at the 310 K isentrope-level on May 9 at 00:00 UTC. The model was initialized at 12:00 UTC on May 6. Circled in red is the extent of the reduced CO-region originating off the Baja California peninsula on May 7 (see Figure 3-18).

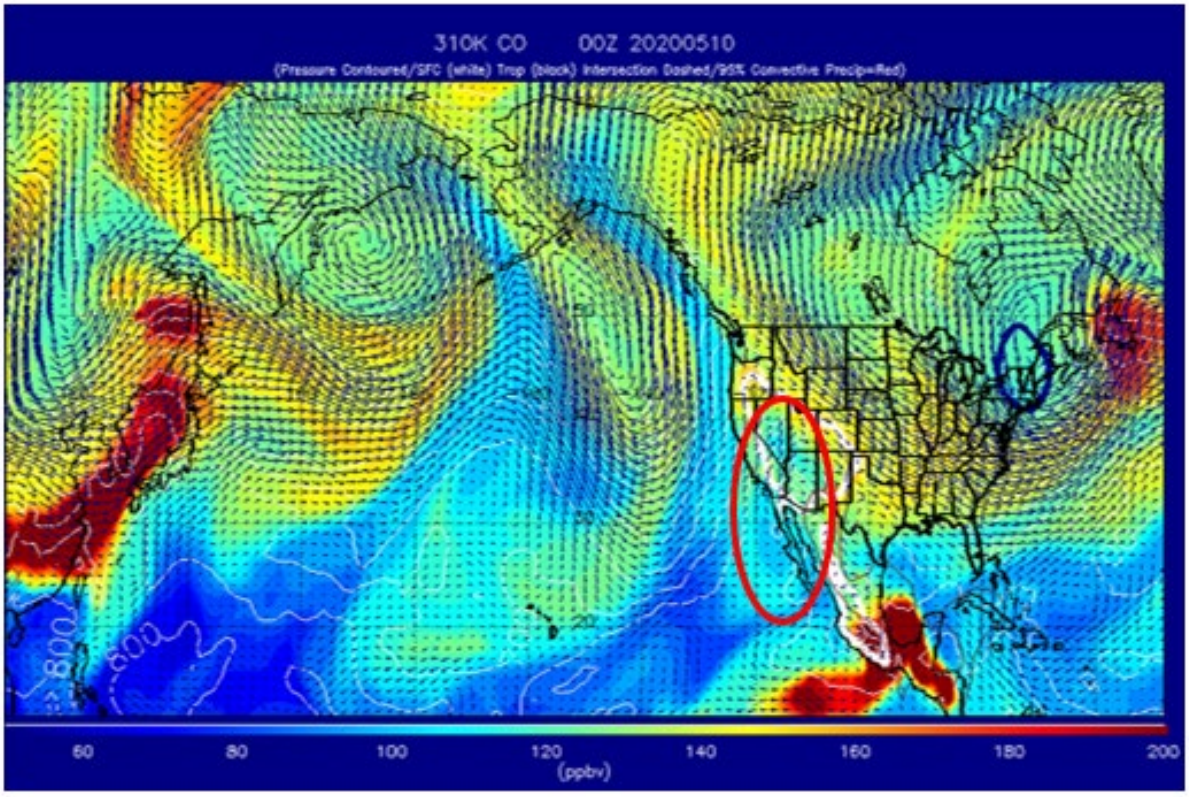


**Figure 3-27.** RAQMS-modeled CO concentrations at the 310 K isentrope-level on the event date (May 10 at 0:00 UTC/May 9 at 16:00 PST). The model was initialized at 12:00 UTC on May 6. Circled in red is the extent of the reduced CO-region originating off the Baja California peninsula on May 7 (see Figure 3-18).

Figure 3-28 shows the modeled CO cross-section concentration from RAQMS at 00:00 UTC on May 10 (May 9 at 16:00 PST), the date of the ozone exceedance. This modeled analysis shows that reduced CO concentrations in the mid-troposphere had extended to higher latitudes by the EE date, aligning with the transport of air northward from the Baja California peninsula shown in Figures 3-25 through 3-27.

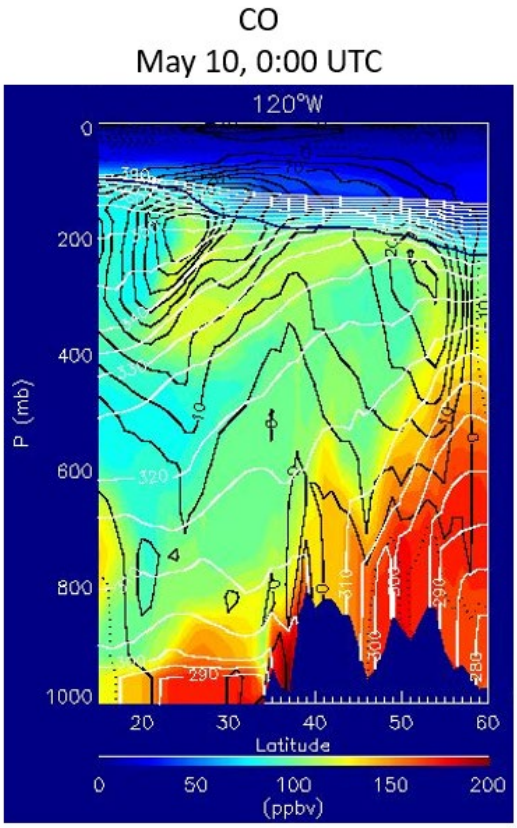


**Figure 3-28.** RAQMS-modeled cross-section of CO along the 120 degrees west longitude line on the event date (May 10 at 0:00 UTC/May 9 at 16:00 PST). The model was initialized at 12:00 UTC on May 9. The "tongue" of reduced CO concentrations extending from the stratosphere into the troposphere has expanded northward compared to on May 7 (see Figure 3-24).

Figure 3-29 also provides the WACCM model analysis of CO at 500 mb on May 7 at 00:00 UTC. Off the coast of Baja California, we see an area of low CO concentrations, which is indicative of stratospheric air and is consistent with the RAQMS data presented previously.

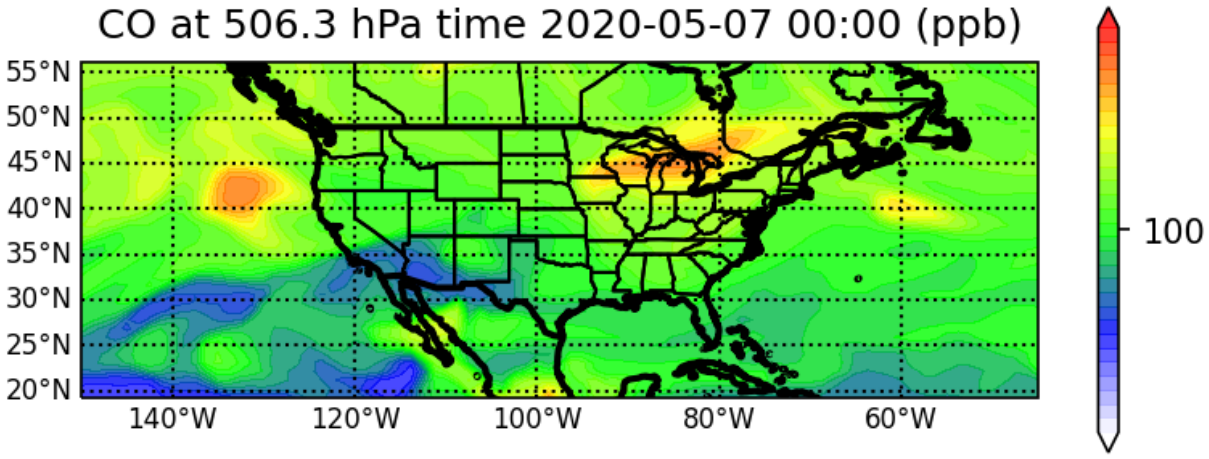


**Figure 3-29.** WACCM-modeled CO concentrations at the 500 mb level on May 7 at 0:00 UTC. The color range extends from 50 to 200 ppb of CO.

Vertical cross sections of ozone can help to identify areas where stratospheric air extended into the troposphere. Figure 3-30 shows a latitude cross section of ozone mixing ratio from MERRA-2 above the SOI source region off the coast of Baja California (-121 to -118 W and 15 to 35 N), averaged over 00:00 and 23:00 UTC on May 7. In this area, we can see a protrusion of high ozone mixing ratio (indicative of stratospheric air) extending into the free troposphere, with enhancements of ozone down to around 300 hPa. Visible satellite images, water vapor retrievals, total column ozone, and ozone cross section data all provide evidence pointing to an SOI event off the coast of Baja California on May 7.

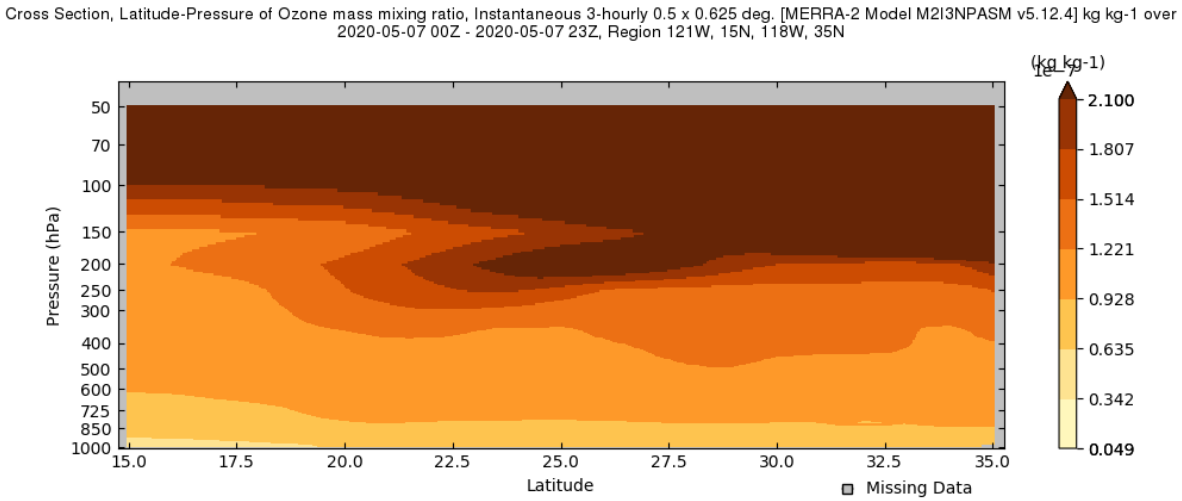


**Figure 3-30.** MERRA-2 ozone mixing ratio cross section over the SOI source region on May 7 from 00:00 through 23:00 UTC. This image provides a latitude-pressure cross section of ozone mixing ratio between -121 to -118 W and 15 to 35 N.

Areas of stratospheric intrusion into the troposphere are often associated with relatively low CO concentrations. Figure 3-31 shows the MERRA-2 modeled mean CO concentration west of Baja California at 488 hPa for the month of May across 2014 through 2020, compared to the modeled CO concentration at 00:00 UTC on May 7 at the same location. Figure 3-32 shows modeled mean CO concentration for the same parameters, but at 288 hPa. During the stratospheric intrusion that led to the May 9 ozone exceedance in Las Vegas, CO concentrations over the SOI area at the 488 hPa and 288 hPa level were below average compared with the May mean. The analysis using MERRA-2 modeled CO is consistent with the analysis presented in Figures 3-25 to 3-27, which also show an area of low CO concentrations over the Pacific Ocean west of Baja California. Near the surface at the 985 hPa level on the event date (May 10 at 00:00 UTC/May 9 at 16:00 PST), CO concentrations over the Las Vegas area were average to slightly below average (Figure 3-33, as indicated by darker shades of blue and purple), but higher than normal CO concentrations extend towards the northwest.

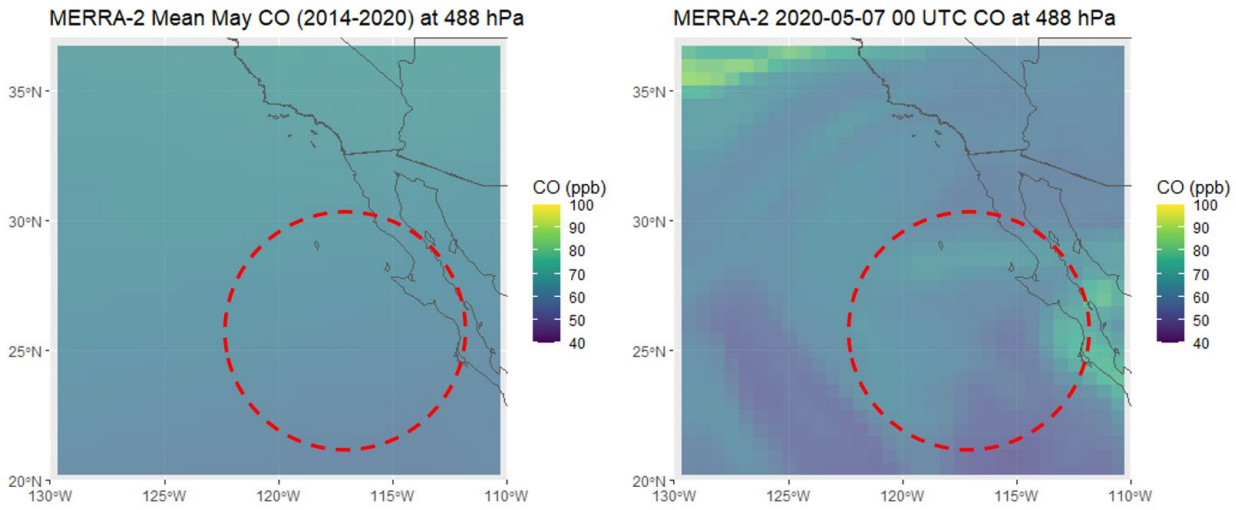


**Figure 3-31.** MERRA-2 mean CO concentrations at the 488 hPa level for the month of May from 2014 – 2020 (left), compared to MERRA-2 CO concentrations at the 488 hPa level on May 7, 2020, at 00:00 UTC (right). The red oval represents the approximate area of stratospheric intrusion.

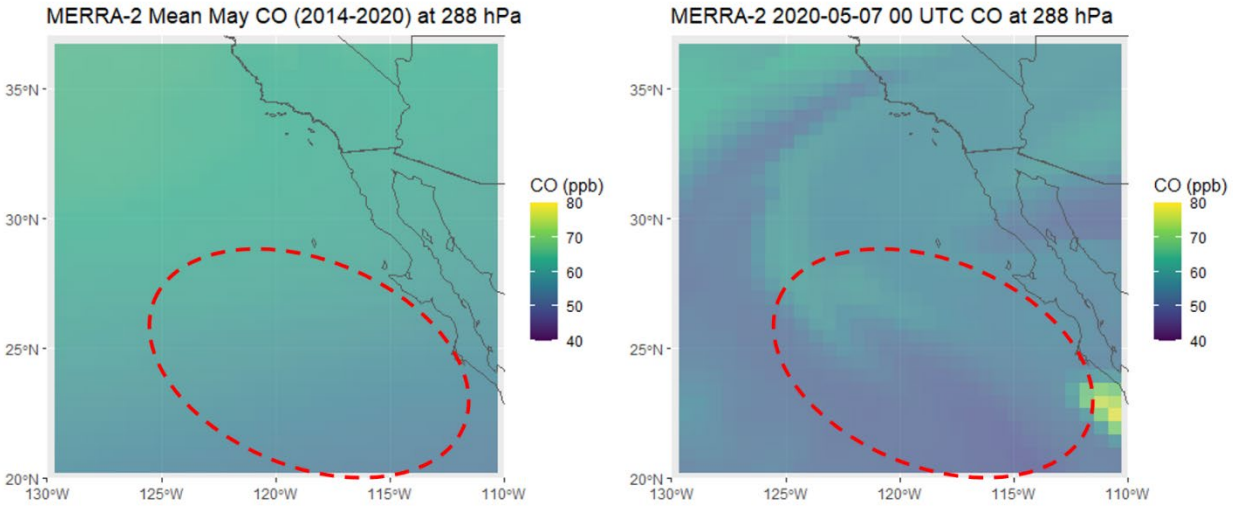


**Figure 3-32.** MERRA-2 mean CO concentrations at the 288 hPa level for the month of May from 2014 – 2020 (left), compared to MERRA-2 CO concentrations at the 288 hPa level on May 7, 2020, at 00:00 UTC (right). The red oval represents the approximate area of stratospheric intrusion.

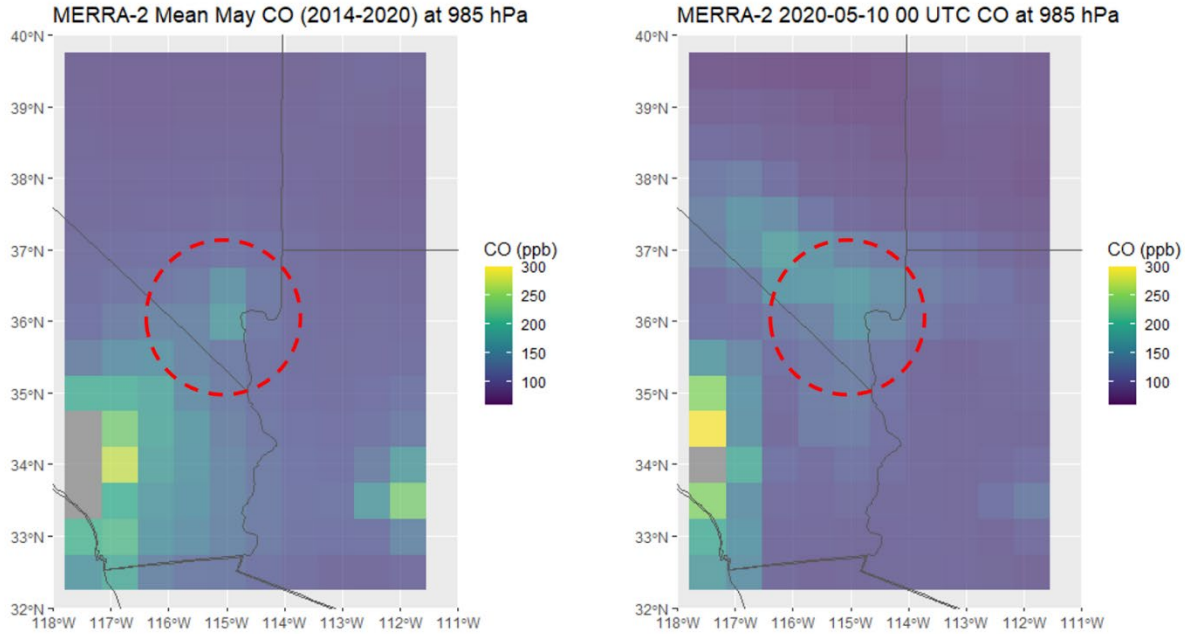


**Figure 3-33.** MERRA-2 mean CO concentrations at the 985 hPa level based on data for the month of May from 2014 – 2020 (left), compared to MERRA-2 CO concentrations at the 985 hPa level on May 10, 2020, at 00:00 UTC (May 9 at 16:00 PST) (right). The red oval represents the approximate area of Clark County.

Modeled values of IPV and ozone and CO concentrations support the hypothesis that stratosphere-to-troposphere mixing occurred off the coast of the Baja California peninsula. This region saw relatively high IPV, enhanced ozone concentrations throughout the upper- and mid-troposphere, and reduced CO levels in the upper- and mid-troposphere, which are all markers of stratospheric air. Further, a series of modeled ozone and CO in the mid-troposphere indicate transport of air from the Baja California peninsula region northward towards Clark County between 0:00 UTC on May 7 and 0:00 UTC on May 10, which aligns well with the modeled HYSPLIT trajectories presented in Section 3.3.1.

## 3.3 Evidence of Stratospheric Air Reaching the Surface

### 3.3.1 HYSPLIT Trajectory Analysis

HYSPLIT trajectories were run to demonstrate the transport of air from a stratospheric intrusion to Clark County. These trajectories show that air was transported from the stratospheric intrusion, generally located to the west of Baja California, Mexico, over the eastern Pacific Ocean to the Clark County area in the days prior to and on May 9, 2020. Combined with satellite observations and modeled analyses described in Sections 3.2.1 and 3.2.2, these trajectories provide evidence that stratospheric ozone was transported to Las Vegas, Nevada.

NOAA's online HYSPLIT model tool[1] was used for the trajectory modeling. HYSPLIT is a commonly used model that calculates the path of a single air parcel from a specific location and height above the ground over a period of time; this path is the modeled trajectory. HYSPLIT trajectories can be used as evidence that high-ozone stratospheric air was transported to an air quality monitor. In addition to horizontal transport, HYSPLIT trajectories can be used to indicate vertical motion and mixing. This type of analysis is important for meeting both Tier 1 and 2 requirements.

The model options used for this study are summarized in **Table 3-7**. The meteorological data from the North American Mesoscale Forecast System (NAM, 12 km resolution) and High-Resolution Rapid Refresh (HRRR, 3 km resolution) model were used.[2] These data are high in spatial resolution, are readily available for HYSPLIT modeling over the desired lengths of time, and are expected to capture fine-scale meteorological variability. The backward trajectory start time was selected to be in the afternoon (i.e., 15:00 PST) when daily ozone concentrations peak. Additionally, the backward trajectory matrix analysis was initiated in the early evening (03:00 UTC or 19:00 PST) to better understand the full event-day transport of ozone and its precursors. As suggested in the EPA's EE guidance (U.S. Environmental Protection Agency, 2016), a backward trajectory length of 72 hours was selected to assess whether stratospheric air from the current day or from the previous two days may have been transported over a long distance to the monitoring sites. Trajectories were initiated at

[1] http://ready.arl.noaa.gov/HYSPLIT.php
[2] ready.noaa.gov/archives.php

50 m, 500 m, and 1,000 m above ground level to capture transport throughout the mixed boundary layer, as stratospheric ozone may be transported aloft and influence concentrations at the surface through vertical mixing. Three backward trajectory approaches available in the HYSPLIT model were used in this analysis, including site-specific trajectories, trajectory matrices, and trajectory frequency. Site-specific back trajectories were run to show direct transport from the SOI to the affected site(s) – this analysis is useful in linking air quality and meteorological impacts at a single location (i.e., an air quality monitor) to a SOI. Matrix back trajectories were run to show the general air parcel transport patterns from the Las Vegas area to the SOI. Similarly, matrix forward trajectories were run to show air parcel transport patterns from the SOI region to the Las Vegas area. Matrix trajectories are useful in analyzing air transport over areas larger than a single air quality site. Trajectory frequency analysis show the frequency with which multiple trajectories initiated over multiple hours pass over a grid cell on a map. Trajectory frequencies are useful in estimating the temporal and spatial patterns of air transport from a source region to a specific air quality monitor. In addition to trajectories from Clark County, we also initiate mid-transport trajectories from JPL to confirm the transport of ozone-rich air to Clark County (see Section 3.3.2 for more details). Together, these trajectory analyses indicate the transport patterns into Clark County on May 9, 2020.

Additionally, a forward trajectory matrix was run for the area to the west of Baja California, over the eastern Pacific Ocean, to examine transport in the direction of Clark County.

**Table 3-7.** HYSPLIT run configurations for each analysis type, including meteorology data set, time period of run, starting location(s), trajectory time length, starting height(s), starting time(s), vertical motion methodology, and top of model height.

| HYSPLIT Parameter | Back Trajectory Analysis – Matrix | Backward Trajectory Analysis – Frequency | Forward Trajectory Analysis – Matrix | Backward Trajectory Analysis – High Resolution |
|---|---|---|---|---|
| Meteorology | 12-km NAM | 12-km NAM | 12-km NAM | 3-km HRRR |
| Time Period | May 7 – May 10, 2020 | May 7 – May 10, 2020 | May 7 – May 10, 2020 | May 6 – May 9, 2020 |
| Starting Location | Evenly spaced grid covering Las Vegas, Nevada. Evenly spaced grid covering area over JPL. | 36.1381 N, 115.2582 W, | Evenly spaced grid covering area west of Baja California in the eastern Pacific Ocean. Evenly spaced grid covering area over JPL. | 36.1381 N, 115.2582 W |
| Trajectory Time Length | 72 hours | 72 hours | 36 hours, 72 hours | 72 hours |
| Starting Heights (AGL) | 500 m, 1,000 m, 2,000 m, 3,700 m | 1,000 m | 500 m, 2,000 m, 3,000 m | 50 m, 500 m, 1,000 m |
| Starting Times | 03:00 UTC, 05:00 UTC | 05:00 UTC | 03:00 UTC, 05:00 UTC | 23:00 UTC |
| Vertical Motion Method | Model Vertical Velocity | Model Vertical Velocity | Model Vertical Velocity | Model Vertical Velocity |
| Top of Model | 10,000 m | 10,000 m | 10,000 m | 10,000 m |

Site-specific backward trajectories were calculated from the Las Vegas Valley (36.1381 N, 115.2582 W) on May 9, 2020. We chose to model all trajectories for sites within the Las Vegas metropolitan area using the Las Vegas Valley location. The hour of 23:00 UTC (i.e., 15:00 PST) was chosen as the model starting time, since ozone concentrations are usually the highest in the afternoon. The high resolution (3 km) backward trajectories from the Las Vegas Valley are shown in Figure 3-34. All three trajectories, each at a different height, follow a similar backward path from the Las Vegas Valley, originating at elevated heights over the area to the west of Baja California in the eastern Pacific Ocean. We also ran additional back-trajectories at multiple mixed layer elevations (up to 4.5 km)

above Clark County on May 9 (details in Section 3.3.3) and found that each elevation modeled followed the same trajectory path as shown in Figure 3-34.

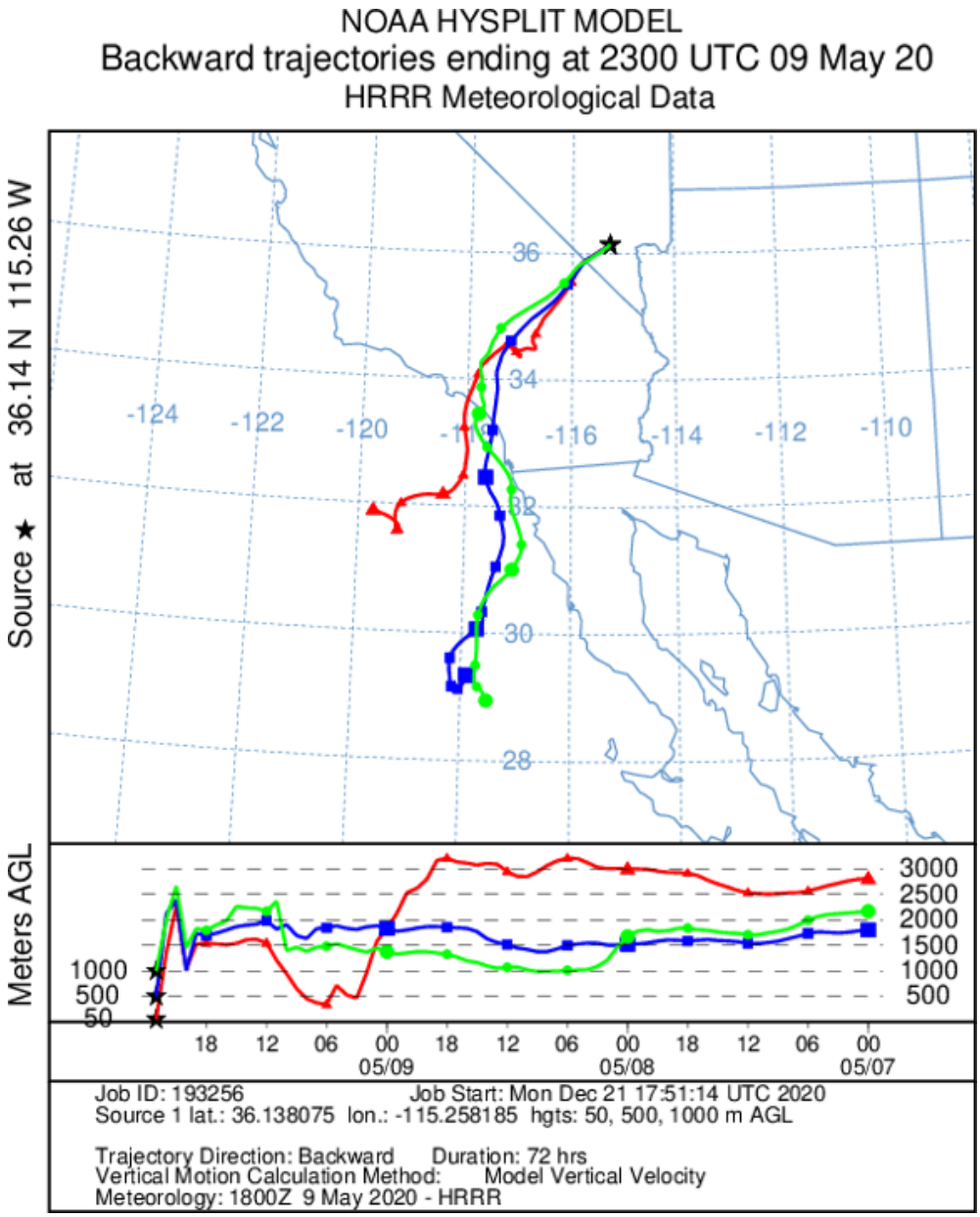


**Figure 3-34.** 72-hour HYSPLIT back trajectories from the Las Vegas Valley, ending on May 9, 2020, at 23:00 UTC (15:00 PST). HRRR 3 km back trajectories are shown for 50 m (red), 500 m (blue), and 1,000 m (blue) above ground level.

To identify variations in meteorological patterns of transported air to Las Vegas, we generated a HYSPLIT trajectory matrix. For this approach, trajectories are run in an evenly spaced grid of source locations. Figure 3-35 shows a 72-hour backward trajectory matrix with source locations encompassing Clark County. The backward trajectories were initiated from the early evening at

03:00 UTC (i.e., 19:00 PST) of May 9, 2020, at a starting height of 1,000 m above ground level (AGL). As shown in the plot, the transported air intersects Las Vegas on May 9. Consistent with the trajectories depicted in Figure 3-34, air was transported from an area to the west of Baja California at elevated heights over the eastern Pacific Ocean, across southern California, and northeast to intersect Las Vegas at 1,000 m AGL.

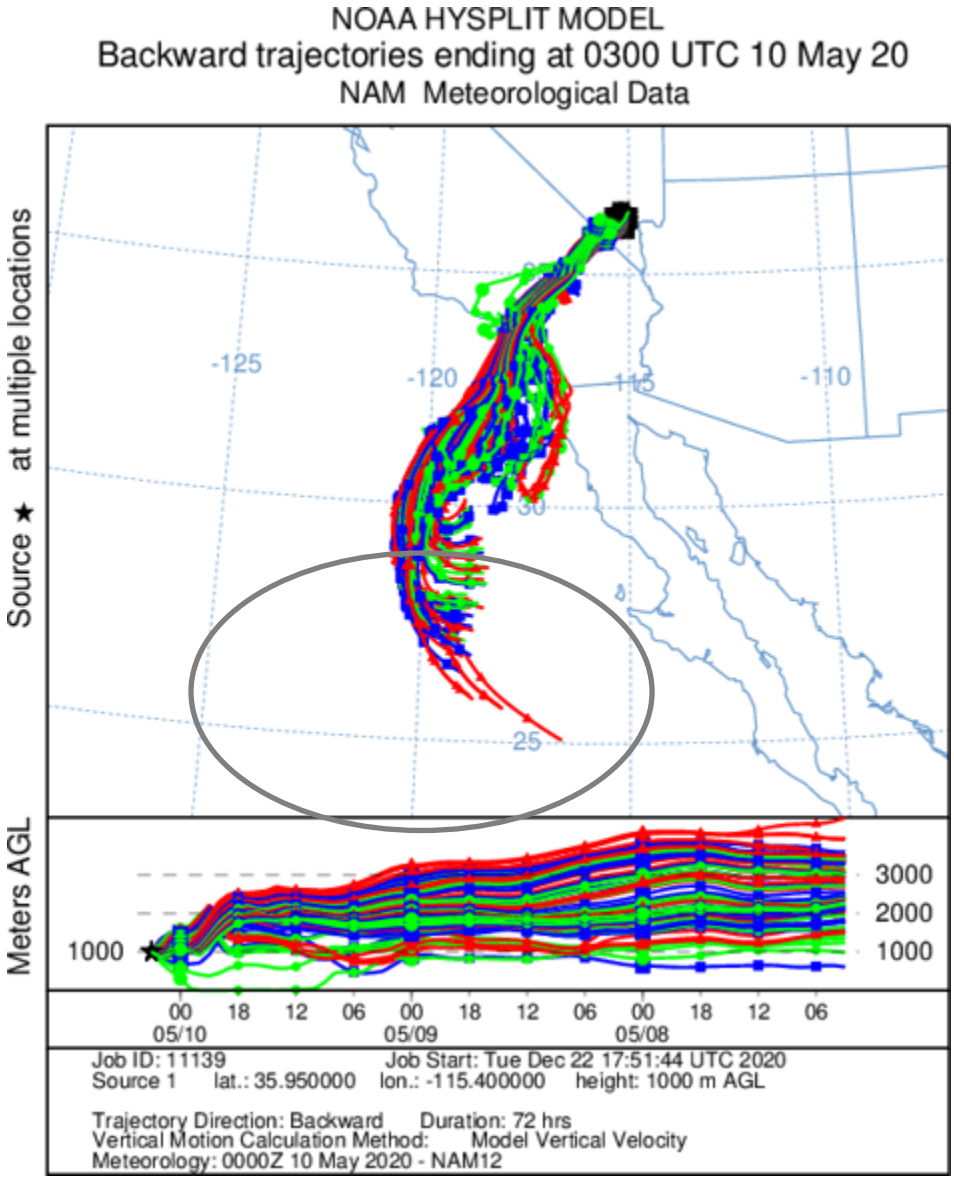


**Figure 3-35.** 72-hour HYSPLIT back trajectory matrix from the Las Vegas Valley, ending on May 10, 2020, at 03:00 UTC (19:00 PST). NAM 12 km back trajectories are shown for 1000 m above ground level. The approximate area of the SOI is shown by the gray circle.

The third trajectory approach used in this analysis was HYSPLIT trajectory frequency. In this option, a trajectory from a single location and height starts every three hours. Using a continuous 0.25-degree

grid, the frequency of trajectories passing through each grid cell is totaled and then normalized by the total number of trajectories. Figure 3-36 shows a 72-hour backward trajectory frequency plot starting from the Las Vegas Valley and 1,000 m AGL on May 9, 2020. The trajectory frequency plot yields similar results as those from the previous two approaches; transported air impacting the Las Vegas Valley on May 9, 2020, most frequently came from the area to the west of Baja California over the eastern Pacific Ocean.

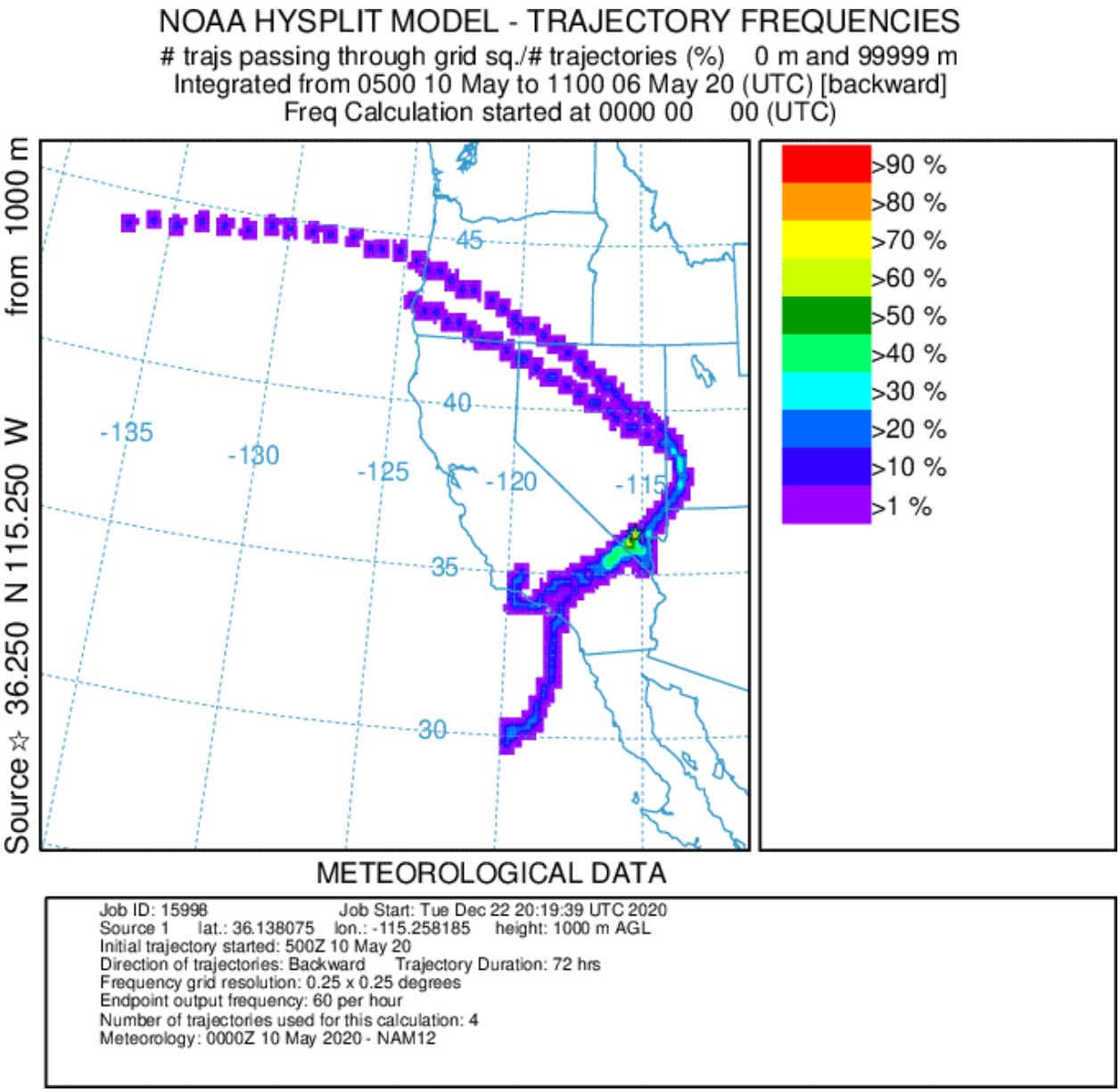


**Figure 3-36.** 72-hour HYSPLIT back trajectories frequency from Las Vegas Valley, ending on May 9, 2020. NAM 12 km back trajectories are shown for 1,000 m above ground level. The colors within the frequency plot indicate the percent of trajectories that pass through a grid square.

Forward trajectories were run from the approximate area of the stratospheric intrusion starting at a height of 3,000 m AGL at 03:00 UTC and 05:00 UTC on May 7 (**Figures 3-37 and 3-38**). This height was chosen based on the highest back trajectory heights from Figures 3-34 and 3-35. Choosing higher starting heights up to 5 km showed similar spatial and vertical results. These trajectories show that air was transported from the approximate area of the stratospheric intrusion to Clark County. These forward trajectories, combined with the back trajectories shown above, further support the transport of free tropospheric air from the area to the west of Baja California over the eastern Pacific Ocean, and descend into Clark County, Nevada.

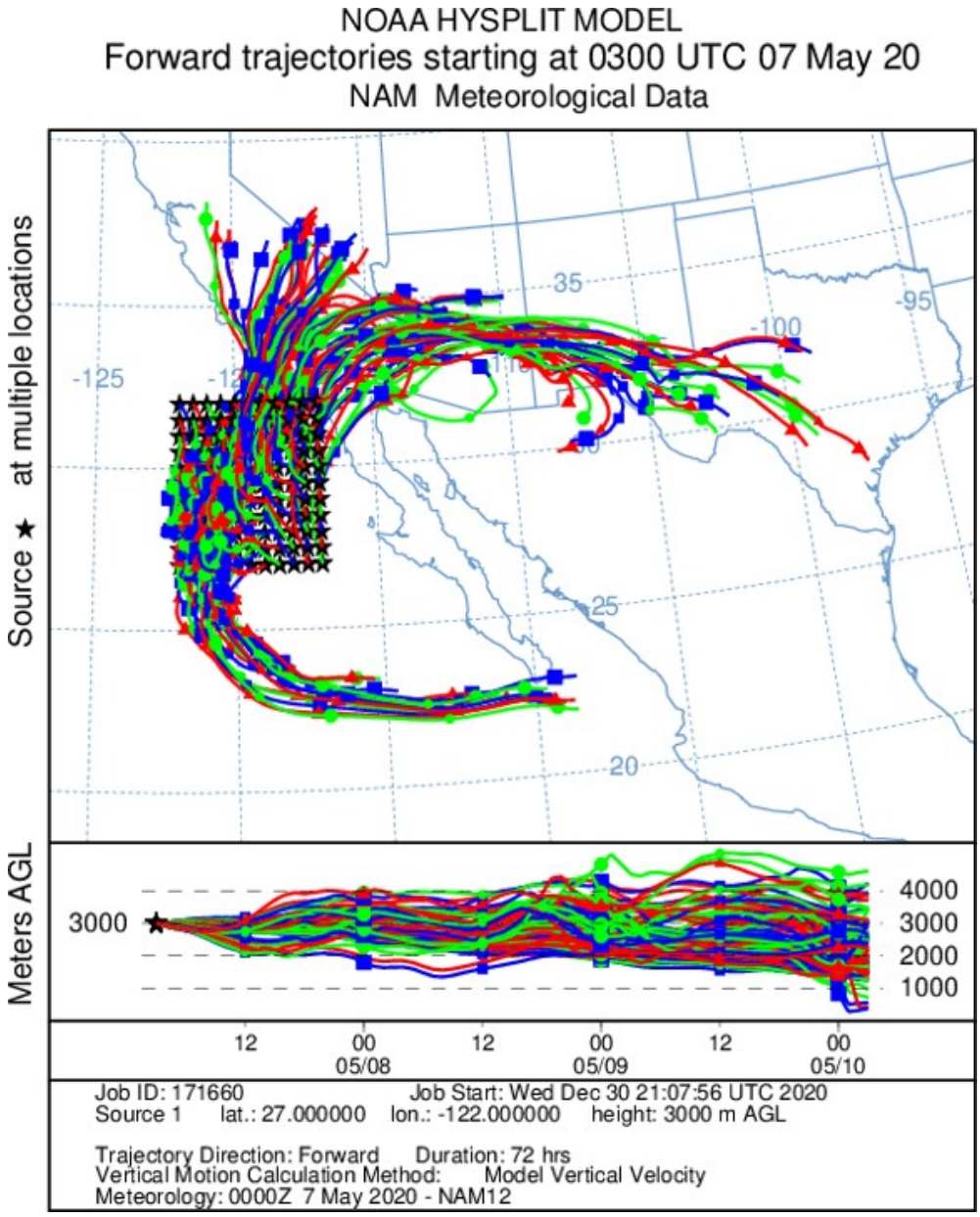


**Figure 3-37.** 72-hour HYSPLIT forward trajectories from the stratospheric intrusion source region initiated on May 7, 2020, at 03:00 UTC. NAM 12 km forward trajectories were initiated at 3,000 m above ground level.

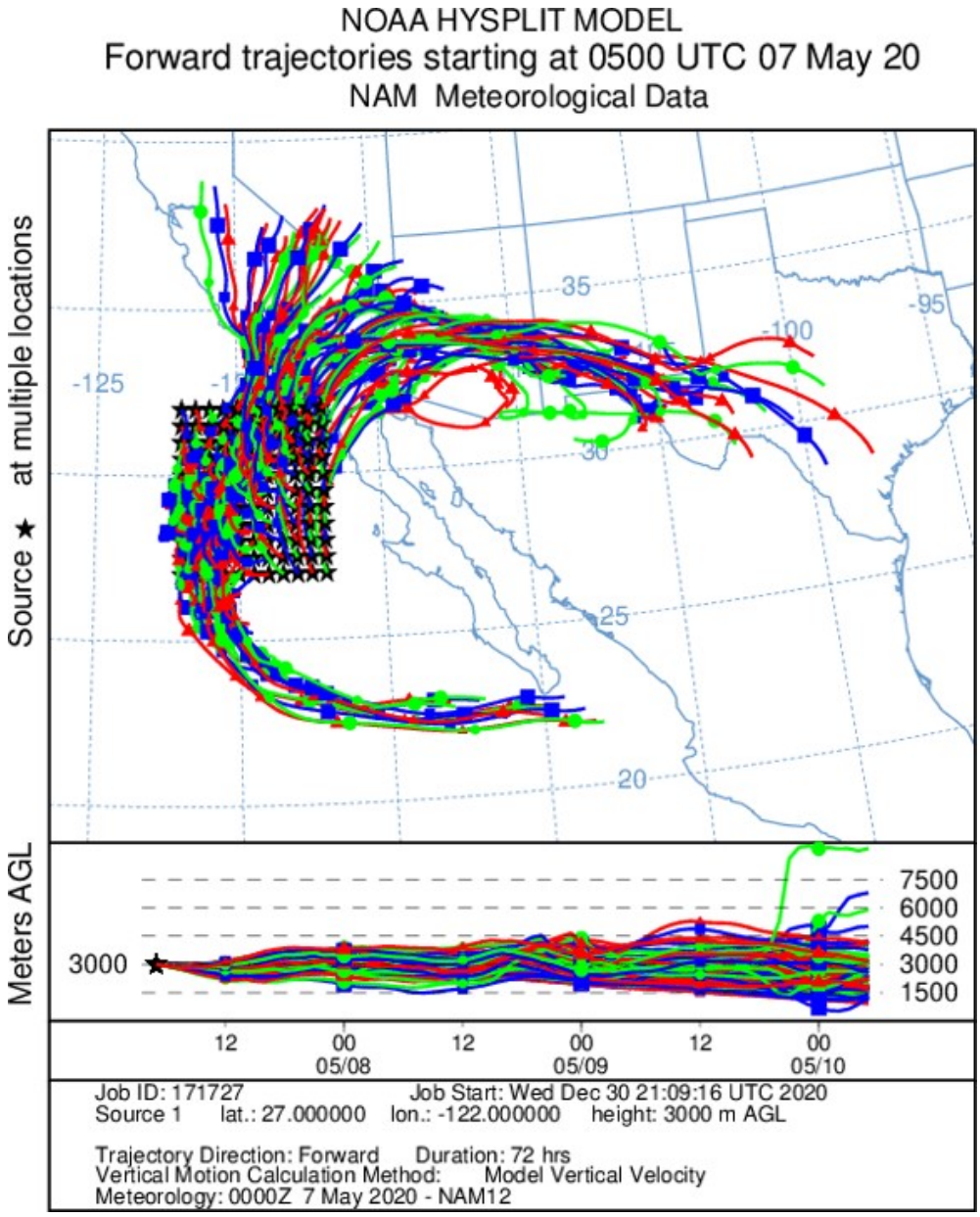


**Figure 3-38.** 72-hour HYSPLIT forward trajectories from the stratospheric intrusion source region initiated on May 7, 2020, at 05:00 UTC. NAM 12 km forward trajectories were initiated at 3,000 m above ground level.

## 3.3.2 Measurements of Tropospheric Mixing

Atmospheric soundings in the form of skew-T diagrams can provide an initial view into the extent of vertical mixing between the stratosphere and the troposphere. Some indications of stratospheric intrusion revealed by a sequence of these atmospheric soundings include the transport of dry, stratospheric air to lower elevations, a lowering of the tropopause, and favorable conditions for

mixing between the surface and higher altitudes. An example of a skew-T diagram, shown in Figure 3-39, shows the change in air temperature (T) and dewpoint temperature ($T_d$) as a function of altitude and corresponding pressure level. Drier air is indicated by a separation between T and $T_d$ (e.g. orange-boxed region). The tropopause is indicated by temperatures reaching a minimum before increasing with height, and represents the boundary between the troposphere and the stratosphere. The air temperature profile follows the dry adiabatic lapse rate (green curve), indicating a well-mixed, dry layer from the surface up to 500 hPa.

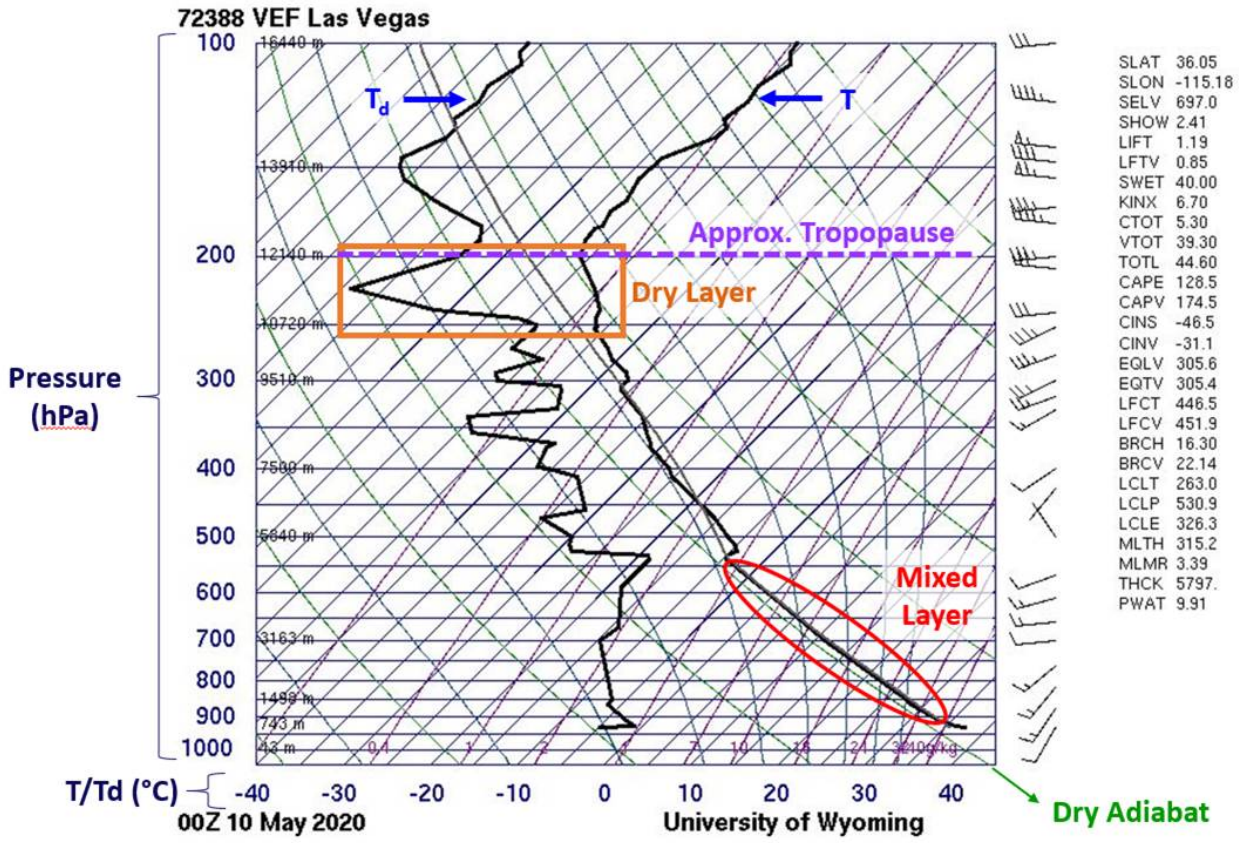


**Figure 3-39.** Skew-T diagram from May 9, 2020, in Las Vegas, Nevada. Red circle denotes deep mixed layer. The approximate (cold-point temperature) tropopause is denoted by the dashed purple line. Dry and wet adiabats are drawn as green and blue lines at a range of initial surface temperatures.

Our analysis of atmospheric soundings during the May 9 event period was guided by an example included in the EPA SOI Guidance that displayed skew-T diagrams from a documented stratospheric intrusion over Grand Junction, Colorado, in 2017 (U.S. Environmental Protection Agency, 2018). This example included two skew-T diagrams, shown in Figure 3-40, with particular characteristics that suggest viable tropospheric mixing to facilitate vertical transport of ozone injected into the mid-troposphere to the surface. The two skew-T diagrams are characterized primarily by the large, very

dry layer at a height greater than approximately 5 km above mean sea level, or 3.5 km above ground level. A temperature inversion, observed from the 00:00 UTC sounding, likely prevented the dry air above from mixing down into the lower troposphere. During the 12:00 UTC sounding 12 hours after the 00:00 UTC sounding and 12 hours before the exceedances occurred, it is clear from the widening of the gap between the dewpoint temperature profile and the temperature profile that dry air mixed into the lower troposphere. The base of the very dry mixed layer also moved down into the atmosphere by about 500 m. Further, the temperature lapse rate of the lower troposphere was approximately dry-adiabatic, indicating that the lower PBL was well-mixed. These skew-Ts provide an example of an SOI above an area and being mixed down into the boundary layer. In the Grand Junction example, the SOI affected surface ozone concentrations and caused an exceedance of the ozone NAAQS.

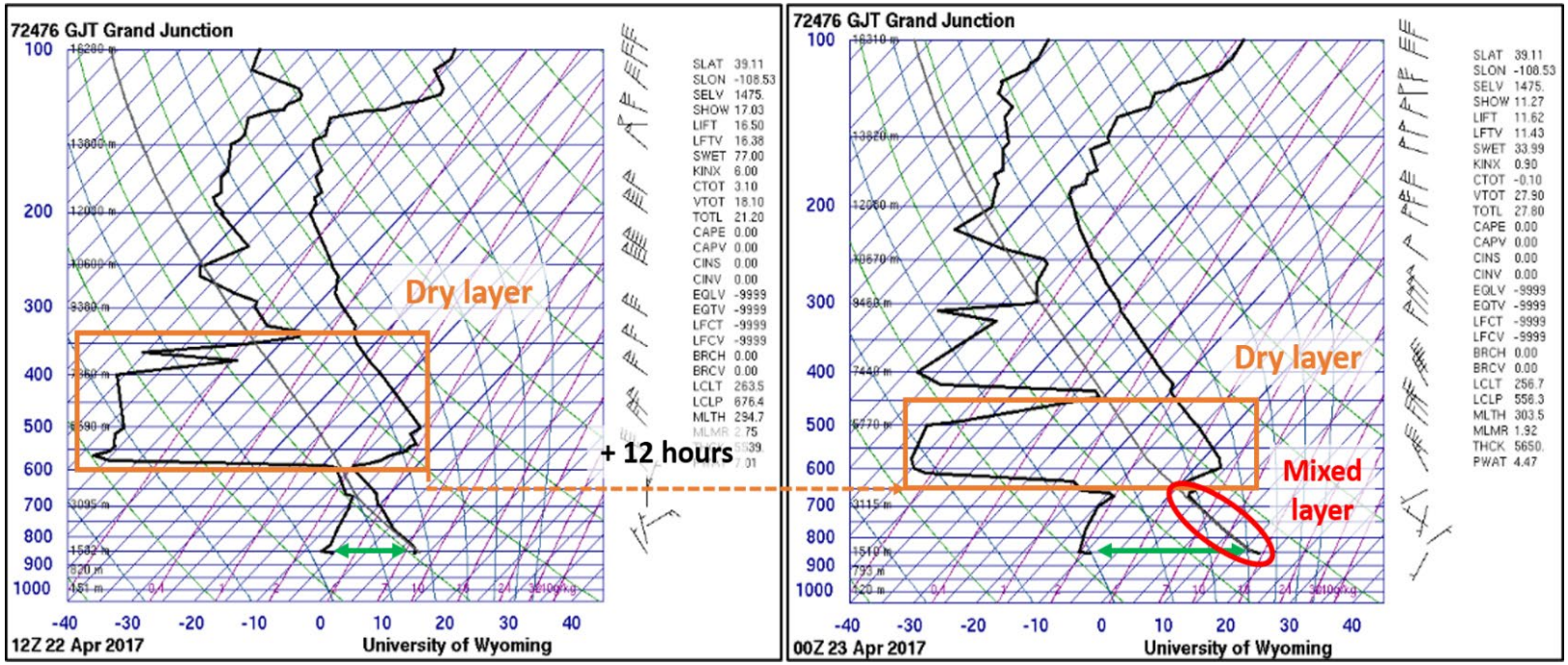


**Figure 3-40** Skew-T diagrams for 12:00 UTC on April 22, 2017, (left), and 00:00 UTC April 23, 2017, (right), both at Grand Junction, Colorado. Orange boxes denote the very dry layer. The red circle denotes the mixed layer. Green arrows indicate the intrusion of very dry air to the surface. The figures were collected directly from EPAs "Guidance on the Preparation of Exceptional Events Demonstrations for Stratospheric Ozone Intrusions."

Figures 3-41 and 3-42 display skew-T diagrams from the San Diego (NKX) National Weather Service office, which lies along the path of transport from the SOI to Clark County, and from the Las Vegas (VEF) National Weather Service office. Soundings were obtained from the University of Wyoming's Upper Air portal.[3]

As shown in Sections 3.2 and 3.3.1, an ozone-rich air mass originated from a stratospheric-tropospheric exchange off the coast of Baja California between 0:00 UTC on May 7 and 0:00 UTC on May 8, and was transported to the Clark County region on May 9. Figures 3-41 and 3-42 show the soundings from the San Diego office, which is the forecasting office closest to this origin during this time period and sits along the path of air transport towards Clark County. Both of these skew-T diagrams, taken 24 hours apart, exhibit a dry layer of air just below tropopause, which provides supporting evidence that dry, stratospheric air penetrated lower into the atmosphere (similar to the Grand Junction example).

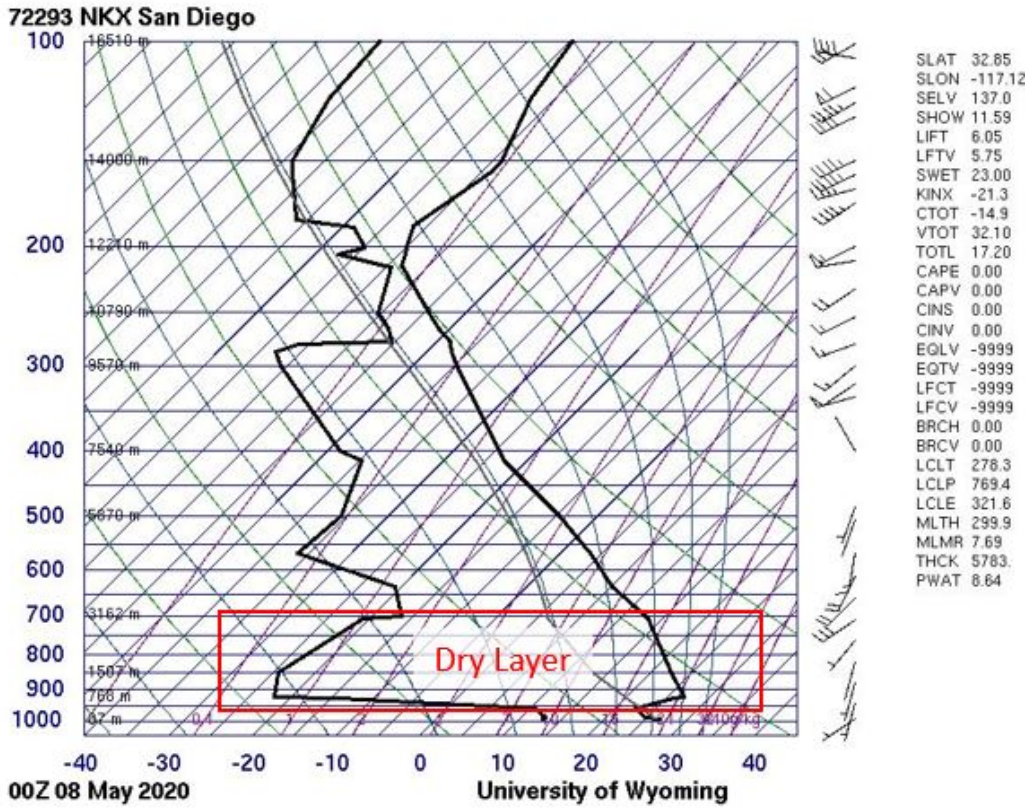


Figure 3-41. Skew-T sounding launched from the San Diego (NKX) National Weather Service office on May 8, 2020, at 0:00 UTC (4 p.m. May 7, local time). A dry layer of air is boxed and labeled in red.

[3] http://weather.uwyo.edu/upperair/sounding.html

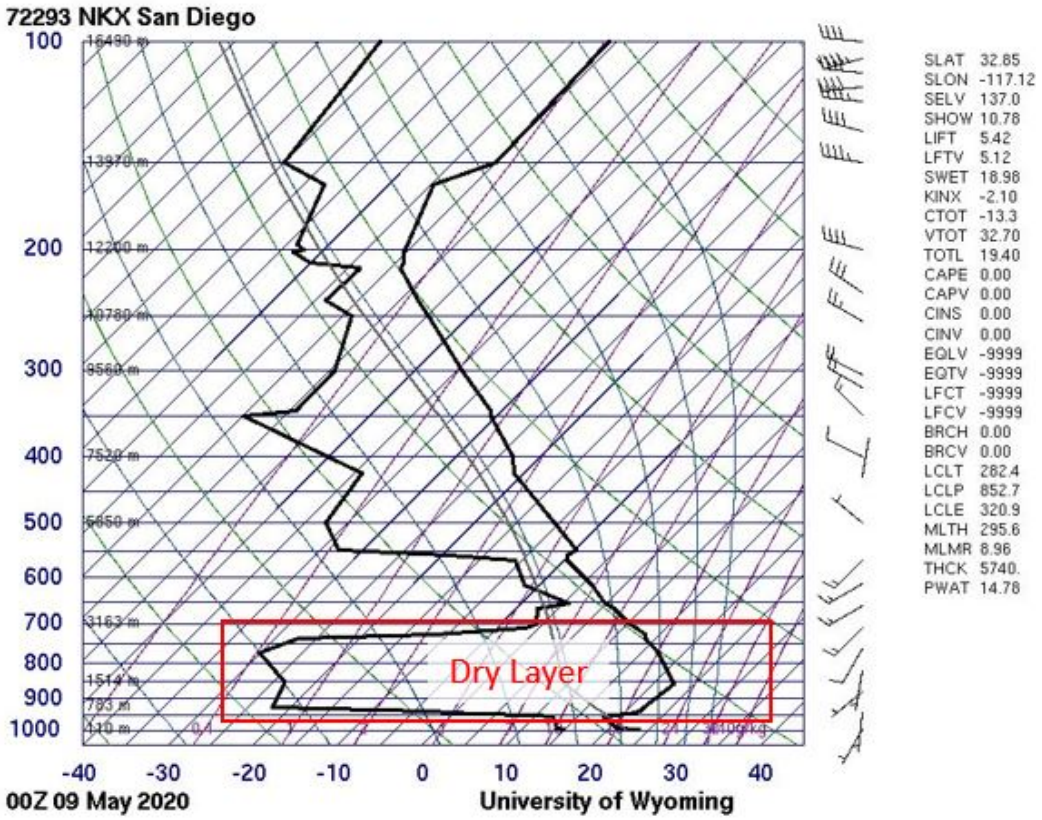


**Figure 3-42.** Skew-T log-P sounding launched from the San Diego (NKX) National Weather Service office on May 9, 2020, at 0:00 UTC (4 p.m. May 8, local time). A dry layer of air is boxed and labeled in red.

Figure 3-43 shows the skew-T diagram for a sounding launched from Las Vegas at 0:00 UTC on May 10 (4 p.m. May 9, local time), the observation location closest to the exceedance event. The temperature lapse rate in the lower-to-mid troposphere follows a dry adiabatic lapse rate, shown in the red circle where the slope of the temperature lapse rate parallels the dry adiabatic lapse rate (green curve). The conditions shown are characteristic of a well-mixed layer from 550 hPa (around 4 km) to the surface. This suggests that air entrained from higher altitudes into the boundary layer could be mixed toward the surface. This sounding also shows dry air at the surface, indicated by the large horizontal distance between the dew point and the temperature, which suggests possible stratospheric influence at the surface in Clark County on May 9.

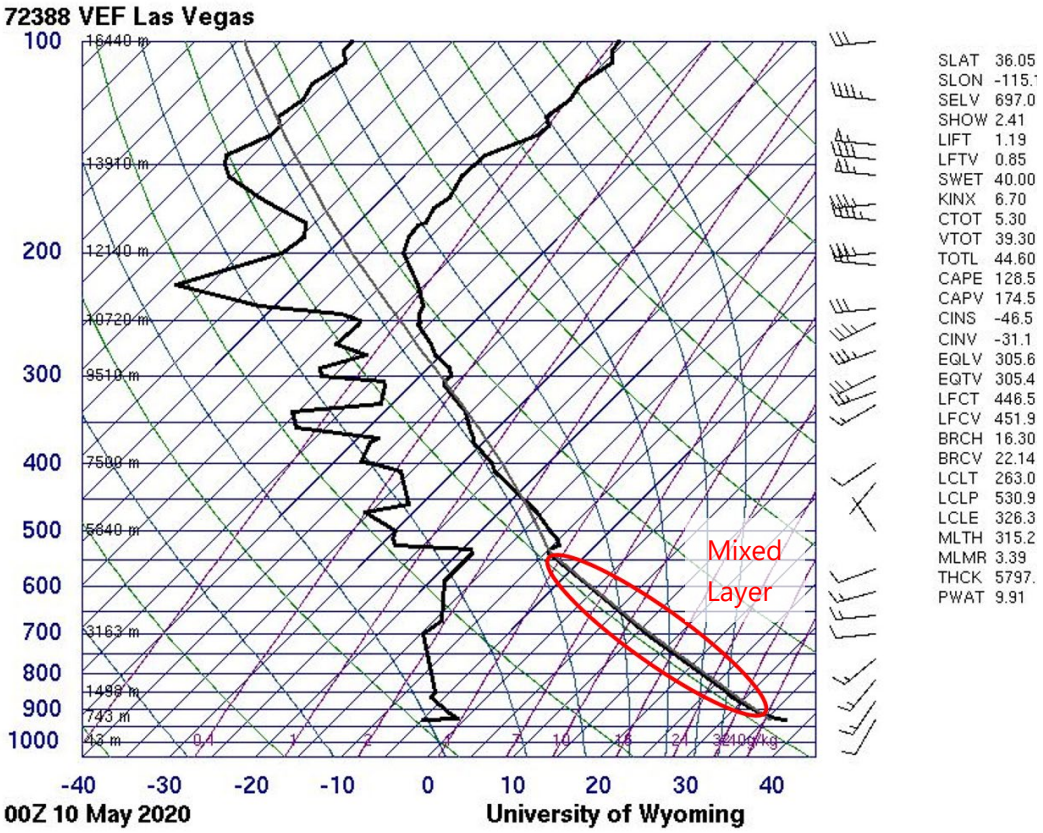


**Figure 3-43.** Skew-T sounding launched from the Las Vegas (VEF) National Weather Service office on May 10, 2020, at 0:00 UTC (4 p.m. May 9, local time). This sounding is the closest observation to the exceedance event on May 9. A mixed layer is shown where the temperature lapse rate (black) parallels the dry adiabatic lapse rate (green). This condition is circled in red.

The JPL Table Mountain Facility (34.38N, 117.68W, 2285 m above sea level) in the San Gabriel mountains north of the Los Angeles, California, basin lies along the transport path from the source region to Clark County (see HYSPLIT trajectories in Section 3.3.1). The ozone differential absorption LIDAR at this site provides ozone concentration vertical profiles at 4:00–6:00 UTC daily from the surface to the lower stratosphere, providing a picture of free tropospheric ozone mixing ratios (Chouza et al., 2020). Figure 3-44 shows the average ozone profile on May 9 from 4:00–6:00 UTC (20:00 to 22:00 PST) relative to the spring 2020 mean ozone profiles at the JPL Table Mountain facility. The temperature profile on the right is shown to confirm that the atmosphere above JPL is fully in the free troposphere (temperature steadily decreasing with height) and no inversions that would prevent mixing are present. Ozone concentrations of 80-110 ppb were observed at 3-6 km above sea level in the free troposphere; these concentrations were 25-50 ppb above the spring 2020 mean ozone profile. These measurements confirm enhanced ozone concentrations along the trajectory between the SOI source region and Clark County.

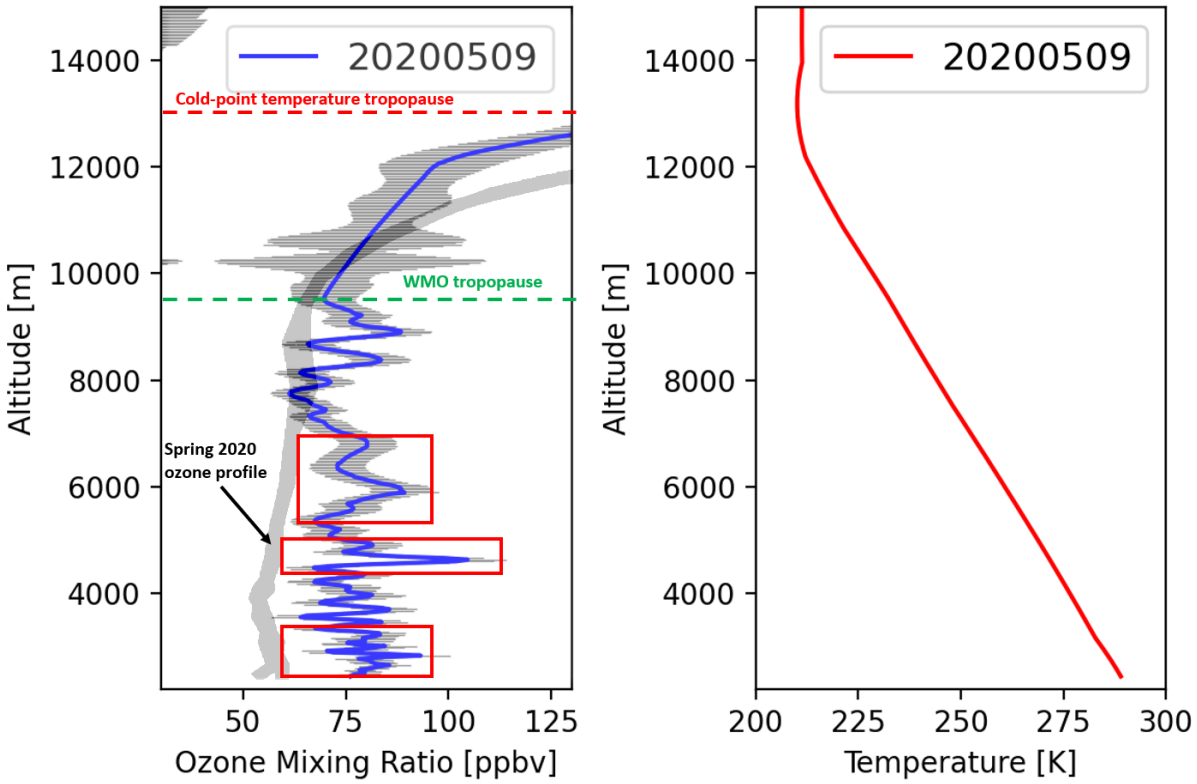


**Figure 3-44.** Ozone mixing ratio and temperature vertical profiles above sea level measured by the TOLNet ozone lidar at the JPL Table Mountain Facility from 4:00-6:00 UTC on May 9, 2020 (8:00-10:00 pm local time on May 8, 2020). The spring 2020 mean ozone profile compiled from the Table Mountain Facility profiles is also shown for comparison (adapted from Chouza et al., 2020). Ozone measurement uncertainty bounds are denoted by the grey shading. Red boxes denote locations of elevated ozone concentration investigated with HYSPLIT trajectories.

**Figures 3-45 through 3-47** show forward and back trajectory matrices of the ozone vertical profile LIDAR data from the JPL Table Mountain site. These trajectories are conducted at altitudes where ozone enhancements were observed in the ozone profile observations. At 3,700 m and 2,000 m altitudes, back trajectories intersect with the stratospheric intrusion source region location at ~5-6 km above sea level over the Pacific Ocean, where upper tropospheric air was influenced by stratospheric-tropospheric exchange (see Sections 2.4 and 3.3.1). Furthermore, the ozone enhancements recorded at the JPL Table Mountain site at 500 m and 2000 m AGL were transported from the free troposphere to altitudes of ≤ 2.5 km, within the deep mixed layer over Clark County (Figure 3-46).

It is important to note that transport of Los Angeles basin pollution is another possible source of high ozone events near the JPL Table Mountain site, the Mojave Desert, and locations downwind, such as Clark County. Previous high ozone events detected at this site involved transport through mountain passes and up-slope flow transport via a mountain chimney effect (Chouza et al., 2020).

Trajectories indicate that air parcels containing the observed ozone enhancement features were transported both within the boundary layer and at higher altitudes in the free troposphere from the Pacific Ocean to the JPL Table Mountain site (Figures 3-45 through 3-47). In addition, all of the trajectories indicate that air parcels transported to Clark County were over the Los Angeles Basin overnight on May 8, when surface ozone concentrations are typically low compared with daytime. Therefore, the evidence prior to the May 9 event indicates an ozone enhancement contribution from transport at upper levels, rather than solely associated with local Los Angeles basin, surface level ozone formation and transport. The combination of the free troposphere ozone concentration profiles, skew-T diagrams, and trajectories to and from the JPL Table Mountain site provide strong evidence for the free tropospheric transport of ozone enhancements towards the deep mixed layer and surface at Clark County on May 9, 2020.

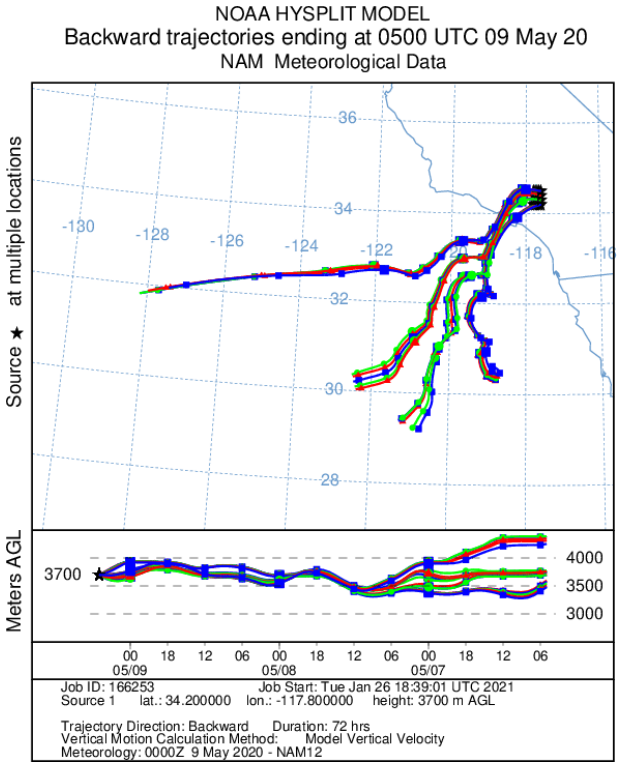


**Figure 3-45.** 72-hr back trajectories from a matrix located close to the JPL Table Mountain Facility at 3,700 m AGL (5,950 m ASL) on the evening before May 9, 2020 (May 9, 5:00 UTC).

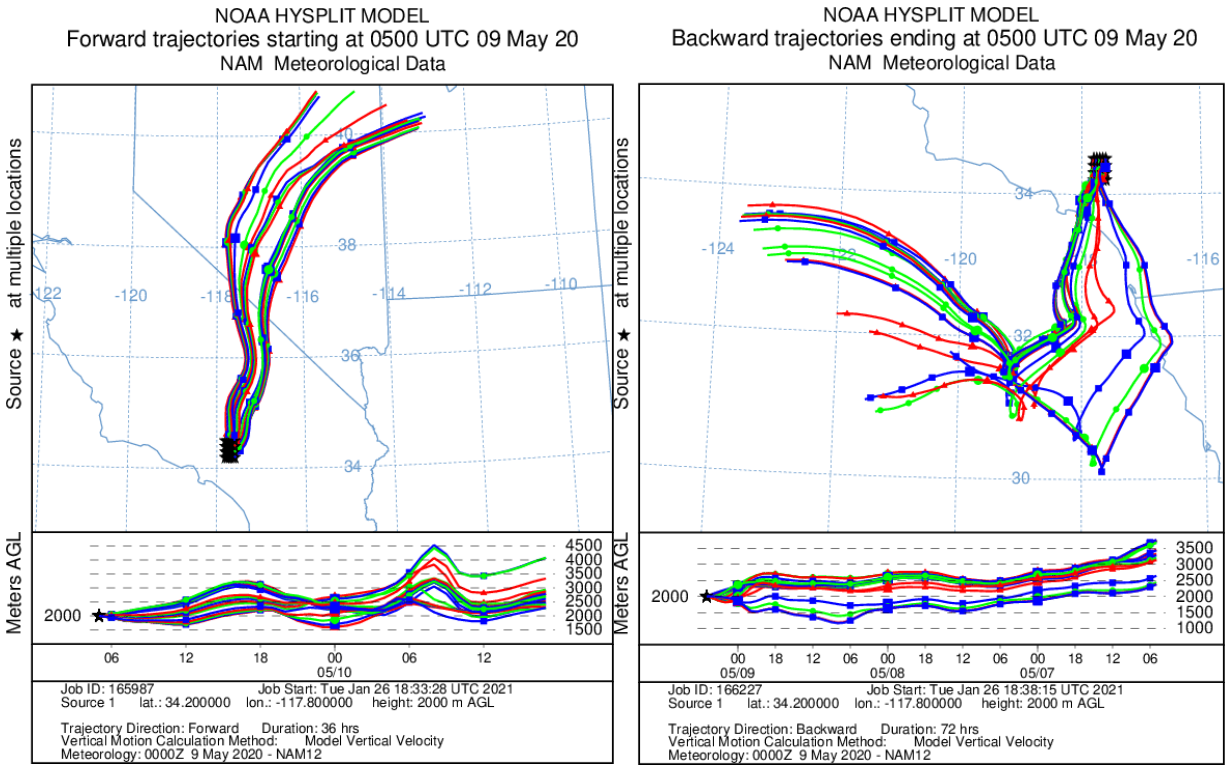


**Figure 3-46.** 72-hr forward (left) and back (right) trajectories from a matrix located close to the JPL Table Mountain Facility at 2,000 m AGL (4,250 m ASL) on the evening before May 9, 2020 (May 9, 5:00 UTC).

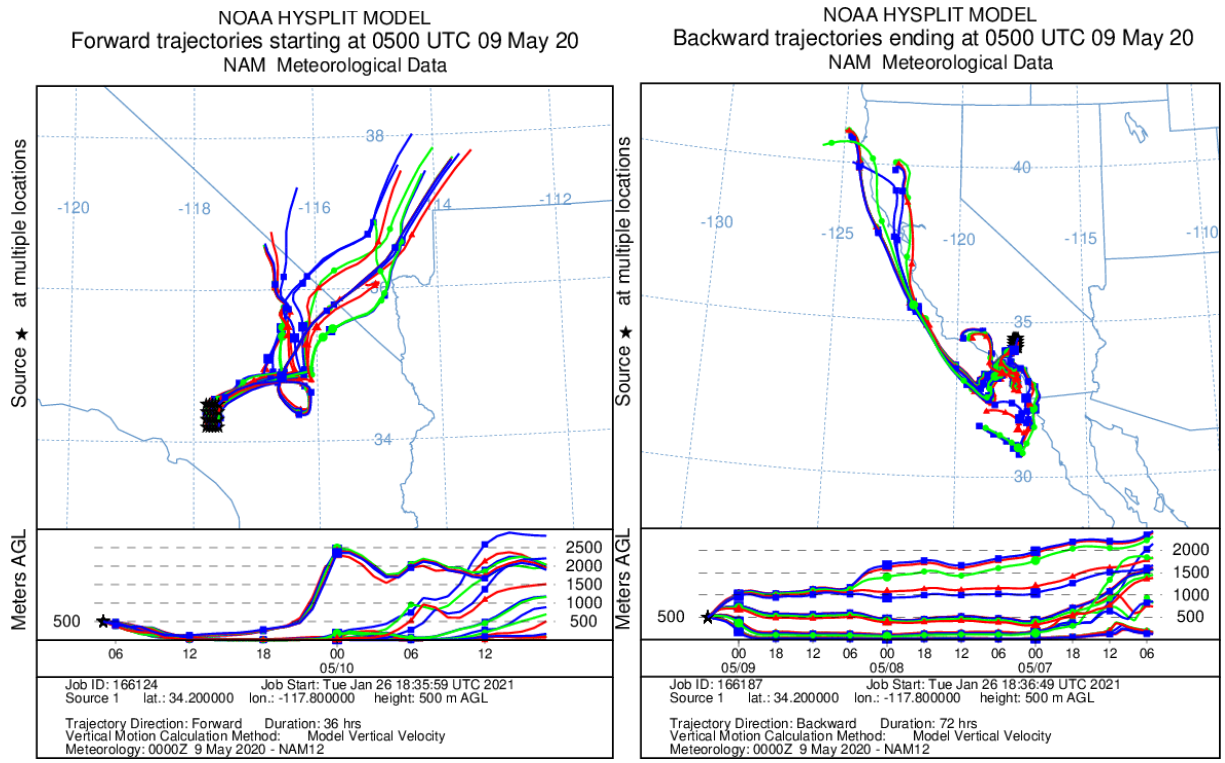


**Figure 3-47.** 72-hr forward (left) and back (right) trajectories from a matrix located close to the JPL Table Mountain Facility at 500 m AGL (2,750 m ASL) on the evening before May 9, 2020 (May 9, 5:00 UTC).

## 3.3.3 Meteorological Conditions

The mesoscale and local meteorological conditions from May 7 to 9 provide evidence for transport of air from Baja California to Clark County, Nevada, and subsequent vertical mixing of upper-level air to the surface. Figure 3-48 depicts upper-level meteorological conditions on May 7, 8 and 9, 2020 at 4:00 PST. The pressure contours over Baja California and the southwestern United States depict an upper-level ridge, identified by the inverted 'v' shape of the brown height contours, indicating high pressure on May 7 through 9. Within a ridge, aloft high air pressure is associated with an influx of air mass from a surface low-pressure system. To the east of a ridge, this configuration results in an influx of sinking air from the high pressure above toward the surface. On May 7 through 9, Clark County, Nevada was to just to the east of the upper-level ridge, indicating that vertical downward mixing from the high pressure above could readily transport and mix ozone into the lower free-troposphere.

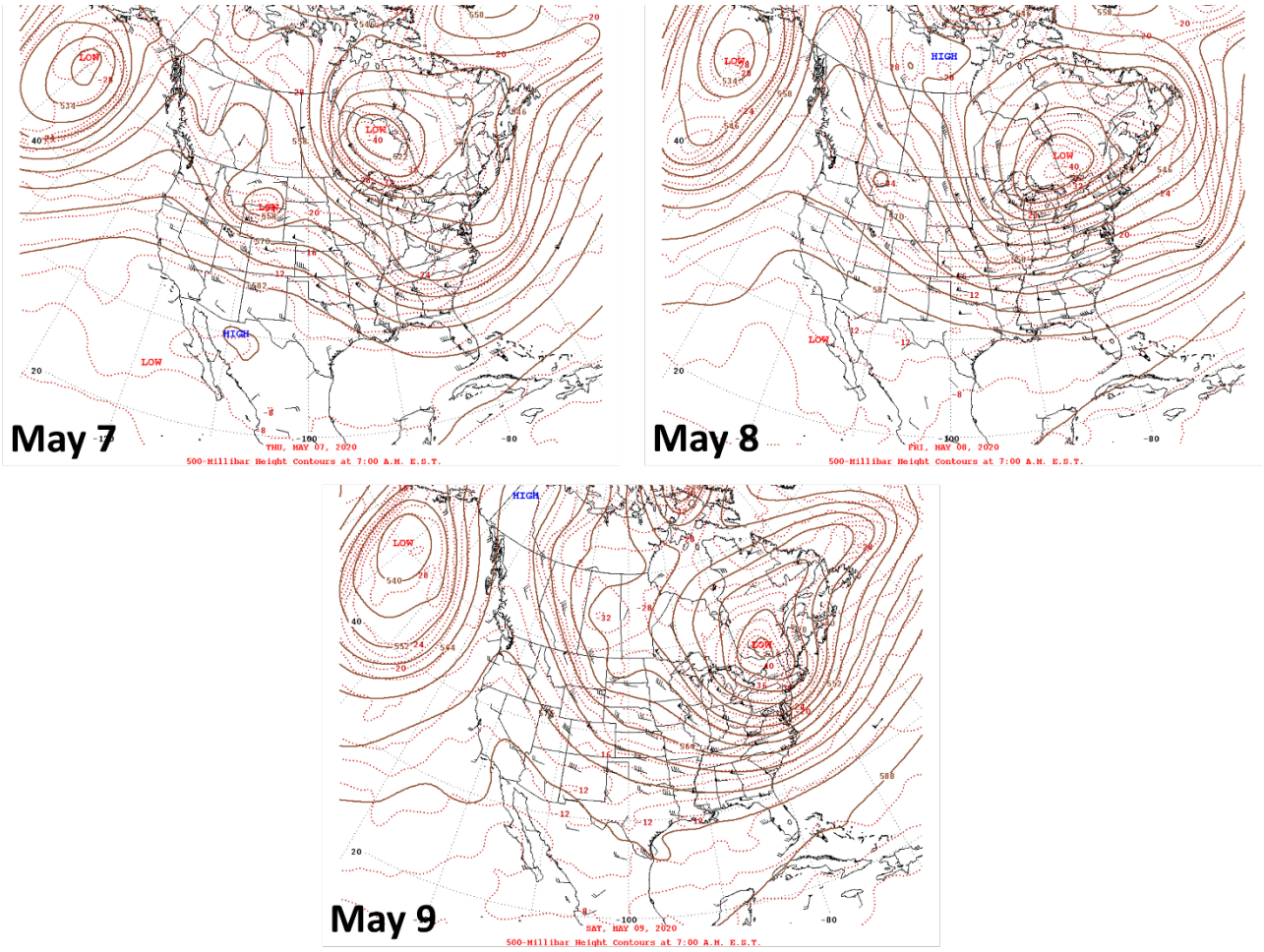


**Figure 3-48.** Daily upper-level (500 mb) meteorological maps for the two days leading up to the exceptional event and during the May 9 exceptional event.

A surface low-pressure system moved over the border of Nevada and California between May 7 and 8 and centered over Clark County, Nevada, on May 9 along with high surface temperatures. The large amount of surface heating, as evident from the skew-T temperature profile, along with low pressure that moved northeastward from southern California, both favor intense vertical mixing via buoyancy between the boundary layer and surface, and potential entrainment into the boundary layer from the free troposphere. After sinking to the lower-free troposphere due to the upper-level ridge, the surface low readily mixed the ozone-rich air into the lowest layer of the atmosphere (**Figure 3-49**). This is consistent with the skew-T diagrams shown in Section 3.3.2, with a characteristically well-mixed PBL from the surface to 550 hPa, and suggests that free tropospheric ozone was mixed down to the surface on May 9 in Clark County.

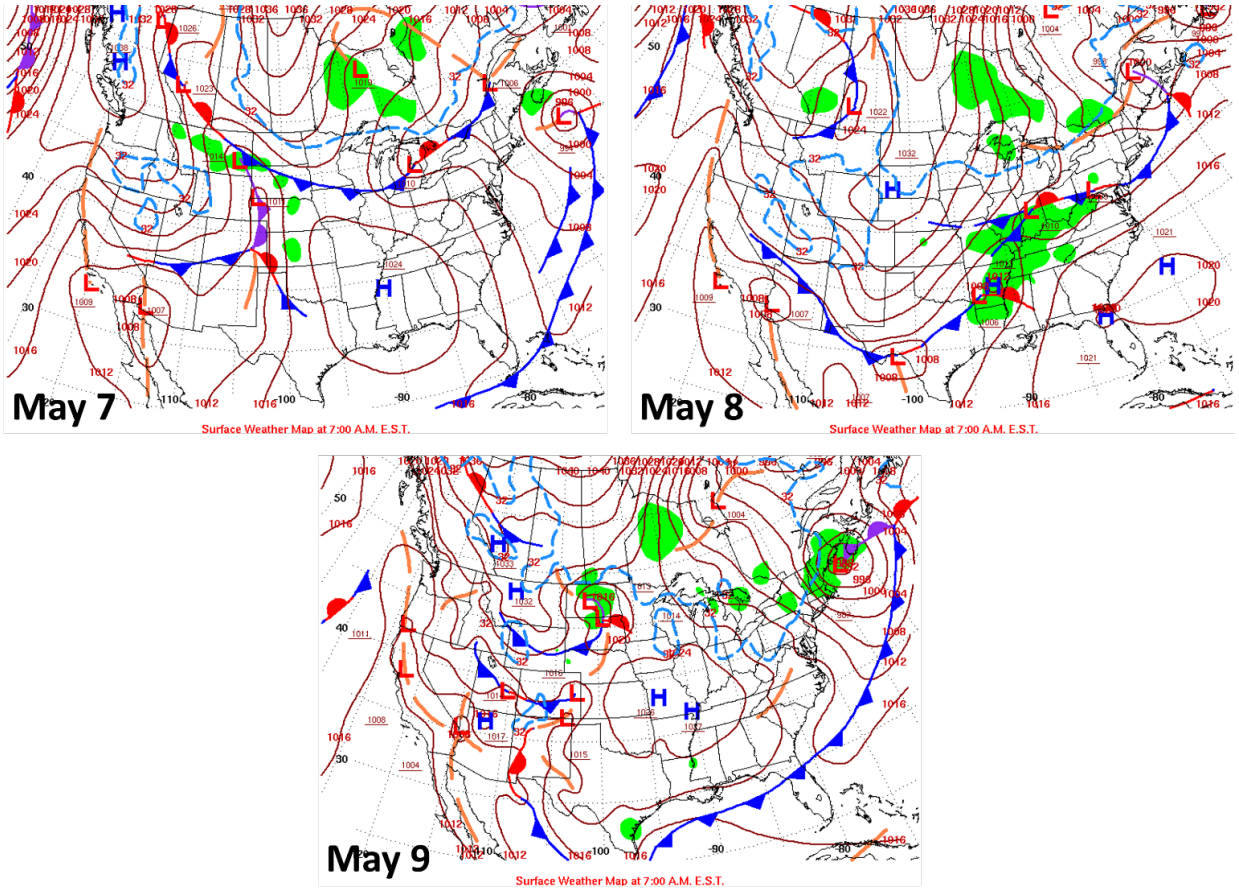


**Figure 3-49.** Daily surface meteorological maps for the two days leading up to and during the May 9 exceptional event.

The planetary boundary layer denotes the atmospheric layer closest to the surface, and the height of the planetary boundary layer describes the vertical extent of surface air characteristics. On May 9, the planetary boundary layer height for the southern region of Clark County, Nevada, was greater than 4 km in altitude, as indicated by the skew T, log P 550 hPa mixed layer (Figure 3-43). The NAM modeled PBL heights on the afternoon of May 9 show that the PBL height of 4 km extended from Clark County to southern California along the transport path from the SOI event (Figure 3-50). Although photochemical production likely occurred on May 9, this analysis and the previous trajectories provide evidence that ozone from the aloft intrusion originating over the eastern Pacific Ocean, west of Baja California, was transported into the deep mixed layers over southern California and southern Nevada and mixed to the surface in Clark County on May 9.

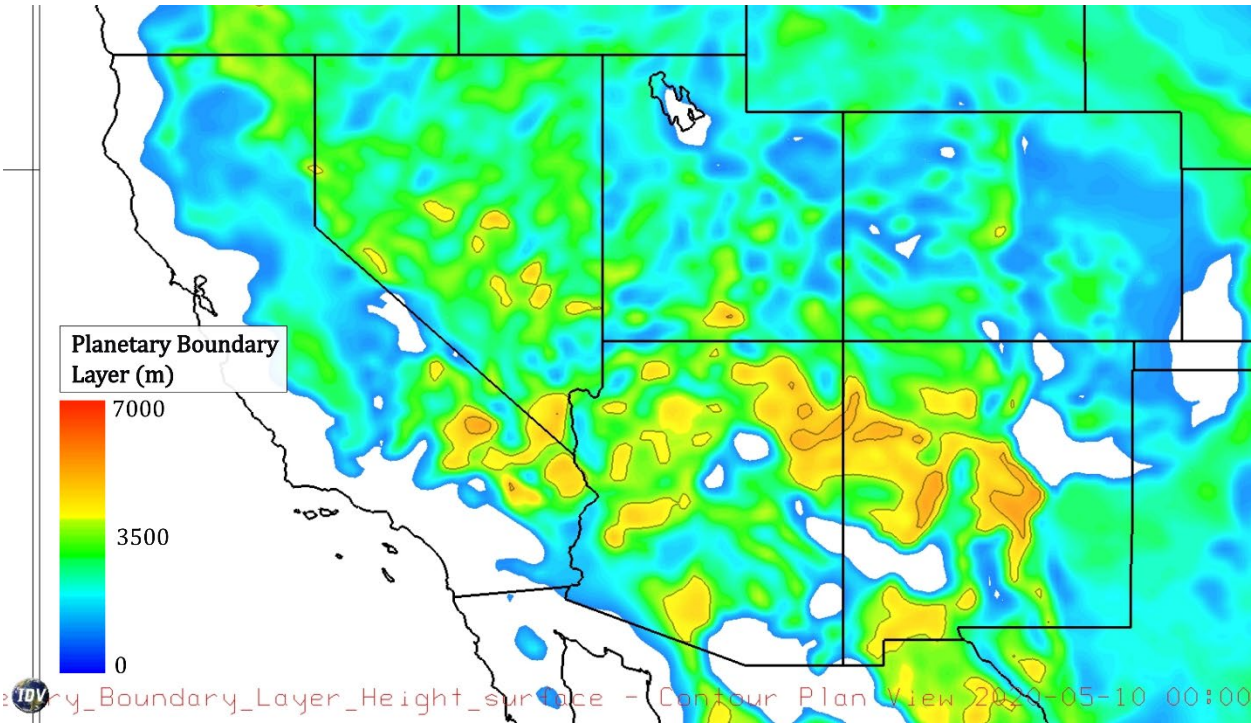


**Figure 3-50.** Planetary boundary layer (PBL) height contour map based on the NAM model for May 9, 2020, at 16:00 PST. The gray lines denote PBL heights above 4 km altitude in 500 m increments.

## 3.4 Impacts of the SOI at the Surface

As stated in Sections 3.2.1, 3.2.2, and 3.3.2, stratospheric air is characterized by high ozone content and low water vapor content relative to tropospheric air. Therefore, stratospheric intrusion and subsequent transport of stratospheric air to the surface should cause meteorological variables at the surface, such as ozone concentrations and relative humidity, to have characteristics similar to stratospheric air.

Figure 3-51 shows ozone, absolute humidity, and air temperature observations from May 9 at the Jerome Mack station compared with their diurnal profiles for the month of May from 2015 through 2019. Absolute humidity has a relatively constant diurnal profile in May and hovers between 5 to 7 grams per cubic meter, with a slight dip in the afternoon. The diurnal temperature profile shows a trough in the early morning, followed by a peak throughout the afternoon and a gradual decrease into the evening. The diurnal profile of ozone is similar to temperature, reaching a maximum in the afternoon and minimum in the early morning. The temperature on May 9 was high compared to the 5-year May average, reaching a magnitude just above the 95$^{th}$ percentile in the late afternoon. Absolute humidity, rather than relative humidity, is displayed in Figure 3-51 to decouple the measurement of humidity from temperature. Throughout most of May 9, absolute humidity values were lower than the lowest 5$^{th}$ percentile of May observations, and were below 1 gram per cubic

meter for much of the afternoon. During the late afternoon on May 9, ozone concentrations were higher than the 5-year 95th percentile of May observations. The extremely low absolute humidity values and high ozone concentrations provide evidence that stratospheric air reached the lower troposphere in Las Vegas on May 9.

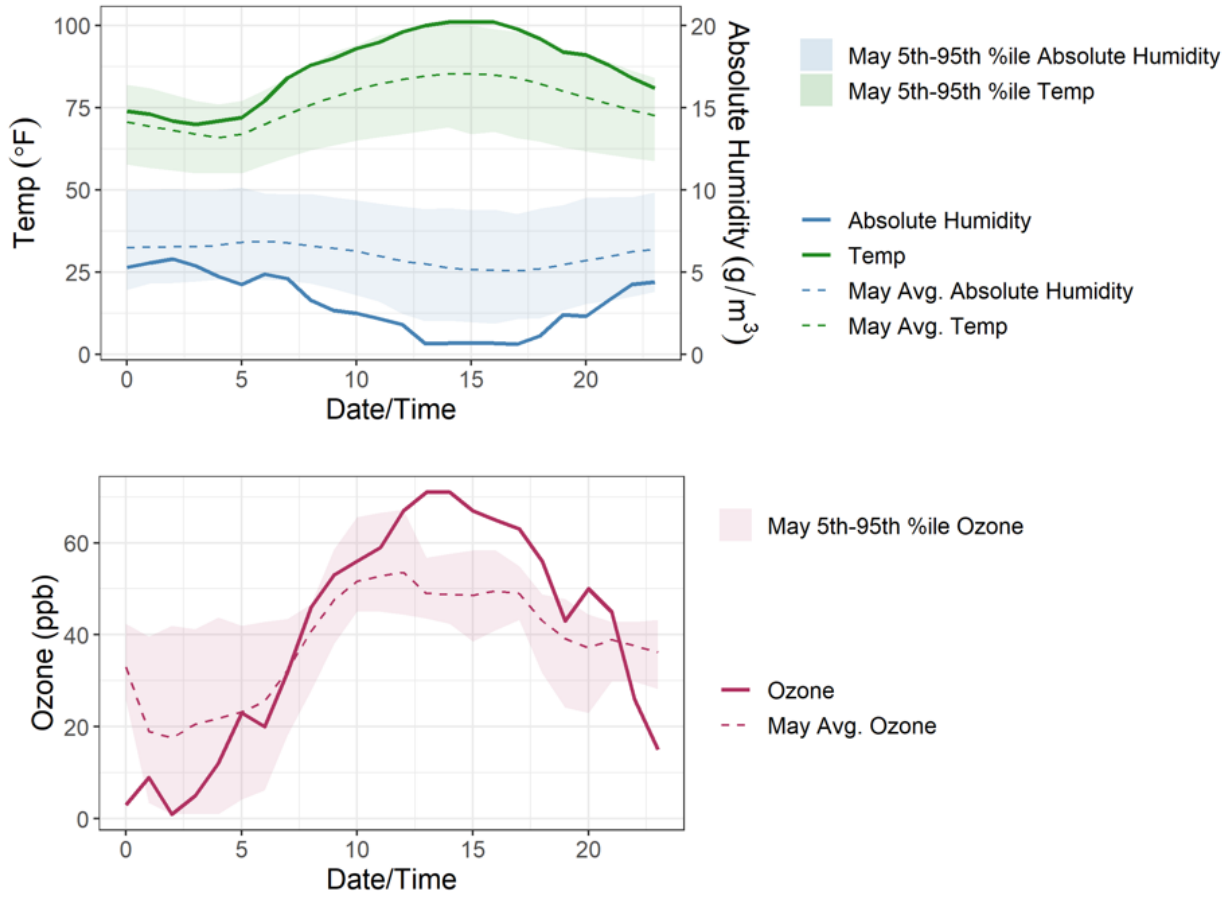


**Figure 3-51.** (Top plot) Diurnal profile of temperature (green) and absolute humidity (blue) at the Jerome Mack station, including temperature and absolute humidity values on May 9 and the 5-year May averages (dotted lines); and, (bottom plot) diurnal profile of ozone at the Jerome Mack station on May 9. Shaded ribbons represent the five-year 5th-95th percentile range.

To determine whether the May 9 event was predominately due to photochemical processes at the surface, we examine whether $NO_x$ was abnormally high during this event. **Figures 3-52 through 3-55** show nitric oxide (NO), nitrogen dioxide ($NO_2$), and ozone observations on May 9 at the Paul Meyer and Walter Johnson stations, and are compared with diurnal profiles for the month of May from 2015 through 2019. NO and $NO_2$ observations are available only from two non-exceedance sites in Clark

County, Jerome Mack and Joe Neal. Plots for these two sites are included in this section to provide a reference for regional NO and $NO_2$ concentrations in Clark County on the day of the event, although these sites should not serve as a direct proxy for concentrations at either of the event sites due to local variation. $NO_2$ concentrations in May usually reach a peak in the early to mid-morning and gradually decrease throughout the day, followed by a gradual increase in the later evening. The diurnal profile of NO is similar to $NO_2$ but does not have a distinct increase into the late evening. $NO_x$ (NO + $NO_2$) is an important ingredient (in addition to VOCs and sunlight) in the creation of ozone in the troposphere. During the afternoon on May 9, ozone concentrations at Paul Meyer and Walter Johnson were higher than the seasonal 95th percentile concentrations. The Jerome Mack and Joe Neal monitoring sites also showed abnormally high ozone concentrations on May 9, although magnitudes remained over the NAAQS for a shorter period than at either exceedance site. During this time, $NO_2$ concentrations were approximately average relative to seasonal average at both reference sites, while NO concentrations were low at Jerome Mack. The average NO and $NO_2$ concentrations at Jerome Mack and Joe Neal during the May 9 event provide evidence that photochemistry alone was unlikely to be responsible for the EE in Clark County on May 9.

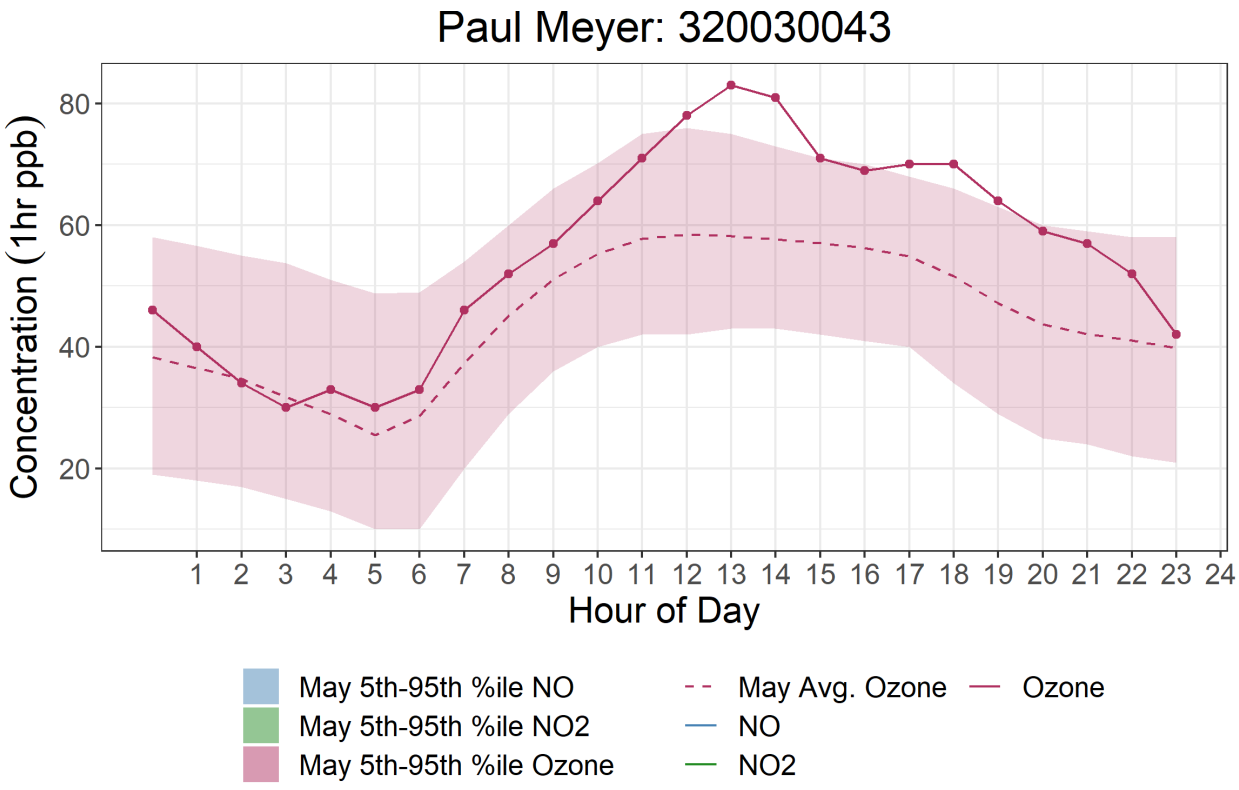


**Figure 3-52.** Diurnal profile of ozone concentrations (red) at the Paul Meyer site on May 9 and the 5-year seasonal average ozone (dotted lines). Shaded ribbons represent the five-year 5th-95th percentile range. NO and $NO_2$ data are not available at Paul Meyer.

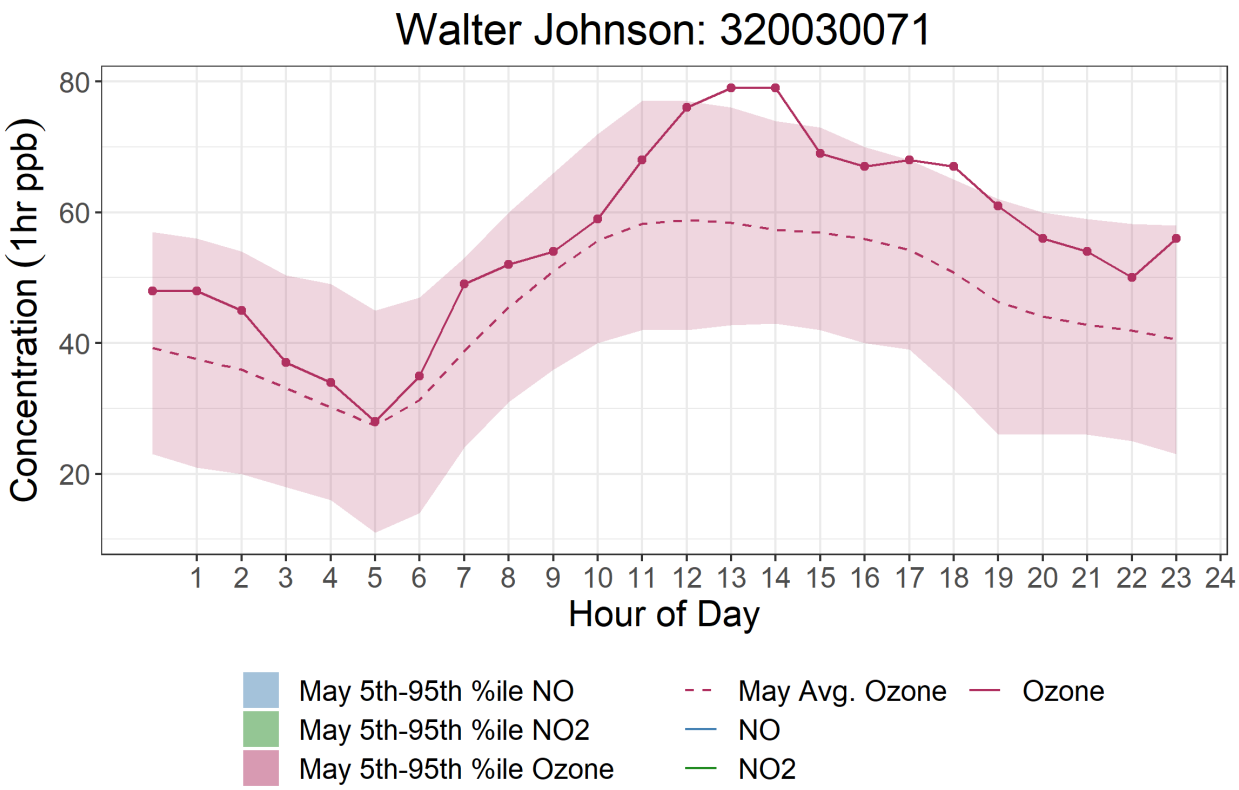


**Figure 3-53.** Diurnal profile of ozone concentrations (red) at the Walter Johnson site on May 9 and the 5-year seasonal average ozone (dotted lines). Shaded ribbons represent the five-year 5th-95th percentile range. NO and $NO_2$ data are not available at Walter Johnson.

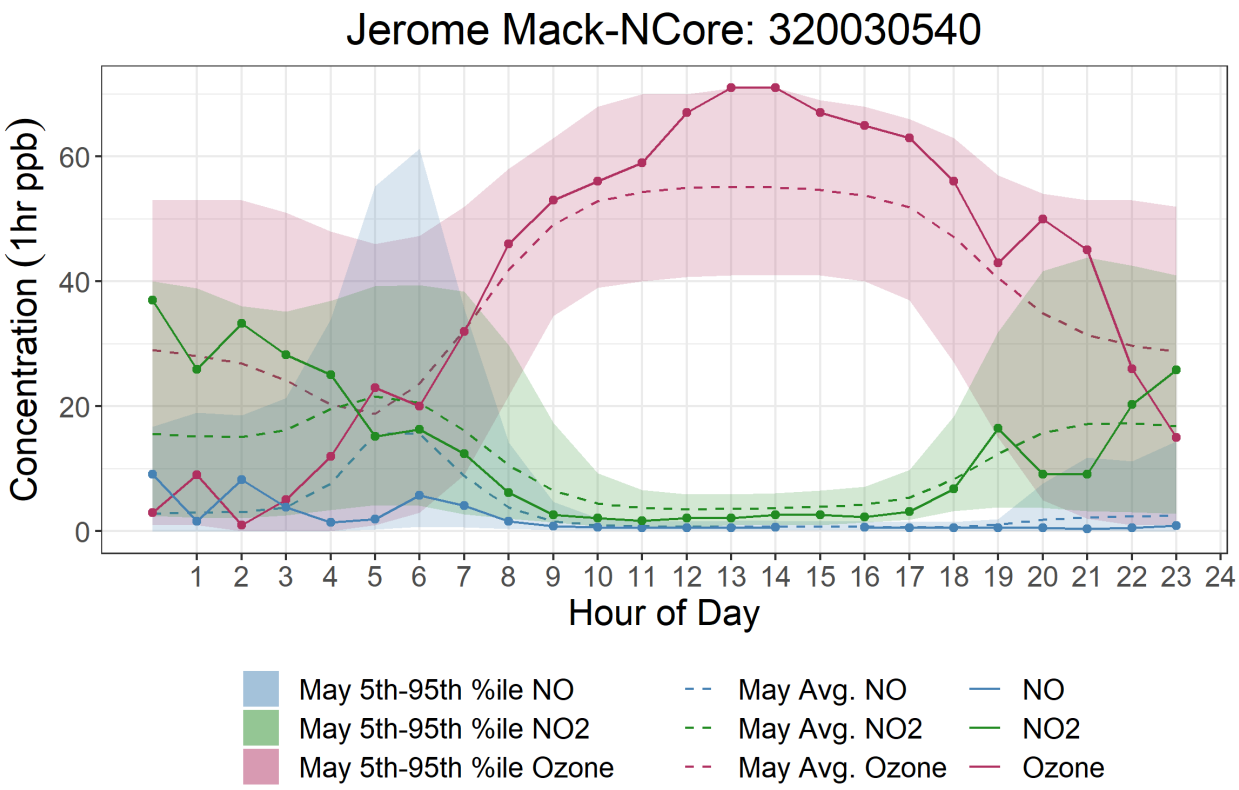


**Figure 3-54.** Diurnal profile of ozone concentrations (red), nitrogen dioxide ($NO_2$) concentrations (green), and nitric oxide (NO) concentrations (blue) at the Jerome Mack monitoring site in Clark County on May 9, compared to the seasonal averages (dotted lines). Shaded ribbons represent the 5th-95th percentile range. $NO_2$ data are available from 2017-2020, and NO and ozone data are available from 2015-2020.

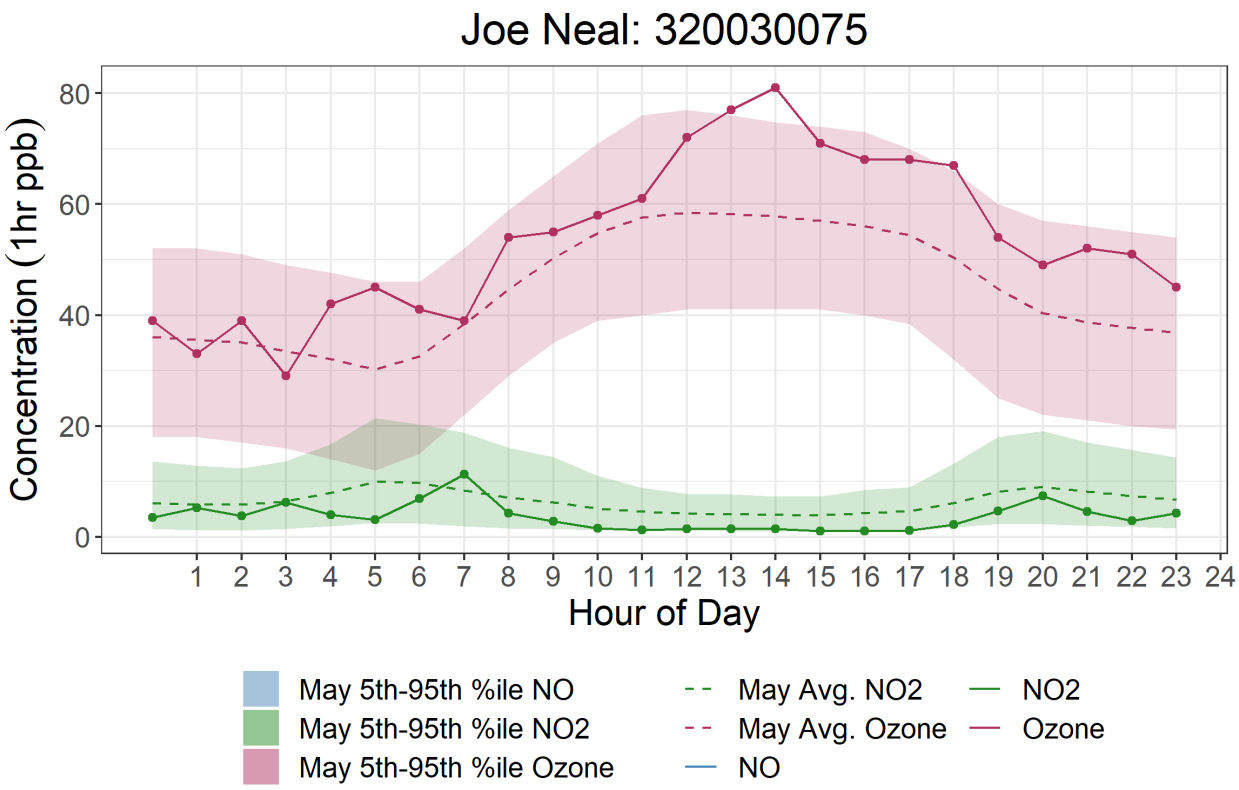


**Figure 3-55.** Diurnal profile of ozone concentrations (red) and nitrogen dioxide ($NO_2$) concentrations (green) at the Joe Neal reference site in Clark County on May 9, compared to the seasonal averages (dotted lines). Shaded ribbons represent the 5th-95th percentile range. $NO_2$ and ozone data are available from 2015-2020.

A map of observed MDA8 ozone concentrations on May 9, 2020, shows elevated ozone levels throughout southern California to the east of Los Angeles, the Central Valley, and southern Nevada within the Clark County border (Figure 3-56). Stations with recorded NAAQS ozone exceedances are colored orange or red. Four stations located in southern California reached MDA8 ozone concentrations between 86 and 106 ppb. In Clark County, the Paul Meyer and Walter Johnson stations exceeded the 2015 ozone NAAQS of 70 ppb on May 9, 2020. These stations were surrounded by stations that observed elevated MDA8 ozone concentrations (from 55 to under 71 ppb), but did not exceed the NAAQS. In Clark County, the highest observed value of 74 ppb was recorded at the Paul Meyer station. The Jean and Indian Springs stations often act as indicators of background ozone concentrations because they are not within the Las Vegas metropolitan area. Although the Indian Springs and Jean stations did not exceed NAAQS on May 9, both stations reached a moderate concentration between 66 and 68 ppb. Regionally high ozone concentrations, along with elevated background ozone recorded at the Indian Springs and Jean stations, provides additional evidence that suggests stratospheric ozone enhanced surface ozone on May 9, 2020.

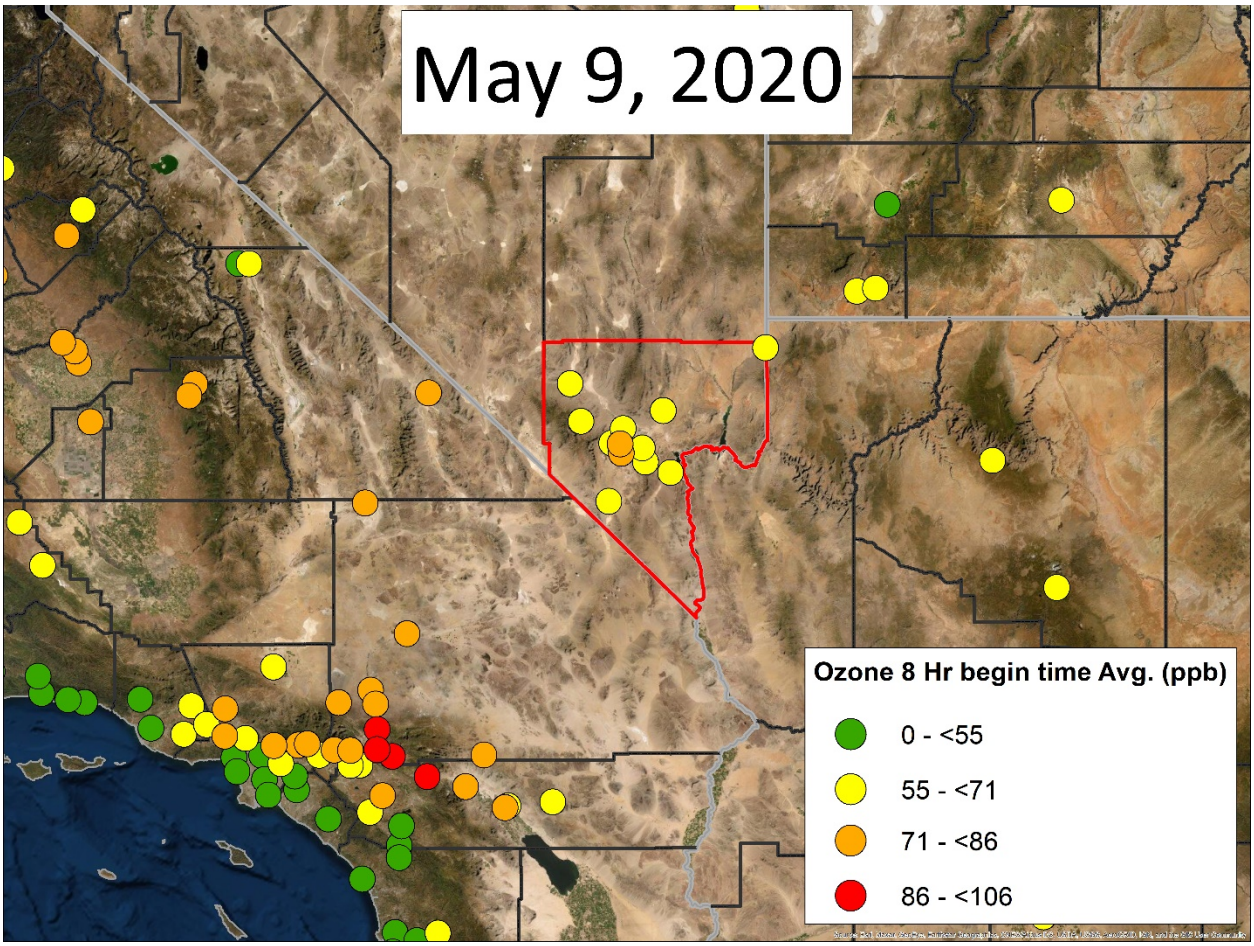


**Figure 3-56.** Observed maximum daily 8-hour average (MDA8) ozone on May 9, 2020, at stations in southern California, southern Nevada, western Arizona, and southwestern Utah.

We also produced maps of daily ozone Air Quality Index (AQI) for the two days leading up to and the day of the May 9 event. These maps show moderate and unhealthy ground-level AQI values (indicated by yellow, orange, and red area) across the southwestern United States, with unhealthy levels expanding between May 7 and 9 (Figure 3-57). Again, regionally high ozone/AQI can be indicative of stratospheric ozone influence. Based on low water vapor, regionally high ozone, and typical concentrations of $NO_x$, we suggest that ozone concentrations on May 9 were enhanced by an upwind SOI event and not purely due to photochemical production or transport from the Los Angeles basin.

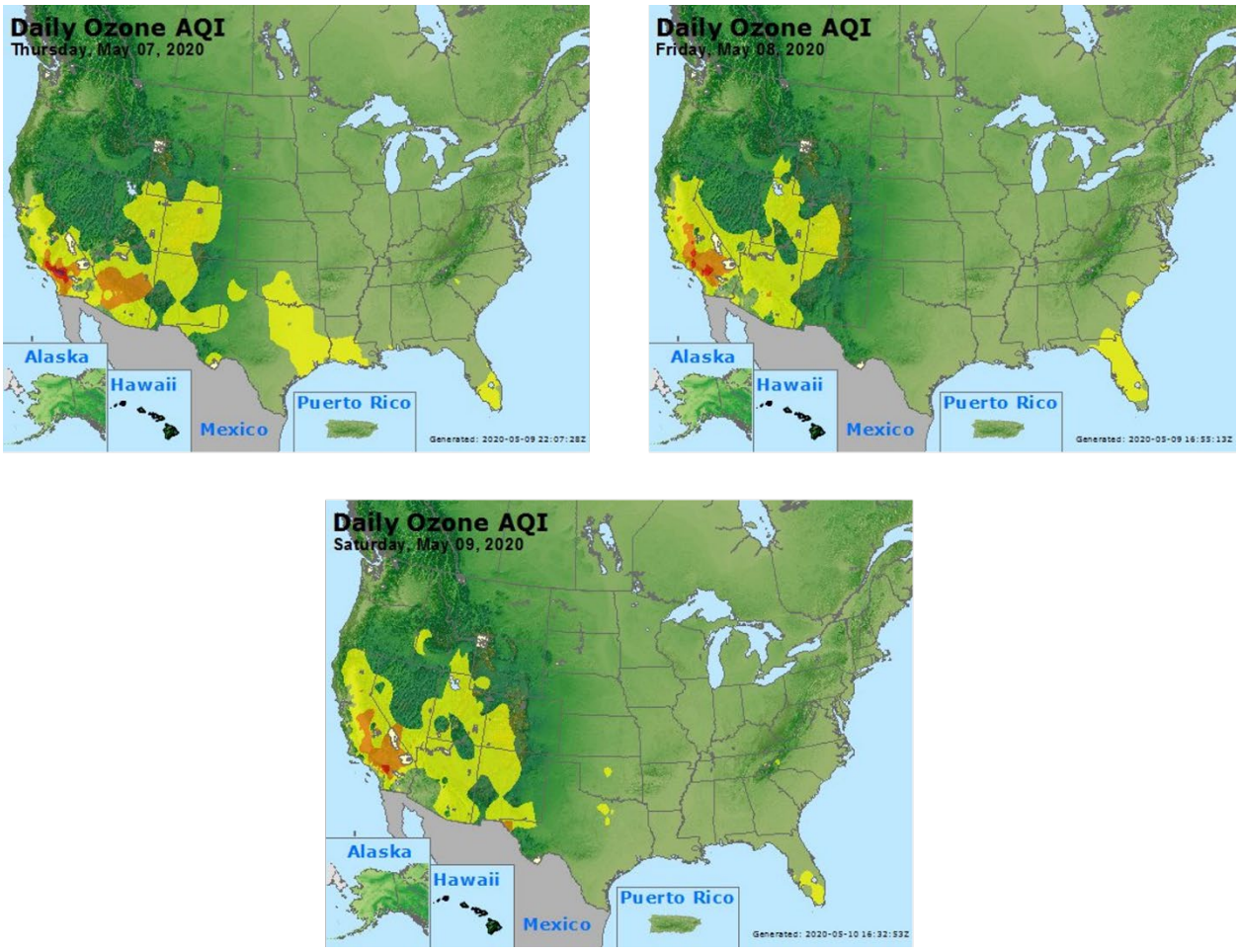


**Figure 3-57.** Daily ozone AQI for the two days before and the day of the May 9 event.

## 3.5 Additional Evidence

### 3.5.1 Matching Day Analysis

Ozone production and transport strongly depend on regional and local meteorological conditions. A comparison of ozone concentrations on suspected exceptional event days with non-event days that share similar meteorology can help identify periods when ozone production was affected by an atypical source. Given that similar meteorological days are likely to have similar ozone concentrations, noticeable differences in the levels of ozone between an event date and meteorologically similar days can lend evidence to a clear causal relationship between an SOI and elevated ozone concentration.

## Identify Meteorologically Similar Days

In order to identify the best matching meteorological days, both synoptic and local conditions were examined from ozone-season days (April 1 through September 30) between 2014 and 2020. Excluded from this set are days with suspected exceptional events in the 2018 and 2020 seasons, as well as dates within 5 days of the event date to ensure that lingering effects of smoke transport or stratospheric intrusion did not appear in the data.

To best represent similar air transport, twice daily HYSPLIT trajectories (initiated at 18:00 and 22:00 UTC) from Clark County for 2014-2020 were clustered by total spatial variance. The calculation, based on the difference between each point along a trajectory, provides seven distinct pathways of airflow into Clark County. The cluster that best represents the trajectory on the exceptional event day was chosen, and ozone-season days within the cluster were then subset for regional meteorological comparison to the exceptional event day.

For the meteorological comparison, a correlation score was assigned to each day from the cluster subset. The National Centers for Environmental Prediction (NCEP) reanalysis data was compiled for the ozone seasons in 2014-2020. Daily average wind speed, geopotential height, relative humidity, and temperature were considered at 1,000 mb and 500 mb. At the surface, daily average atmospheric pressure, maximum temperature, and minimum temperature were utilized. Pearson product-moment coefficient of linear correlation (pattern correlation) was calculated between the exceptional event date and each cluster-subset ozone-season day in 2014-2020 for each parameter. The pattern correlation calculates the similarity between two mapped variables at corresponding grid locations within the domain. The statistic was calculated using a regional domain of 30 °N – 45 °N latitude and 125°W – 105°W longitude. The correlation score for each day was defined as the average pattern correlation of all parameters at each height level. The correlations scores were then ranked by the highest correlation for 1,000 mb, surface, and finally 500 mb. Dates within 5 days of the exceptional event were removed from the similar day analysis to ensure the data are mutually exclusive. 50 dates with the highest rank correlation scores were then chosen as candidate matching days for further analysis.

Local meteorological conditions for the subset of candidate matching days were then compared to conditions on May 9, 2020, and filtered to identify five or more days that best matched the event date. Meteorological maps at the surface and at 500 mb, as well as local meteorological data describing temperature, wind, moisture, instability, mixing layer height, and cloud cover, were examined. The data source for each parameter is summarized in **Table 3-8**.

**Table 3-8.** Local meteorological parameters and their data sources.

| Meteorological Parameter | Data Source |
|---|---|
| Maximum Daily Temperature | Jerome Mack - NCore Monitoring Site |
| Average Daily Temperature | Jerome Mack - NCore Monitoring Site |
| Resultant daily wind direction | Jerome Mack - NCore Monitoring Site (calculated vector average) |
| Resultant daily wind speed | Jerome Mack - NCore Monitoring Site (calculated vector average) |
| Average daily wind speed | Jerome Mack - NCore Monitoring Site |
| Average daily relative humidity (RH) | Jerome Mack - NCore Monitoring Site |
| Precipitation | Jerome Mack - NCore Monitoring Site |
| Total daily global horizontal irradiance (GHI) | UNLV Measurement and Instrumentation Data Center (MIDC) in partnership with NREL (https://midcdmz.nrel.gov/apps/daily.pl?site=UNLV&start=20060318&yr=2021&mo=4&dy=29) |
| 4:00 p.m. local standard time (LST) mixing layer mixing ratio | Upper air soundings from KVEF (http://weather.uwyo.edu/upperair/sounding.html) |
| 4:00 p.m. LST lifted condensation level (LCL) | Upper air soundings from KVEF (http://weather.uwyo.edu/upperair/sounding.html) |
| 4:00 p.m. LST convective available potential energy (CAPE) | Upper air soundings from KVEF (http://weather.uwyo.edu/upperair/sounding.html) |
| 4:00 p.m. LST 1,000-500 mb thickness | Upper air soundings from KVEF (http://weather.uwyo.edu/upperair/sounding.html) |
| Daily surface meteorological map | NOAA's Weather Prediction Center Daily Weather Maps (https://www.wpc.ncep.noaa.gov/dailywxmap/index.html) |
| Daily 500 mb meteorological map | NOAA's Weather Prediction Center Daily Weather Maps (https://www.wpc.ncep.noaa.gov/dailywxmap/index.html) |

## Matching Day Analysis

The meteorological conditions on May 9, 2020, were not abnormal for the region at this time of year. Table 3-9 displays the percentile ranking of each examined meteorological parameter at the Jerome Mack- NCore site in the 30-day period surrounding May 9 (April 24 through May 24) across the years of 2014 through 2020, All examined meteorological parameters fall within the $10^{th}$ to $90^{th}$ percentile. As is typical for Clark County, there was no precipitation.

**Table 3-9.** Percentile rank of meteorological parameters on May 9, 2020, compared to the 30-day period surrounding May 9 over seven years (April 24 through May 24, 2014-2020).

| Date | Max Temp (°F) | Avg Temp (°F) | Resultant Wind Direction (°) | Resultant Wind Speed (mph) | Avg Wind Speed (mph) | Avg RH (%) | Precip. (in) | Total GHI (kWh/m$^2$) | Mixing Layer Mixing Ratio (g/kg) | LCL (mb) | CAPE (J/kg) | 500-1,000 mb Thickness (m) |
|---|---|---|---|---|---|---|---|---|---|---|---|---|
| 2020-05-09 | 35 | 18 | NA | 11 | 13 | 40 | NA | 24 | 19 | 23 | 77 | 15 |

The subset of synoptically similar days identified by the methodology above was further filtered based on parameters listed in Table 3-8 to match local meteorological conditions that existed on the event date. Table 3-10 shows the eight days that best match the meteorological conditions that existed on May 9, 2020, as well as the MDA8 ozone concentration at each site that experienced an exceedance on May 9. Three days from 2020 are included in Table 3-10—May 10, June 1, and June 5. These three days are particularly valuable comparisons to include in this analysis since they occurred under similar abnormal anthropogenic emissions—a result of Covid-19 restrictions—as the event date. Surface and upper-level maps for May 9 and each date listed in Table 3-10 show highly consistent conditions. All dates show a surface low pressure system and an upper-level ridge over Clark County. Most dates also show a region of high pressure at the surface that was directly east of the surface low pressure over Clark County. Surface and upper-level maps are included in Appendix B.

Table 3-10 shows the average MDA8 ozone concentration across these eight days with an expected range defined by one standard deviation, a conservative estimate given the small sample size. The average MDA8 ozone concentration across these eight days is well below the 70 ppb ozone standard at both sites that recorded an exceedance on May 9, with ozone concentration ranging from 58 to 60 ppb. Further, the upper end of the provided range at each site also falls below the ozone standard. None of these matching days exceeded the 70 ppb ozone standard at either site. This includes the matching days from 2020 that better match the levels of anthropogenic emissions that existed on May 9, 2020. This goes to show that an ozone exceedance on May 9 was unexpected based on meteorological conditions alone. If meteorology were the sole cause of the ozone exceedance on May 9, we would expect to see similarly high ozone levels on each of the similar days listed in Table 3-10, especially those with even warmer temperatures and higher GHI than experienced on May 9 alongside other similar conditions. With deep mixed layer depth, indicated by the lifted condensation layer (LCL), there is increased vertical dispersion of surface ozone. Therefore, lower ozone concentrations would be expected. This is evident in the similar meteorological days, which had an average LCL of 528 mb, but not seen in the May 9 event, which had an LCL height of 530 mb. These findings lend weight to the assertion that an external source of ozone contributed to the ozone exceedance on May 9, 2020.

**Table 3-10.** Top eight matching meteorological days to May 9, 2020. WJ and PM refer to monitoring sites Walter Johnson and Paul Meyer, respectively. Average MDA8 ozone concentration of meteorologically similar days is shown plus-or-minus one standard deviation rounded to the nearest ppb.

| Date | Max Temp (°F) | Avg Temp (°F) | Resultant Wind Direction (°) | Resultant Wind Speed (mph) | Avg Wind Speed (mph) | Avg RH (%) | Precip. (in) | Total GHI (kWh/m$^2$) | Mixing Layer Mixing Ratio (g/kg) | LCL (mb) | CAPE (J/kg) | 500-1,000 mb Thickness (m) | MDA8 Ozone Concentration (ppb) | |
|---|---|---|---|---|---|---|---|---|---|---|---|---|---|---|
| | | | | | | | | | | | | | PM | WJ |
| 2020-05-09 | 101 | 87.08 | 208.32 | 0.97 | 2.89 | 10.33 | 0 | 8.26 | 3.39 | 530 | 128 | 5797 | 74 | 71 |
| 2014-05-16 | 99 | 86.54 | 221.62 | 2.55 | 3.92 | 11.62 | 0 | 7.48 | 2.01 | 482 | 0 | 5814 | 64 | 61 |
| 2014-06-12 | 101 | 92.96 | 198.7 | 6.01 | 7.77 | 12.42 | 0 | 8.82 | 2.65 | 496 | 0 | 5852 | 68 | 67 |
| 2015-06-15 | 107 | 96.75 | 210.65 | 4.05 | 6.05 | 14.58 | 0 | 8.52 | 5.86 | 560 | 105 | 5905 | 60 | 58 |
| 2015-08-23 | 105 | 94.21 | 191.25 | 2.08 | 3.34 | 17.04 | 0 | 7.45 | 5.8 | 566 | 0 | 5883 | 51 | 49 |
| 2017-05-05 | 99 | 86.12 | 210.72 | 3.67 | 5.47 | 15.12 | 0 | 7.6 | 3.62 | 539 | 152 | 5793 | 60 | 62 |
| 2019-06-13 | 107 | 95.46 | 218.59 | 5.25 | 6.93 | 11.29 | 0 | 8.96 | 3.34 | 510 | 0 | 5874 | 62 | 61 |
| 2020 Dates | | | | | | | | | | | | | | |
| 2020-06-05 | 102 | 92.96 | 157.18 | 5.75 | 6.80 | 10.79 | 0 | 8.11 | 3.55 | 530 | 0 | 5834 | 54 | 52 |
| 2020-06-01 | 101 | 89.75 | 183.96 | 1.90 | 3.86 | 11.5 | 0 | 7.97 | 3.75 | 543 | 0 | 5814 | 56 | 54 |
| Average MDA8 Ozone Concentration of Meteorologically Similar Days | | | | | | | | | | | | | **59** ± 6 | **58** ± 6 |

### 3.5.2 GAM Statistical Modeling

Generalized additive models (GAM) are a type of statistical model that allows the user to predict a response based on linear and non-linear effects from multiple variables (Wood, 2017a). These models tend to provide a more robust prediction than Eulerian photochemical models or simple comparisons of similar events (Simon et al., 2012; Jaffe et al., 2013; U.S. Environmental Protection Agency, 2016). Camalier et al. (2007) successfully used GAM modeling to predict ozone concentrations across the eastern United States using meteorological variables with $R^2$ values of up to 0.8. Additionally, previous concurred exceptional event demonstrations and associated literature, i.e., Sacramento Metropolitan Air Quality Management District (2011), Alvarado et al. (2015), Louisiana Department of Environmental Quality (2018), Arizona Department of Environmental Quality (2016), and Pernak et al. (2019) used GAM modeling to predict ozone events that exceed the NAAQS standards, some in EE cases. By comparing the GAM-predicted ozone values to the actual measured ozone concentrations (i.e., residuals), we can determine the effect of outside influences, such as wildfires or stratospheric intrusions, on ozone concentrations each day (Jaffe et al., 2004). High, positive residuals suggest a non-typical source of ozone in the area but cannot specifically identify a source. Gong et al. (2017) and McClure and Jaffe (2018) used GAM modeling, in addition to ground and satellite measurements of wildfire pollutants, to estimate the enhancement of ozone during wildfire smoke events. Similar to other concurred EE demonstrations, we used GAM modeling of meteorological and transport variables to estimate the MDA8 ozone concentrations at multiple sites across Clark County for 2014-2020. To estimate the effect of wildfire smoke on ozone concentrations, we can couple the GAM residual results (observed MDA8 ozone–GAM-predicted MDA8 ozone) with the other analyses to confirm that the non-typical enhancement of ozone is due to a stratospheric intrusion on May 9, 2020.

Using the same GAM methodology as prior concurred EE demonstrations and the studies mentioned above, we examined more than 30 meteorological and transport predictor variables, and through testing, compiled the 16 most important variables to estimate MDA8 ozone each day at eight monitoring sites across Clark County, Nevada (Paul Meyer, Walter Johnson, Joe Neal, Green Valley, Boulder City, Jean, Indian Springs, and Jerome Mack). As suggested by EPA guidance (U.S. Environmental Protection Agency, 2016), we used meteorological variables measured at each station (the previous day's MDA8 ozone, daily min/max temperature, average temperature, temperature range, wind speed, wind direction, or pressure), if available (see Table 2-1). If meteorological variables were not available at a specific site, we supplemented the data with National Centers for Environmental Prediction (NCEP) reanalysis meteorological data to fill any data gaps. We also tested filling data gaps with Jerome Mack meteorological data and found results had no statistical difference. We used sounding data from KVEF (Las Vegas Airport) to provide vertical meteorological components; soundings are released at 00:00 and 12:00 UTC daily. Variables such as temperature, relative humidity, wind speed, and wind direction were averaged over the first 1000 m above the surface to provide near-surface, vertical meteorological parameters. Other sounding variables, such as Convective Available Potential Energy (CAPE), Lifting Condensation Level (LCL) pressure, mixing layer potential temperature, mixed layer mixing ratio, and 500-1,000 hPa thickness provided

additional meteorological information about the vertical column above Clark County. We also initiated HYSPLIT GDAS 1°x1° 24-hour back trajectories from downtown Las Vegas (36.173° N, -115.155° W, 500 m agl) at 18:00 and 22:00 UTC (10:00 a.m. and 2:00 p.m. local standard time) each day to provide information on morning and afternoon transport during critical ozone production hours. We clustered the twice per day back trajectories from 2014-2020 into seven clusters. Figure 3-58 shows the clusters, percentage of trajectories per cluster, and heights of each trajectory cluster. We identified a general source region for each cluster: (1) Northwest U.S., (2) Stagnant Las Vegas, (3) Central California, (4) Long-Range Transport, (5) Northern California, (6) Southern California, and (7) Baja Mexico. Within the GAM, we use the cluster value to provide a factor for the distance traveled by each back trajectory. Additionally, day of year (DOY) was used in the GAM to provide information on season and weekly processes. The year (2014, 2015, etc.) was used a factor for the DOY parameter to distinguish interannual variability.

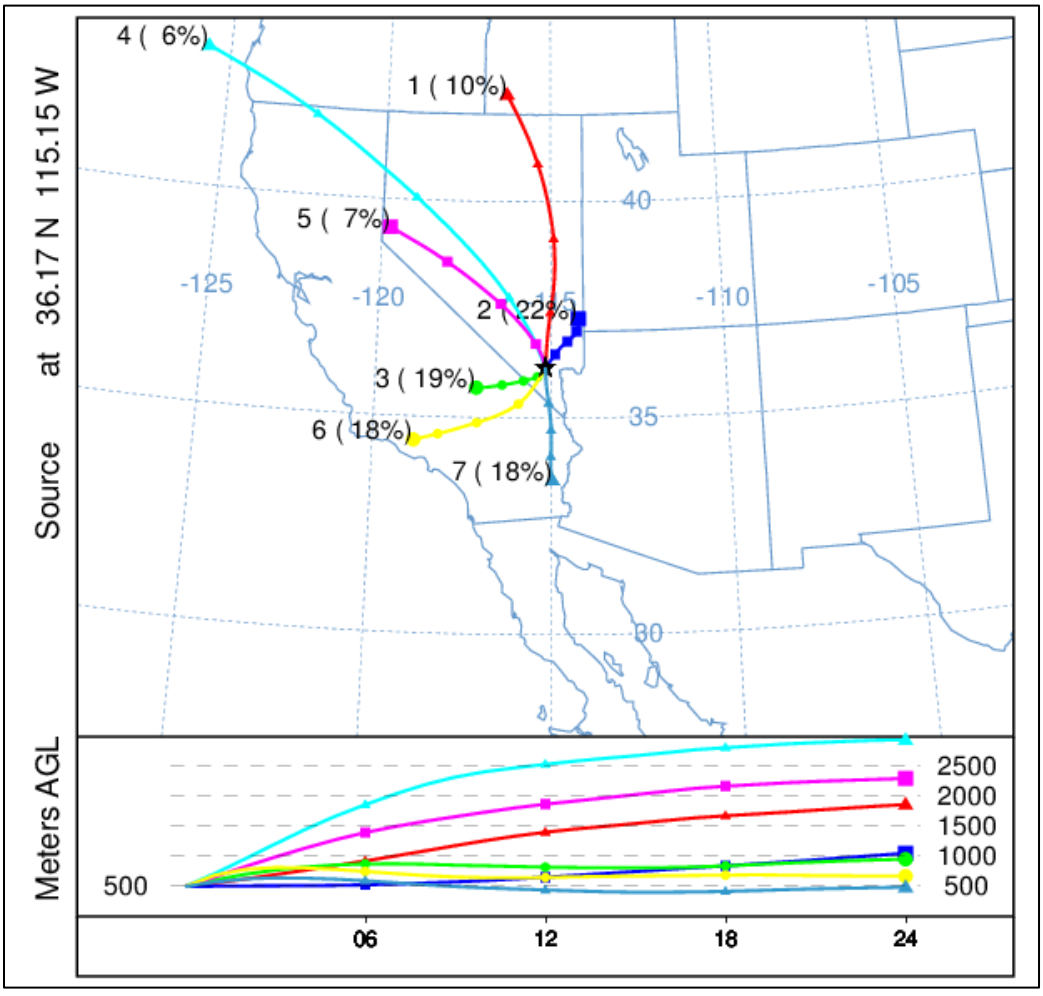


**Figure 3-58.** Clusters for 2014-2020 back trajectories. Seven unique clusters were identified for the twice daily (18:00 and 22:00 UTC) back-trajectories for 2014-2020 initiated in the middle of the Las Vegas Valley. The percentage of trajectories per cluster is shown next to the cluster number. The height of each cluster is shown below the map.

Once all the meteorological and transport variables were compiled, we inserted them into the GAM equation to predict MDA8 ozone:

$$g(MDA8\ O_{3,i}) = f_1(V1_i) + f_2(V2_i) + f_3(V3_i) + \cdots + residual_i$$

where $f_i$ are fit functions calculated from penalized cubic regression splines of observations (allowing non-linearity in the fit), Vi are the variables, and $i$ is the daily observation. All variables were given a cubic spline basis except for wind direction, which used a cyclic cubic regression spline basis. For DOY and back trajectory distances, we used year factors (i.e., 2014-2020) and cluster factors (i.e., 1-7) to distinguish interannual variability and source region differences. The factors provide a different smooth function for each category (Wood, 2017b). For example, the GAM smooth of DOY for 2014 can be different than 2015, 2016, etc. In order to optimize the GAM, we first must adjust knots or remove any variables that are over-fitting or under-performing. We used the "mgcv" R package to summarize and check each variable for each monitoring site (Wood, 2020). A single GAM equation (using the same variables) was used for each monitoring site for consistency. During the initial optimization process, we removed the proposed 2018 and 2020 EE days from the dataset. We also ran 10 cross-validation tests by randomly splitting data 80/20 between training/testing for each monitoring site to ensure consistent results. All cross-validation tests showed statistically similar results with no large deviations for different data splits. We used data from each site during April-September ozone seasons for 2014 through 2020, which is consistent with other papers modeling urban ozone (e.g., Pernak et al., 2019; McClure and Jaffe, 2018; Solberg et al., 2018; Solberg et al., 2019) and ozone concentrations during the periods with exceptional events are within the representative range of ozone in the GAM model.

Table 3-11 shows the variables used in the GAM and their F-value. The F-value suggests how important each variable is (higher value = more important) when predicting MDA8 ozone. Any bolded F-values had a statistically significant correlation ($p < 0.05$). $R^2$, the positive 95$^{th}$ quantile of residuals, and normalized mean square residual values for each monitoring site are listed at the bottom of the table.

**Table 3-11.** GAM variable results. F-values per parameter used in the GAM model are shown for each site. Units and data source for each parameter in the GAM model are shown on the right of the table. 95th quantile, $R^2$, and normalized mean square residual information is shown at the bottom of the table.

| Parameters | Paul Meyer | Walter Johnson | Joe Neal | Green Valley | Jerome Mack | Boulder City | Jean | Indian Springs | Unit | Source |
|---|---|---|---|---|---|---|---|---|---|---|
| Day of Year (DOY) factored by Year (2014-2020) | **8.11** | **7.09** | **7.65** | **11.8** | **7.94** | **7.11** | **8.68** | **7.53** | -- | -- |
| Previous Day MDA8 Ozone | **37.9** | **22.7** | **41.5** | **18.1** | **27.9** | **31.3** | **105.5** | **123.8** | ppb | Monitor Data |
| Average Daily Temperature | 1.92 | **2.90** | **4.80** | 0.05 | 1.83 | 2.13 | 0.12 | 1.83 | K | Monitor Data/NCEP Reanalysis |
| Maximum Daily Temperature | 1.37 | **2.74** | **2.48** | 0.16 | 0.38 | 0.02 | 1.30 | 1.52 | K | |
| Temperature Range (TMax - TMin) | **4.12** | 2.13 | 1.38 | 1.74 | 1.77 | 1.51 | 0.50 | 0.54 | K | |
| Average Daily Pressure | **5.54** | **6.42** | **6.74** | **4.64** | **2.94** | 0.22 | 2.17 | 0.24 | hPa | |
| Average Daily Wind Speed | **11.1** | **5.03** | **7.49** | **5.02** | **15.3** | 0.07 | 0.49 | 2.19 | knots | |
| Average Daily Wind Direction | 0.47 | **1.04** | 0.24 | **1.35** | **2.43** | 0.69 | 0.11 | **2.48** | deg | |
| 18 UTC HYSPLIT Distance factored by Cluster | 1.70 | 1.82 | 1.69 | 0.92 | 2.52 | 2.97 | 1.66 | 1.03 | km | HYSPLIT Back-Trajectories |
| 22 UTC HYSPLIT Distance factored by Cluster | 1.03 | 0.74 | 1.47 | 1.47 | 1.20 | 1.26 | 1.19 | 0.50 | km | |
| 00 UTC Convective Available Potential Energy | 3.50 | 0.13 | 0.37 | 1.17 | 1.16 | 0.57 | **5.71** | **6.49** | J/kg | Sounding Data |
| 00 UTC Lifting Condensation Level Pressure | 1.36 | **2.78** | 2.29 | 2.41 | **3.76** | 0.38 | 1.43 | 0.38 | hPa | |
| 00 UTC Mixing Layer Potential Temperature | 0.65 | 0.79 | 1.72 | 0.10 | 1.23 | 0.97 | 1.09 | 2.53 | K | |
| 00 UTC Mixed Layer Mixing Ratio | **2.10** | **2.76** | **2.85** | **3.09** | **3.07** | **2.42** | 0.69 | 1.04 | g/kg | |
| 00 UTC 500-1000 hPa Thickness | **2.91** | 0.43 | 1.70 | 1.60 | 1.69 | **4.11** | **2.18** | 1.83 | m | |
| 12 UTC 1km Average Relative Humidity | **12.4** | **14.6** | **17.8** | **21.3** | **37.5** | **26.0** | **11.1** | 2.18 | % | |
| | | | | | | | | | | |
| 95th Quantile of Positive Residuals (ppb) | 10 | 10 | 10 | 10 | 9 | 9 | 9 | 10 | | |
| $R^2$ | 0.55 | 0.58 | 0.60 | 0.58 | 0.61 | 0.58 | 0.57 | 0.55 | | |
| Normalized Mean Square Residual | 3.6E-06 | 7.3E-04 | 6.1E-05 | 1.3E-04 | 3.1E-05 | 1.3E-04 | 1.2E-04 | 1.5E-04 | | |

Table 3-12 provides GAM residual and fit results for all sites for the ozone seasons of 2014 through 2020. Overall, the residuals are low for all data points, and similarly low for all non-EE days. However, the 2018 and 2020 EE day residuals are significantly higher than the non-EE day results, meaning there are large, atypical influences on these days. Figure 3-59 shows non-EE vs EE median residuals with the 95$^{th}$ confidence intervals denoted as notches in the boxplots. We show the data in both ways to provide specific values, as well as illustrate the difference in non-EE vs EE residuals. Since the 95$^{th}$ confidence intervals for median EE residuals are above and do not overlap with those for non-EE residuals at any site in Clark County, we can state that the median residuals are higher and statistically different ($p<0.025$). The $R^2$ for each site ranged between 0.55 and 0.61, suggesting a good fit for each monitoring site, and similar to the results in prior studies and EE demonstrations mentioned previously ($R^2$ range of 0.4-0.8). We also provide the positive 95$^{th}$ quantile MDA8 ozone concentration, which is used to estimate a "No Fire" MDA8 ozone value based on the EPA guidance (U.S. Environmental Protection Agency, 2016). We also provide the median residuals (and confidence interval) for all non-EE days with observed MDA8 at or above 60 ppb; this threshold was needed to build a sufficient sample size with a representative distribution, and derive the median and 95% confidence interval. It should be noted that four out of the seven years modeled by the GAM were high wildfire years, and these values likely include a significant amount of wildfire days. We were not able to systematically remove wildfire influence by subsetting the Clark County ozone data based on HMS smoke, HMS smoke and $PM_{2.5}$ concentrations, and low wildfire years. These methods produced a significant number of false positives and negatives, and yielded datasets that were still affected by wildfire smoke. Therefore, these values should be considered an upper estimate of residuals for high ozone days. We see that the median residuals for 2018 and 2020 EE days are significantly higher than those on non-EE high observed ozone days since their confidence intervals do not overlap (or are comparable for the Jerome Mack station). The non-EE day residuals on days where observed MDA8 was at or above 60 ppb were determined to be normally distributed with a slight positive skew (median skewness = 0.39).

**Table 3-12.** Overall 2014-2020 GAM median residuals and 95% confidence interval range in square brackets for each site modeled. Sample size is shown in parentheses below the residual statistics. For sample sizes less than ten, we include a range of residuals in square brackets instead of the 95% confidence interval. Residual results are split by non-EE days and the 2018 and 2020 EE days. $R^2$ for each site is also shown along with the positive 95th quantile result.

| Site Name | All Residuals (ppb) | Non-EE Day Residuals (ppb) | 2018 & 2020 EE Day Residuals (ppb) | $R^2$ | Positive 95th Quantile (ppb) | Non-EE Day Residuals when MDA8 ≥ 60 ppb (ppb) |
|---|---|---|---|---|---|---|
| Boulder City | 0.22 [-0.04, 0.48] (1,132) | 0.22 [-0.04, 0.48] (1,130) | 12.05 [10.38-13.72] (2) | 0.58 | 9 | 4.05 [3.55, 4.55] (200) |
| Green Valley | 0.17 [-0.15, 0.48] (948) | 0.10 [-0.21, 0.41] (934) | 7.38 [5.40, 9.36] (14) | 0.58 | 10 | 3.76 [3.28, 4.23] (271) |
| Indian Springs | 0.13 [-0.18, 0.44] (1,014) | 0.08 [-0.22, 0.38] (1,010) | 12.30 [9.37-17.19] (4) | 0.55 | 10 | 4.79 [4.26, 5.32] (201) |
| Jean | 0.21 [-0.06, 0.48] (1,149) | 0.20 [-0.07, 0.47] (1,146) | 12.57 [9.59-13.90] (3) | 0.57 | 9 | 3.40 [2.94, 3.85] (290) |
| Jerome Mack | 0.09 [-0.19, 0.36] (1,152) | 0.05 [-0.22, 0.32] (1,141) | 6.83 [4.21, 9.45] (11) | 0.61 | 9 | 3.83 [3.32, 4.33] (242) |
| Joe Neal | 0.23 [-0.08, 0.54] (1,113) | 0.17 [-0.13, 0.47] (1,097) | 7.77 [5.79, 9.75] (16) | 0.60 | 10 | 3.32 [2.92, 3.71] (377) |
| Paul Meyer | 0.21 [-0.08, 0.50] (1,159) | 0.10 [-0.19, 0.39] (1,137) | 8.11 [6.34, 9.88] (22) | 0.55 | 10 | 3.58 [3.19, 3.97] (388) |
| Walter Johnson | 0.27 [-0.03, 0.57] (1,163) | 0.19 [-0.10, 0.48] (1,141) | 7.16 [5.11, 9.21] (22) | 0.58 | 10 | 3.53 [3.13, 3.93] (379) |

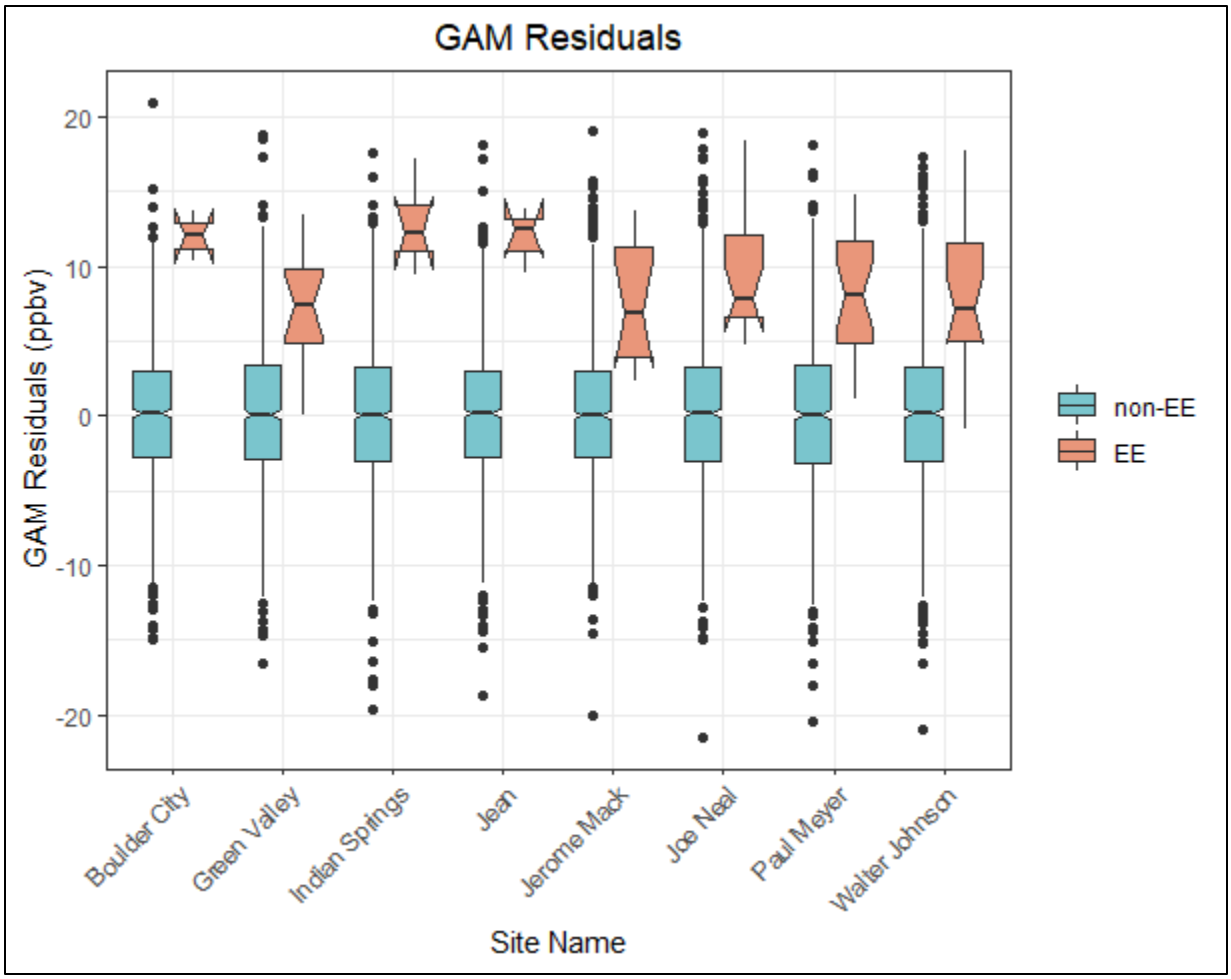


**Figure 3-59.** Exceptional event vs. non-exceptional event residuals. Non-exceptional events (non-EE in blue) and exceptional events (EE in orange) residuals are shown for each site modeled in Clark County. The notches for each box represent the 95$^{th}$ confidence interval. This figure illustrates the information in Table 3-12.

Overall, the GAM results show low bias and consistently significantly higher residuals on EE days compared with non-EE days. We also evaluated the GAM performance on verified high ozone, non-smoke days by looking at specific case studies. This was done to assess whether high-ozone days, such as the EE days, have a consistent bias that is not evident in the overall or high ozone day GAM performance. Out of the seven years used in the GAM model, four were high wildfire years in California (2015, 2017, 2018, and 2020). Since summer winds in Clark County are typically out of California (44% of trajectories originate in California according to the cluster analysis [not including transport through California in the Baja Mexico cluster]), wildfire smoke is likely to affect a large portion of summer days and influence ozone concentrations in Clark County. We identified specific case studies where most monitoring sites in Clark County had an MDA8 ozone concentration greater than or equal to 60 ppb and had no wildfire influence; "no wildfire influence" was determined by

inspecting HMS smoke plumes and HYSPLIT back trajectories for each day and confirming no smoke was over, near, or transported to Clark County. We found one to two examples from each year used in the GAM modeling, and required that at least half of the case study days needed to include an exceedance of the ozone NAAQS. **Table 3-13** shows the results of these case studies. Most case study days, including NAAQS exceedance days, show positive and negative residuals even when median ozone is greater than or equal to 65 ppb in Clark County, similar to the results for the entire multi-year dataset. GAM residuals on non-EE days when MDA8 is at or above 60 ppb have a median of 3.69 [95% confidence interval: 3.47, 3.88] (see Table 3-12). The high ozone, non-smoke case study days all show median residuals within or below the confidence interval of the high ozone residuals (from Table 3-12), meaning that the GAM model is able to accurately predict high ozone, non-smoke days within a reasonable range of error. Two additional factors indicate the GAM has good performance on normal, high ozone days: (1) the median residuals for the case studies are mostly lower than the 95% confidence interval of high ozone residuals (i.e., includes non-EE wildfire days), and (2) the case study days were verified as non-smoke days. Thus, residuals above the 95$^{th}$ confidence interval of the median residuals, such as those on the EE days, are statistically higher than on days with comparable high ozone concentrations, and not biased high because of the high ozone concentrations on these days.

**Table 3-13.** GAM high ozone, non-smoke case study results. Median GAM residuals for ten days in 2014-2020 are shown where most monitoring sites had MDA8 ozone concentrations of 60 ppb or greater. Sites used to calculate the MDA8 and GAM residual median/range are listed in the Clark County AQS site number column by site number.

| Date | Clark County AQS Site Number | Median (Range) of Observed MDA8 Ozone (ppb) | Median (Range) GAM Residual (ppb) |
|---|---|---|---|
| 5/17/2014 | 0601, 0075, 1019, 0540, 0043, 0071 | 66 (64-71) | 1.66 (-0.53-4.28) |
| 6/4/2014 | 0601, 0075, 0540, 1019, 0043, 0071 | 69 (66-72) | 3.46 (1.70-4.80) |
| 6/3/2015 | 1019, 0043, 0075, 0540, 7772, 0601, 0071 | 71 (65-72) | 3.01 (-0.34-5.77) |
| 6/20/2015 | 0601, 0298, 7772, 1019, 0540, 0075, 0043, 0071 | 65 (63-70) | 1.40 (-6.20-5.28) |
| 6/3/2016 | 0298, 1019, 0075, 0540, 0043, 0071 | 65 (63-71) | 3.89 (1.89-5.26) |
| 7/28/2016 | 0075, 0071, 0298, 0540, 0043 | 70 (63-72) | 0.24 (-5.95-3.67) |
| 6/17/2017 | 0601, 0075, 0071, 1019, 0540, 0298, 0043 | 66 (63-72) | 1.85 (-1.94-7.01) |
| 6/4/2018 | 0601, 0298, 7772, 1019, 0540, 0075, 0043, 0071 | 65 (60-67) | 3.06 (-0.91-3.60) |
| 5/5/2019 | 0601, 0298, 7772, 1019, 0540, 0075, 0043, 0071 | 65 (62-67) | 1.28 (-2.00-3.42) |
| 5/15/2020 | 0298, 0043, 0075, 0071 | 63 (63-65) | 1.52 (1.09-3.49) |

We also evaluate the bias of GAM residuals versus predicted MDA8 ozone concentrations in Figure 3-60. Residuals (i.e., observed ozone minus GAM-predicted MDA8 ozone) should be independent of the GAM-predicted ozone value, meaning that the difference between the actual ozone concentration on a given day and the GAM output should be due to outside influences and not well described by meteorological or seasonal values (i.e., variables used in the GAM prediction). Therefore, in a well-fit model, positive and negative residuals should be evenly distributed across all

GAM-predicted ozone concentrations and on average zero. In Figure 3-60, we see daily GAM residuals at all eight monitoring sites in Clark County from 2014-2020, the residuals are evenly distributed across all GAM-predicted ozone concentrations, with no pattern or bias at high or low MDA8 fit concentrations. This evaluation of bias in the model is consistent with established literature and other EE demonstrations (Gong et al., 2018; McVey et al., 2018; Pernak et al., 2019; Texas Commission on Environmental Quality, 2021), and indicate a well-fit model. In Figure 3-61, we also provide a histogram of the residuals at each monitoring site modeled in Clark County. This analysis shows that residuals at each site are distributed normally around a median near zero, and none of the distributions shows significant tails at high or low residuals (median skew = 0.05 with 95% confidence interval [-0.03, 0.12]). This analysis of error in the model and our results are consistent with previously concurred EE demonstrations (Arizona Department of Environmental Quality, 2016) and previous literature (Jaffe et al., 2013; Alvarado et al., 2015; Gong et al., 2018; McClure and Jaffe, 2018; Pernak et al., 2019). Appendix C provides GAM residual analysis from the concurred ADEQ and submitted TCEQ demonstrations that compare well with our GAM residual results. Based on these analysis methods, bias in the model is low throughout the range of MDA8 prediction values and confirms that the GAM can be used to predict MDA8 ozone concentrations in Clark County.

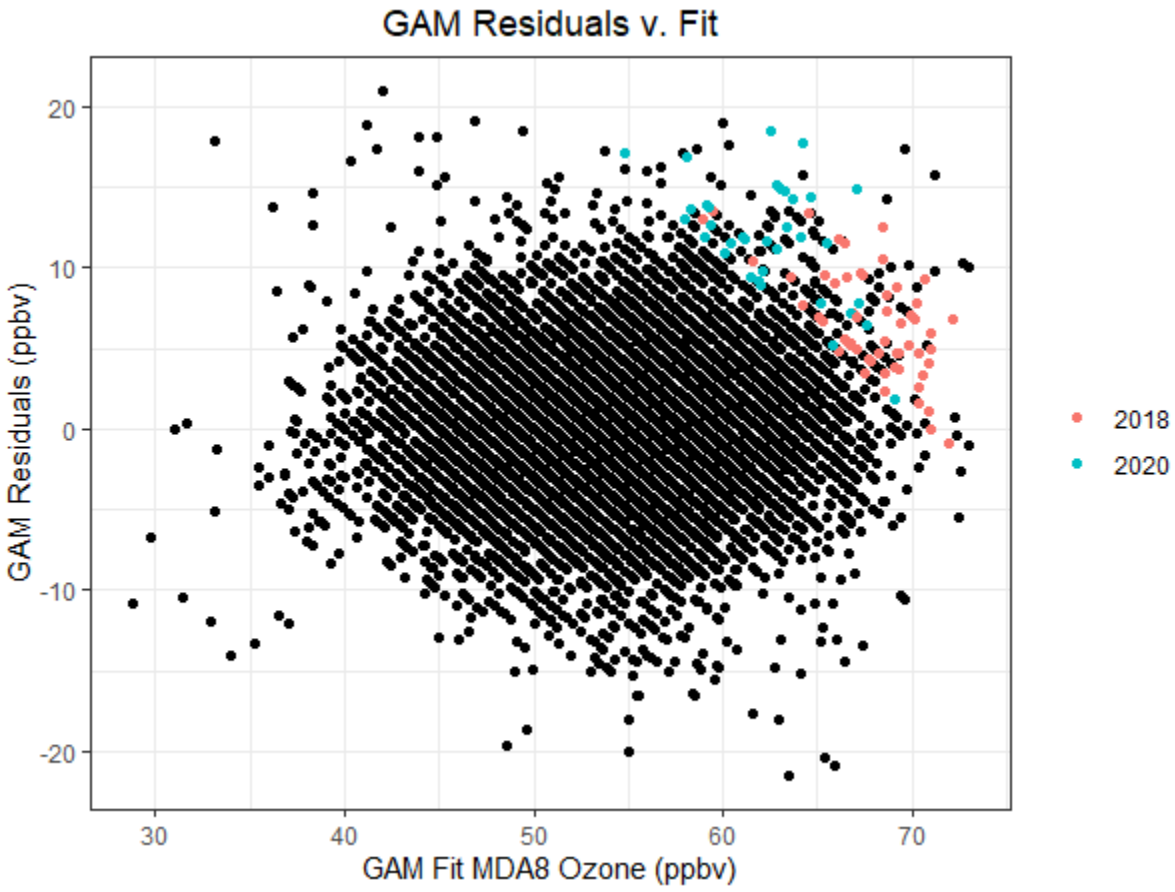


**Figure 3-60.** Daily GAM residuals for 2014-2020 vs GAM Fit (Predicted) MDA8 Ozone values. 2018 and 2020 exceptional events residuals are shown in red and blue.

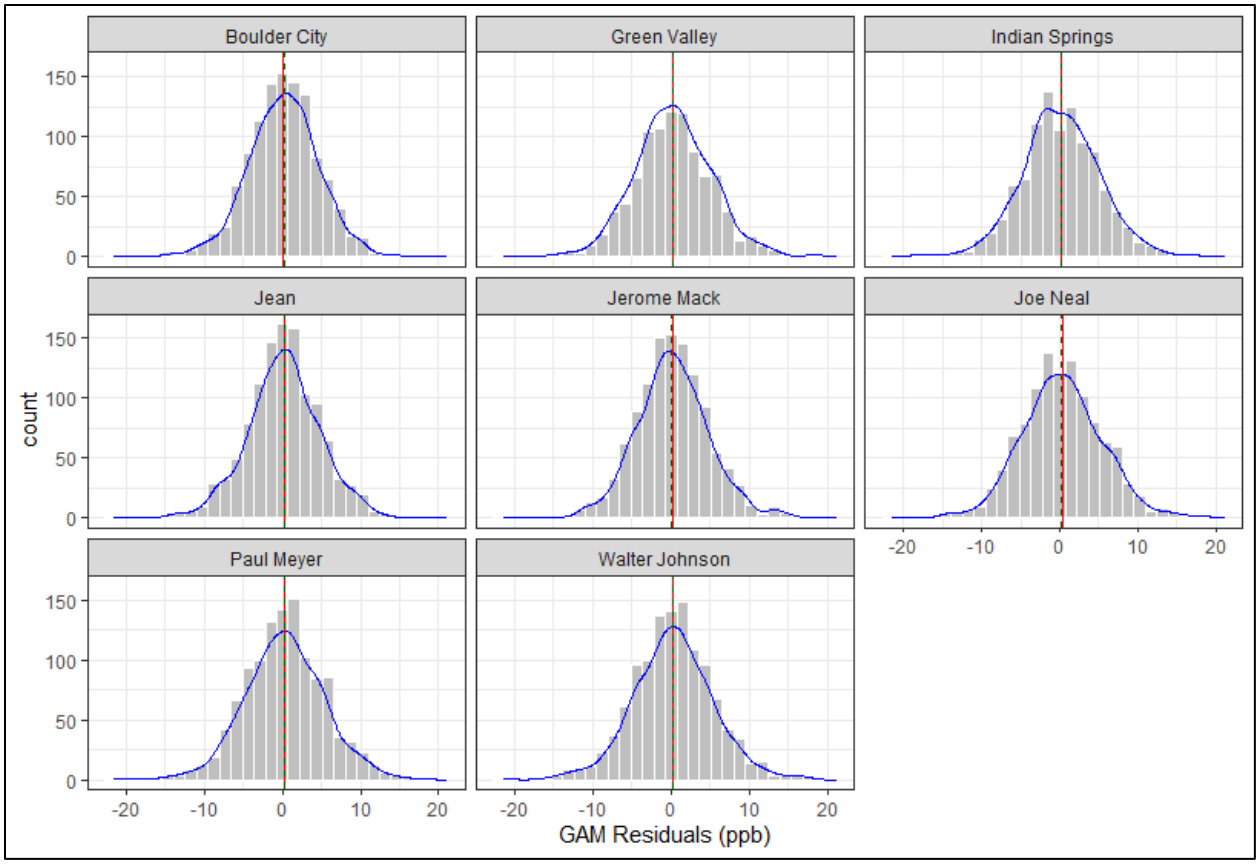


**Figure 3-61.** Histogram of GAM residuals at all modeled Clark County monitoring sites. The red line indicates the mean and the green dashed line indicates the median. The blue line provides the density distribution.

Within the GAM model, we include HYSPLIT 24-hour distance values, which are factored by cluster, to provide source region and stagnation information into the algorithm. A major upwind pollution source for Las Vegas is the Los Angeles Basin (see the Southern California cluster), which is around 400 km away. Since the GAM model uses source region and distance traveled information to help predict daily MDA8 ozone concentrations, contributions from LA should be accounted for in the algorithm. Based on this, we can assess whether GAM residuals on LA-source region days were significantly different from other source regions. In Figures 3-62 and 3-63, we subset the GAM results by removing any potential EE days. From these results, we find that both morning (18:00 UTC) and afternoon (22:00 UTC) trajectory data have similar distributions for all clusters. The notches in the box plots (representing the 95$^{th}$ confidence interval) provide an estimate of statistical difference, and show that the median of residuals is near zero for all clusters. The Northwest U.S. cluster at 18:00 UTC shows slightly negative residuals, while the Long-Range Transport cluster shows slightly positive residuals for both 18:00 and 22:00 UTC. The Southern California cluster shows a median residual of around zero for both 18:00 and 22:00 UTC trajectories, with significant overlap between the 95$^{th}$ confidence intervals of most other clusters (not statistically different). Additionally, the number of data points per cluster (bottom of each figure) corresponds well with transport from California being

dominant for the April through September time frame. Overall, this analysis provides evidence that even when the Los Angeles Basin (Southern California cluster) is upwind of Las Vegas, the GAM model performs well (low median residuals), and the results are statistically similar to most of the other clusters. This implies that when residuals are large, the Los Angeles Basin influence is unlikely to be the only contributor to enhancements in MDA8 ozone.

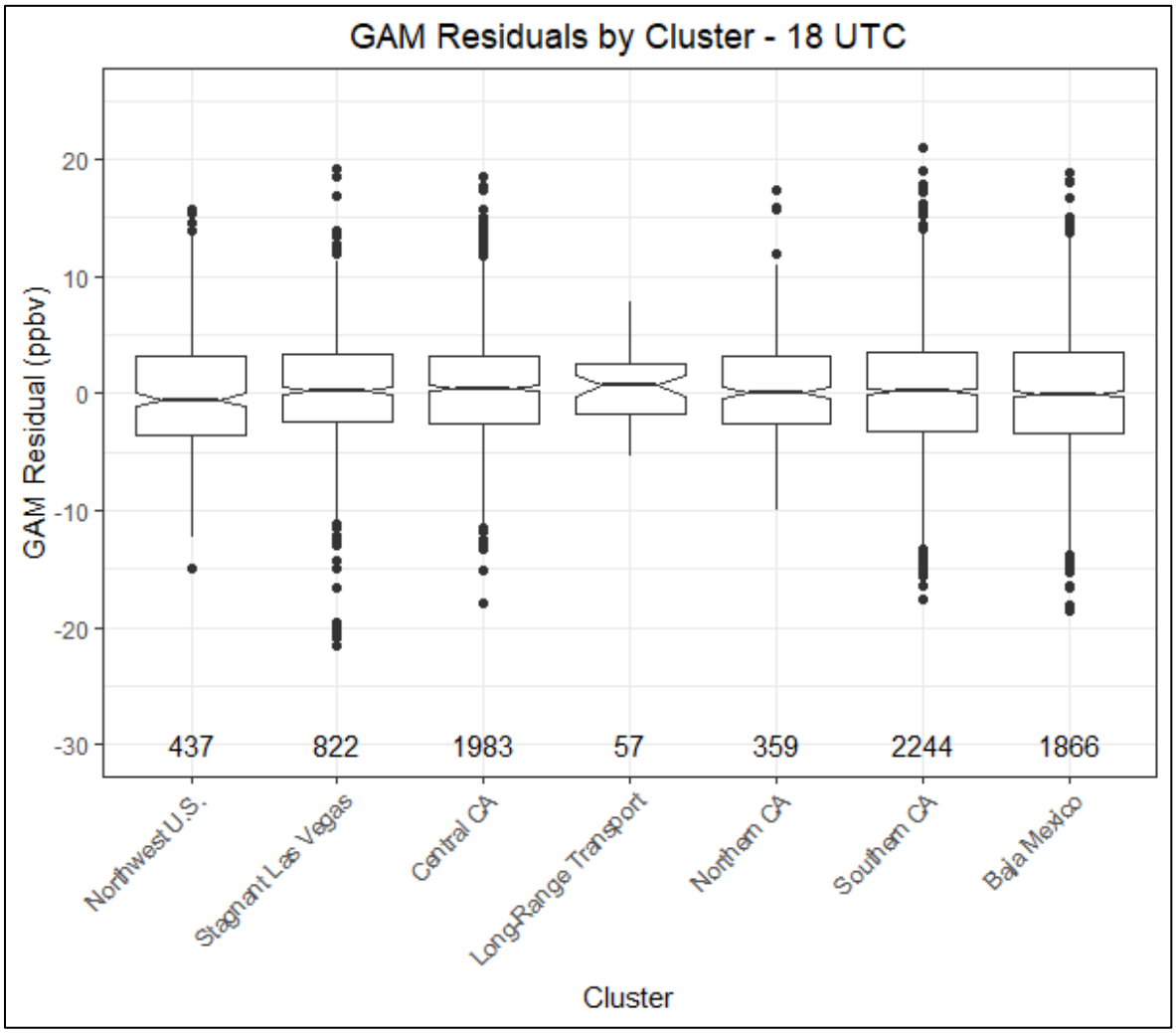


**Figure 3-62.** GAM cluster residual results for 18:00 UTC. The cluster is determined by grouping 24-hour back trajectories from Las Vegas based on their path. Clusters were created by using back trajectory results from Clark County between 2014 and 2020 were used (removed EE days).

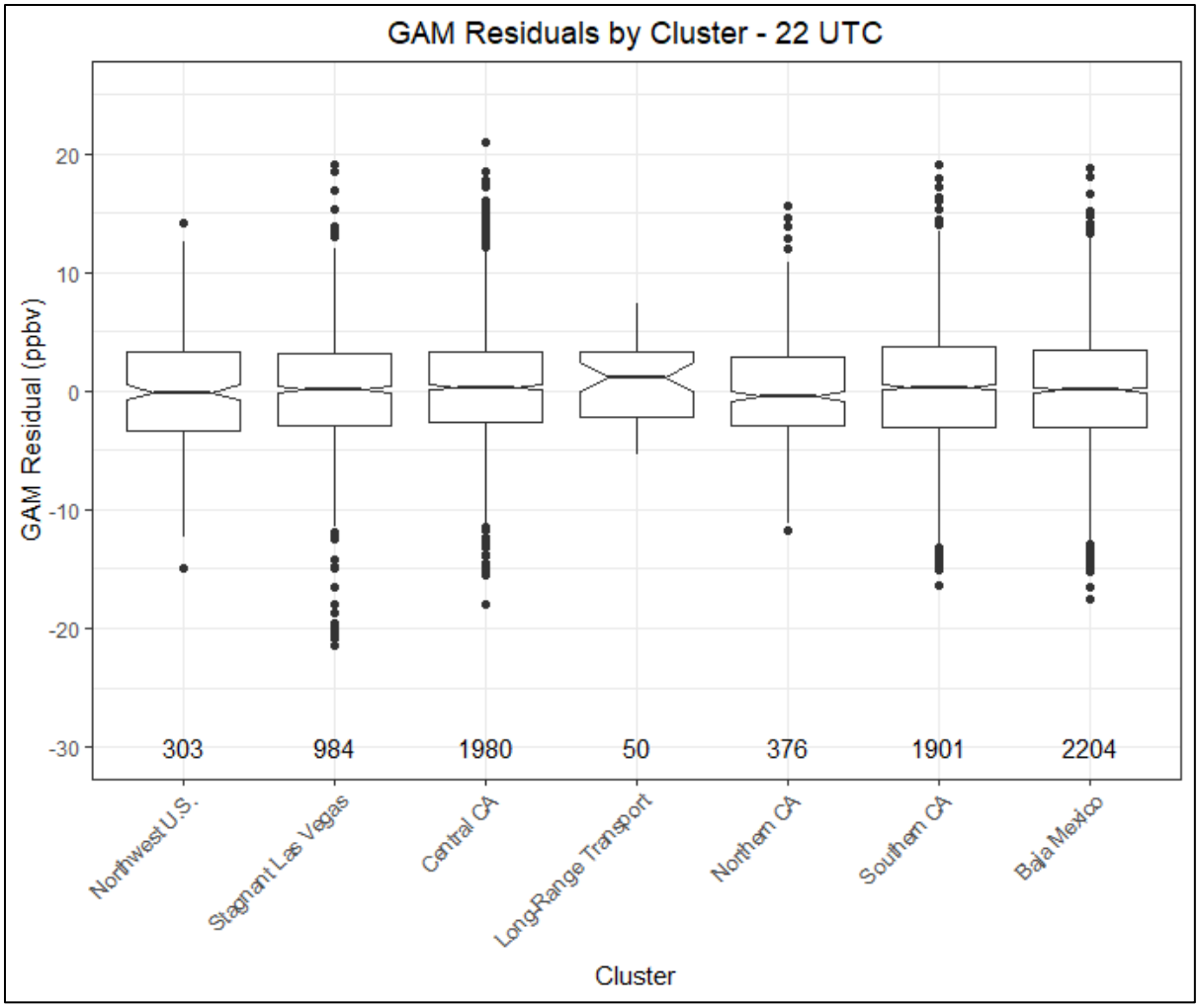


**Figure 3-63.** GAM cluster residual results for 22:00 UTC. The cluster is determined by grouping 24-hour back trajectories from Las Vegas based on their path. Clusters were created by using back trajectory results from Clark County between 2014 and 2020 were used (removed EE days).

Mobile emissions sources decreased throughout the U.S. after COVID restrictions went into place in March 2020. Based on emission inventories from Las Vegas, on-road emissions make up a significant portion of the $NO_x$ emissions inventory (see Sections 2.3 and 2.5 for more details). Based on traffic data from the Nevada Department of Transportation, on-road traffic in Clark County in 2020 was significantly different than 2019 through early to mid-June (depending on the area where traffic volume was measured [see Section 2.5 for more details]). Figure 3-64 provides a scatter plot of MDA8 ozone observed versus GAM fit for all eight monitoring sites, separated by year. The linear regression fit, slope, and intercept do not show large difference between 2020 and other modeled years. Figure 3-65 provides a more in-depth look at the most heavily affected months due to COVID restrictions and traffic changes (April – May 2020). The 95$^{th}$ confidence interval (shown as a notch in the box plots) show overlap between 2020 and most other years (except 2015 and 2016). The May 6,

9, and 28 EE days are included in the 2020 box. This analysis shows that there was not a statistically different GAM response in 2020 compared with other years; this is confirmed in the COVID analysis section (Section 2.5) where we show that MDA8 ozone during April-May 2020 in Las Vegas was not statistically different from previous years. Overall, ozone in Clark County did not change significantly and, similarly, GAM results were not significantly affected.

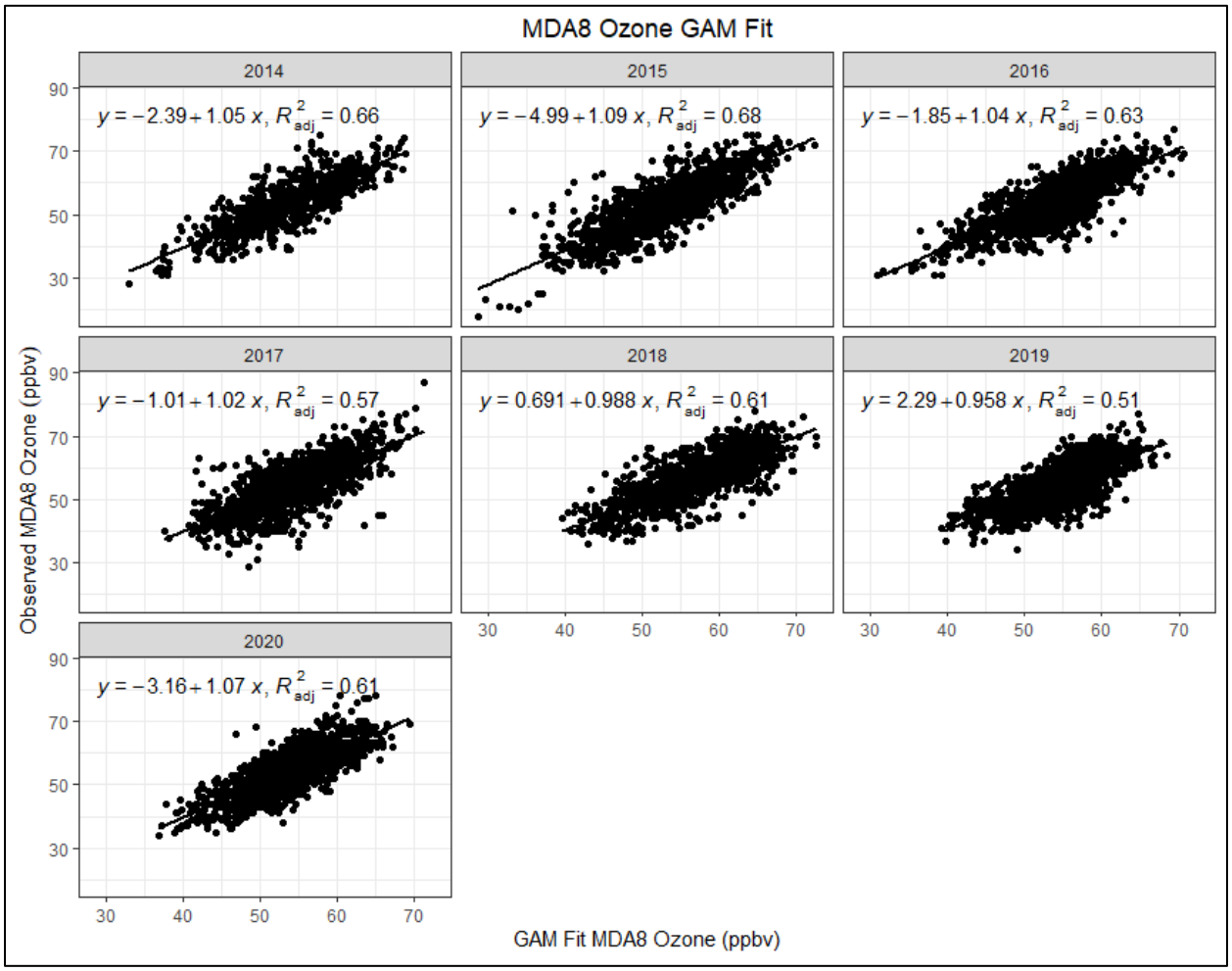


**Figure 3-64.** Observed MDA8 ozone vs GAM fit ozone by year. The relationship between observed MDA8 ozone and GAM fit ozone at all eight modeled monitoring sites in Clark County is broken out by year with linear regression and fit statistics shown (slope, intercept, and $r^2$). EE days are not included in the regression equations.

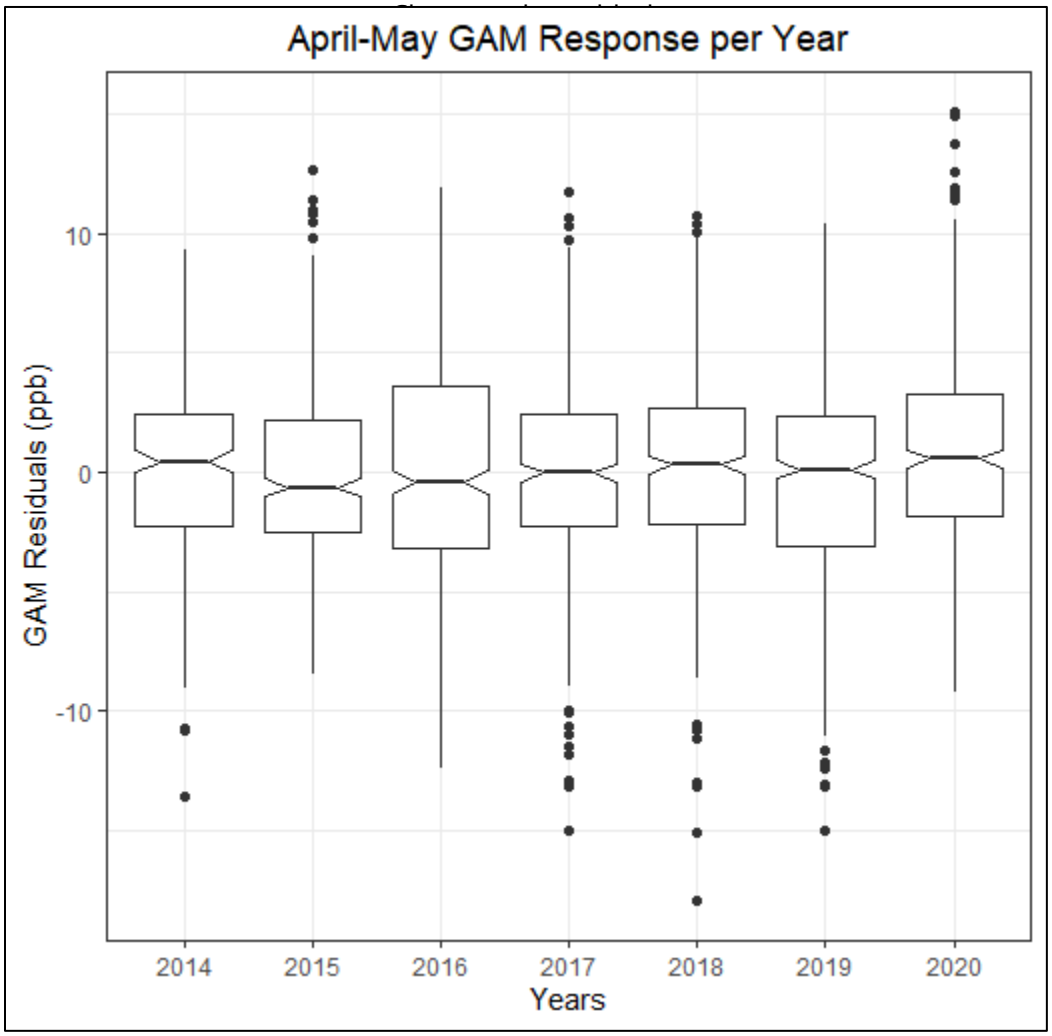


**Figure 3-65.**April-May Interannual GAM Response. April-May residuals per year (2014-2020) are plotted for all eight modeled monitoring sites in Clark County. May 6, 9, and 28 potential EE days are included.

Figure 3-66 provides the observed MDA8 ozone versus GAM Fit MDA8 from 2014 through 2020 for the sites affected on May 9, 2020 (the Paul Meyer and Walter Johnson stations). We marked the possible 2020 (red), 2018 (blue), and other (purple) EE days to show that observed MDA8 ozone on these days is higher than those predicted by the GAM. The other (purple) points are from 2014-2016 suspected wildfire events, as indicated in EPA AQS record. We also highlight the May 9 EE day as a large red triangle in each figure. Linear regression statistics (slope, intercept, and $R^2$) are also provided for context. Both linear regressions show a slope near unity and a low intercept value (around 4 ppb) with a good fit $R^2$ value.

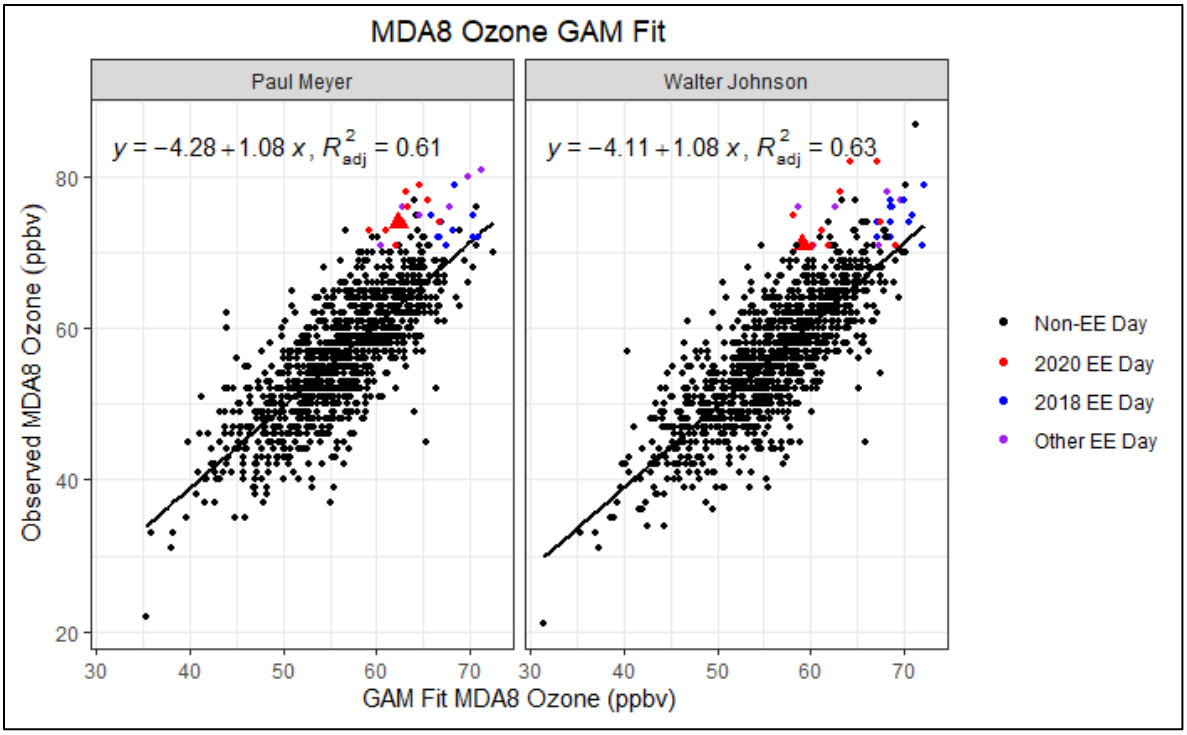


**Figure 3-66.** GAM MDA8 Fit versus Observed MDA8 ozone for EE affected sites on May 9, 2020. Black circles indicate data not associated with the 2018 or 2020 EE days, red circles indicate 2020 EE days, blue circles indicate 2018 EE days, and purple circles indicate 2014-2016 EE days. May 9 is shown as a red triangle. The black line is the linear regression of the data and statistics (equation and $R^2$ value [$R^2_{adj}$ is the same as $R^2$]) are shown in the top of each sub-figure.

Table 3-14 provides the GAM results for May 9, 2020, at each monitoring site affected by the EE. GAM residuals show a modeled wildfire impact of 12 ppb for all monitoring sites, with MDA8 GAM prediction values well below the 0.070 ppm standard. These values suggest that there was a significant, non-typical enhancement in MDA8 ozone concentrations at the affected Clark County monitoring sites on May 9, 2020.

**Table 3-14.** May 9 GAM results and residuals for each site. The GAM residual is the difference between observed MDA8 ozone and the GAM Prediction. We also estimate the minimum predicted fire influence based on the positive 95$^{th}$ quantile and GAM prediction value.

| Site Name | MDA8 $O_3$ Concentration (ppm) | MDA8 GAM Prediction (ppm) | GAM Residual (ppm) |
|---|---|---|---|
| Paul Meyer | 0.074 | 0.062 | 0.012 |
| Walter Johnson | 0.071 | 0.059 | 0.012 |

Finally, Figure 3-67 shows a two-week time series of observed MDA8 ozone values at sites across Clark County and GAM prediction values at those sites. May 9, 2020 (and May 6, 2020, which is another EE filed concurrently with this one), shows the large gap between observed MDA8 ozone and GAM-predicted values. Outside of the possible EE day, the GAM prediction values are close to the observed values (with the exception of May 11, which could have had an outside influence on MDA8 ozone less than 70 ppb), suggesting that immediately before and after the event, we are able to accurately predict typical fluctuations in ozone on non-event days.

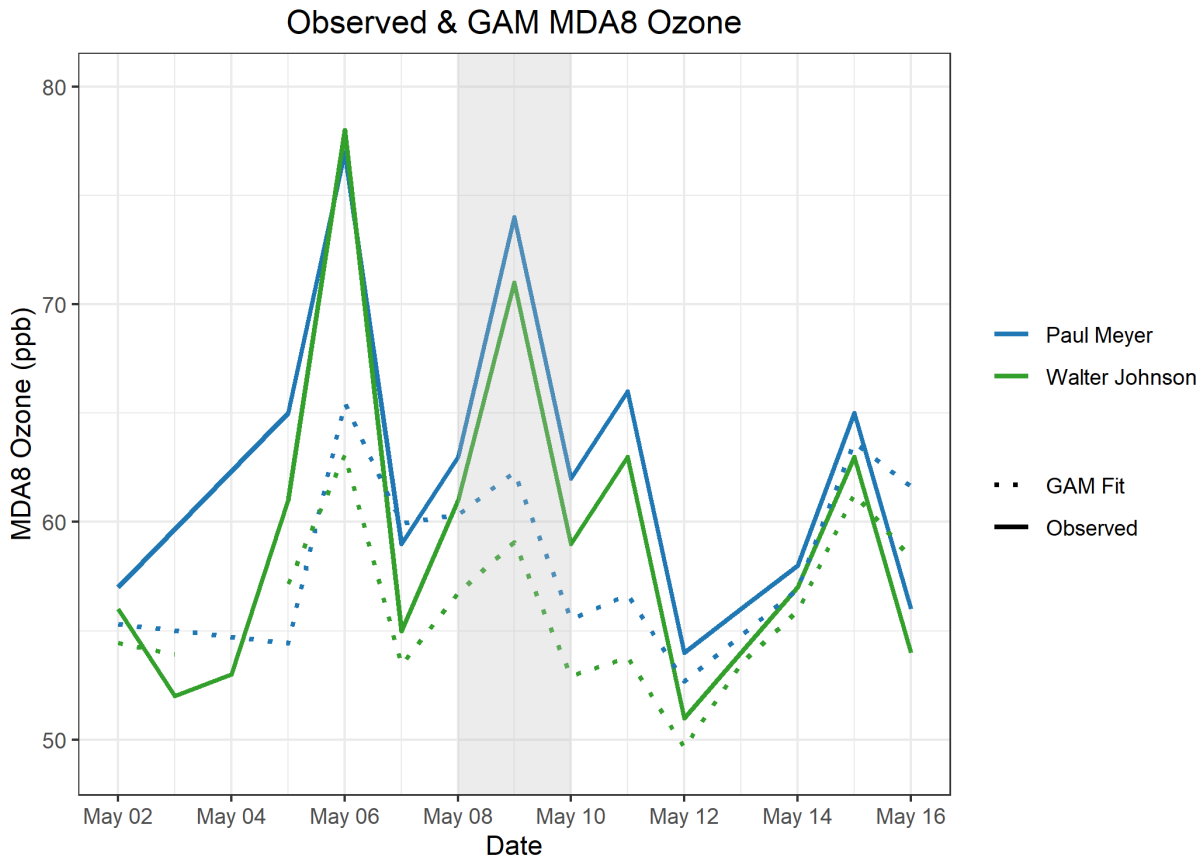


**Figure 3-67.** GAM time series showing observed MDA8 ozone for two weeks before and after the May 9 EE (solid lines). The GAM MDA8 ozone fit value is also shown for two weeks before and after May 9 (dotted line).

Overall, the GAM evidence clearly demonstrates that a non-typical source of ozone significantly impacted concentrations on May 9, 2020, at both EE-affected Clark County sites. Additionally, based on evidence in Figures 3-62 and 3-63, the high residuals on May 9 are unlikely to be a GAM overprediction based solely on unaccounted influence from the Los Angeles Basin. When the GAM evidence is coupled with stratospheric intrusion evidence from Sections 3.1 through 3.5, we suggest

by weight of evidence that the enhancement in ozone is due to a stratospheric intrusion off the coast of Baja California that was transported to Clark County, Nevada.

## 3.6 Clear Causal Relationship Conclusions

The analyses conducted in this report support the impact of a stratospheric intrusion off the coast of Baja California, which was transported to Clark County, Nevada, and enhanced ozone concentrations on May 9, 2020. We find that:

1. Visible satellite imagery, model results, tropospheric measurements, and back trajectories support the conclusion of ozone-rich air being transported from the source region off the coast of Baja California to Clark County between May 7 00:00 UTC and the EE date.
2. A large mixing layer, supported by (a) skew-T sounding diagrams and boundary layer modeling and (b) meteorological analyses from the source region and Clark County, support the transport and mixing of ozone-rich air down to the surface in Clark County on the EE date.
3. Comparisons with non-event concentrations, regionally high ozone concentrations on the EE date, meteorologically similar day analysis, and GAM statistical modeling support the conclusion that the ozone concentrations seen in Clark County were well above typical summer concentrations and likely due to outside influences, such as an upwind SOI.

The analyses presented in this report fulfill the requirements for both a Tier 1 and 2 stratospheric intrusion EE demonstration, and all conclusions for each type of analysis are summarized in Table 3-15. The effect of the SOI event in Clark County caused ozone exceedances at the Paul Meyer and Walter Johnson monitoring stations. Even a small enhancement in ozone concentrations from an SOI on May 9—in addition to typical photochemical production and transport of anthropogenic ozone and ozone precursors—can push MDA8 ozone concentrations above the NAAQS threshold. Since stratospheric intrusions are classified as natural events, and we provide a clear causal relationship between the SOI event and the monitored exceedances, we conclude that the ozone exceedance event on May 9, 2020, in Clark County was not reasonably controllable or preventable.

**Table 3-15.** Results for each tier analysis of the May 9, 2020, exceptional event.

| Type of Analysis | Requirement | Finding |
|---|---|---|
| Historical Comparison | • ≥ 5 years of peak daily ozone data with other high event days flagged.<br>• Table with percentile ranks of days.<br>• Historical diurnal profile comparison (Tier 2). | • The May 9 ozone exceedance occurred during a typical ozone season and event concentrations were significantly higher than non-event concentrations.<br>• Percentile ranks for all affected sites were ≥ 97th percentile |
| Event overview | • Spatial and temporal depictions of ozone during the event.<br>• Description of surface and upper air meteorological conditions during the event.<br>• Begin to establish the complex relationship between the intrusion and eventual impact at surface (Tier 2). | • The SOI source region of the coast of Baja California shows stratospheric-tropospheric exchange on May 7 from 00:00 to 23:00 UTC.<br>• Ozone-rich air is transported across southern California (across the JPL Table Mountain area) and descends into Clark County during the May 9 EE. |
| Establish stratospheric intrusion | Several of following are likely needed:<br>• Water vapor imagery<br>• Total column ozone<br>• Meteorological evidence | • Visible water vapor, ozone satellite imagery, and meteorological data were consistent with an SOI event off the coast of Baja California on May 7.<br>• Model results of IPV, ozone, and CO are also consistent with an SOI in the source region on May 7. |
| Establish stratospheric air reached surface | Several of following are likely needed:<br>• LIDAR, rawinsonde data<br>• Meteorological evidence<br>• Online AQ model cross sections<br>• Trajectory models | • Trajectory analysis to and from the source region and Clark County show transport of an ozone-rich air mass.<br>• Meteorological and LIDAR analysis show the transport of ozone from the source region along with intermediate measurements of ozone between the source region and Clark County.<br>• Model cross-sections of ozone and CO data confirm a descending branch of high ozone and low CO from an SOI event. |
| Impacts at the surface | Several of following are likely needed:<br>• Coincidence between high ozone and meteorological/AQ conditions characteristic of stratospheric intrusions<br>• statistical model evidence of impacts | • Surface measurement on May 9 in Clark County show abnormally low water vapor and abnormally high ozone, with moderate/low $NO_x$ levels. This suggests SOI influence, but not unusually high photochemical influence on ozone concentrations.<br>• Meteorologically similar day analysis shows that average MDA8 ozone across similar days was well below the ozone NAAQS and 10 ppb lower than the May 9 exceedance at all affected sites.<br>• GAM statistical modeling of May 9 indicates an outside source of ozone enhancing ozone concentrations during the EE. |

# 4. Natural Event

The Exceptional Events Rule (81 FR 68216) states that a "[n]atural event, which may recur, is one in which human activity plays little or no direct causal role." The preamble to the Exceptional Events rule notes that the EPA considers stratospheric ozone intrusions to be natural events, as humans have no direct impact on their occurrence. The Clark County Department of Environment and Sustainability has shown through the analyses provided in Section 3.6 of this demonstration that the hypothesized stratospheric intrusion, which existed simultaneously with local photochemical production of ozone, contributed to identified ozone exceedances at the Walter Johnson and Paul Meyer monitoring sites on May 9. Through these analyses and the fact that stratospheric intrusions are purely natural, the Clark County Department of Environment and Sustainability has satisfied the "human activity that is unlikely to recur at a particular location or a natural event" element of 40 CFR 50.14(c)(3).

# 5. Not Reasonably Controllable or Preventable

The documentation provided in Section 3.6 of this demonstration shows that the suspected stratospheric intrusion contributed to the identified ozone exceedances at the Walter Johnson and Paul Meyer monitoring sites on May 9. Through these analyses and the fact that stratospheric intrusions are purely natural events that cannot be prevented or controlled, the Clark County Department of Environment and Sustainability has satisfied the "not reasonably controllable or preventable" criterion.

# 6. Public Comment

This exceptional event demonstration will undergo a 30-day public comment period concurrent with EPA's review beginning July 1, 2021. A copy of the public notice, along with any comments received and responses to those comments, will be submitted to EPA after the comment period has closed, consistent with the requirements of 40 CFR 50.14(c)(3)(v). **Appendix D** contains documentation of the public comment process.

# 7. Conclusions and Recommendations

The analyses conducted in this report support the conclusion that an SOI event occurred off the coast of Baja California and ozone-rich air from that event was transported into Clark County, Nevada, on May 9, 2020, affecting ozone concentrations. This EE demonstration has provided the following elements required by the EPA guidance for SOIs (U.S. Environmental Protection Agency, 2018):

1. A narrative conceptual model that describes the SOI event off the coast of Baja California and how the transport of ozone-rich air led to ozone exceedances downwind in Clark County (Section 1.4).
2. A clear causal relationship between the SOI and the May 9 exceedance through ground and satellite-based measurements, trajectories, comparison with non-event concentrations, vertical profile analysis, and statistical modeling (Section 3).
3. Event ozone concentrations at or above the 97th percentile when compared with the last five years of observations (yearly and ozone season-only) at each site and among the four highest ozone days at each site (excluding other 2018 and 2020 EE events – Section 3).
4. Stratospheric intrusions are considered to be natural events, as humans have no direct impact on their occurrence (Section 4).
5. Demonstrated that transport from an SOI event is neither reasonably controllable or preventable (Section 5).
6. This demonstration went through the public comment process via Clark County's Department of Environment and Sustainability (Section 6).

The major conclusions and supporting analyses found in this report are:

1. Visible satellite imagery, model results, tropospheric measurements, and back trajectories support the conclusion of ozone-rich air being transported from the source region off the coast of Baja California to Clark County between May 7 00:00 UTC and the EE date.
2. A large mixing layer, supported by skew-T sounding diagrams, boundary layer modeling, and meteorological analyses from the source region and Clark County, support the narrative of transport and mixing of ozone-rich air being mixed down to the surface in Clark County on the EE date.
3. Comparisons with non-event concentrations, regionally high ozone concentrations on the EE date, meteorologically similar day analysis, and GAM statistical modeling support the conclusion that the ozone concentrations seen in Clark County were well above typical ozone season concentrations and likely due to outside influences, such as an upwind SOI.

The analyses presented in this report fulfill the requirements for both a Tier 1 and 2 stratospheric intrusion EE demonstration, and all conclusions for each type of analysis are summarized in Table 3-15. The effect of the SOI event in Clark County caused ozone exceedances at the Paul Meyer and Walter Johnson monitoring stations. Even a small enhancement in ozone concentrations from an SOI on May 9—in addition to typical photochemical production and transport of anthropogenic ozone and ozone precursors—can push MDA8 ozone concentrations above the NAAQS threshold. Since stratospheric intrusions are classified as natural events and we provide a clear causal relationship between the SOI event and the monitored exceedances, we conclude that the ozone exceedance event on May 9, 2020, in Clark County was not reasonably controllable or preventable.

# 8. References


Alvarado M., Lonsdale C., Mountain M., and Hegarty J. (2015) Investigating the impact of meteorology on $O_3$ and $PM_{2.5}$ trends, background levels, and NAAQS exceedances. Final report prepared for the Texas Commission on Environmental Quality, Austin, TX, by Atmospheric and Environmental Research, Inc., Lexington, MA, August 31.

Arizona Department of Environmental Quality (2016) State of Arizona exceptional event documentation for wildfire-caused ozone exceedances on June 20, 2015 in the Maricopa nonattainment area. Final report, September. Available at https://static.azdeq.gov/pn/1609_ee_report.pdf.

Camalier L., Cox W., and Dolwick P. (2007) The effects of meteorology on ozone in urban areas and their use in assessing ozone trends. *Atmospheric Environment*, 41, 7127-7137, doi: 10.1016/j.atmosenv.2007.04.061.

Chouza F., Leblanc T., Brewer M., Wang P., Piazzolla S., Pfister G., Kumar R., Drews C., Tilmes S., and Emmons L. (2020) The impact of Los Angeles basin pollution and stratospheric intrusions on the surrounding San Gabriel Mountains as seen by surface measurements, lidar, and numerical models. *Atmos. Chem. Phys. Discuss.*, 2020, 1-29. Available at https://acp.copernicus.org/preprints/acp-2020-1208/.

Clark County Department of Air Quality (2019) Ozone Advance program progress report update. August.

Clark County Department of Environment and Sustainability (2020) Revision to the Nevada state implementation plan for the 2015 Ozone NAAQS: emissions inventory and emissions statement requirements. September. Available at https://files.clarkcountynv.gov/clarknv/Environmental%20Sustainability/SIP%20Related%20Documents/O3/20200901_2015_O3%20EI-ES_SIP_FINAL.pdf?t=1617690564073&t=1617690564073.

Code of Federal Regulations (1997) Title 40, Part 58, Appendix D. Network design for SLAMS, NAMS, and PAMS.

Gong X., Kaulfus A., Nair U., and Jaffe D.A. (2017) Quantifying $O_3$ impacts in urban areas due to wildfires using a generalized additive model. *Environ. Sci. Technol.*, 51(22), 13216-13223, doi: 10.1021/acs.est.7b03130.

Gong X., Hong S., and Jaffe D.A. (2018) Ozone in China: spatial distribution and leading meteorological factors controlling $O_3$ in 16 Chinese cities. *Aerosol and Air Quality Research*, 18(9), 2287-2300. Available at http://dx.doi.org/10.4209/aaqr.2017.10.0368.

Jaffe D.A., Bertschi I., Jaegle L., Novelli P., Reid J.S., Tanimoto H., Vingarzan R., and Westphal D.L. (2004) Long-range transport of Siberian biomass burning emissions and impact on surface ozone in western North America. *Geophys. Res. Let.*, 31(L16106).

Jaffe D.A., Wigder N., Downey N., Pfister G., Boynard A., and Reid S.B. (2013) Impact of wildfires on ozone exceptional events in the western U.S. *Environ. Sci. Technol.*, 47(19), 11065-11072, doi: 10.1021/es402164f, October 1. Available at http://pubs.acs.org/doi/abs/10.1021/es402164f.

Kroll J.H., Heald C.L., Cappa C.D., Farmer D.K., Fry J.L., Murphy J.G., and Steiner A.L. (2020) The complex chemical effects of COVID-19 shutdowns on air quality. *Nature Chemistry*, 12(9), 777-779, doi: 10.1038/s41557-020-0535-z. Available at https://doi.org/10.1038/s41557-020-0535-z.

Langford A.O. (2014) Las Vegas ozone study (LVOS). Final report prepared for the Clark County Department of Air Quality, Las Vegas, NV, by the National Oceanic and Atmospheric Administration Earth System Research Laboratory, Chemical Sciences Division, Boulder, CO, MOU #CBE 602948-13, July 25. Available at https://csl.noaa.gov/projects/lvos/LVOSfinalreportCBE602948-13.pdf.

Langford A.O., Senff C.J., Alvarez R.J., Brioude J., Cooper O.R., Holloway J.S., Lin M.Y., Marchbanks R.D., Pierce R.B., Sandberg S.P., Weickmann A.M., and Williams E.J. (2015) An overview of the 2013 Las Vegas Ozone Study (LVOS): impact of stratospheric intrusions and long-range transport on surface air quality. *Atmospheric Environment*, 109, 305-322, doi: 10.1016/j.atmosenv.2014.08.040, 2015/05/01/. Available at http://www.sciencedirect.com/science/article/pii/S1352231014006426.

Langford A.O. and Senff C.J. (2019) Fires, asian, and stratospheric transport-Las Vegas ozone study (FAST-LVOS). Report prepared for the Clark County Department of Air Quality, Las Vegas, NV, by the National Oceanic and Atmospheric Administration Earth System Research Laboratory, Chemical Sciences Division, Boulder, CO, and the Cooperative Institute for Research in Environmental Sciences, University of Colorado, Boulder, CO, CBE 604318-16, December. Available at https://csl.noaa.gov/projects/fastlvos/FAST-LVOSfinalreport604318-16.pdf.

Louisiana Department of Environmental Quality (2018) Louisiana exceptional event of September 14, 2017: analysis of atmospheric processes associated with the ozone exceedance and supporting data. Report submitted to the U.S. EPA Region 6, Dallas, TX, March. Available at https://www.epa.gov/sites/production/files/2018-08/documents/ldeq_ee_demonstration_final_w_appendices.pdf.

McClure C.D. and Jaffe D.A. (2018) Investigation of high ozone events due to wildfire smoke in an urban area. *Atmospheric Environment*, 194, 146-157, doi: 10.1016/j.atmosenv.2018.09.021, 2018/12/01/. Available at http://www.sciencedirect.com/science/article/pii/S1352231018306137.

McVey A., Pernak R., Hegarty J., and Alvarado M. (2018) El Paso ozone and $PM_{2.5}$ background and totals trend analysis. Final report prepared for the Texas Commission on Environmental Quality, Austin, Texas, by Atmospheric and Environmental Research, Inc., Lexington, MA, June. Available at https://www.tceq.texas.gov/assets/public/implementation/air/am/contracts/reports/da/582188176307-20180629-aer-ElPasoOzonePMBackgroundTotalsTrends.pdf.

National Weather Service Forecast Office (2020) Las Vegas, NV: general climatic summary. Available at https://www.wrh.noaa.gov/vef/lassum.php.

Parker H.A., Hasheminassab S., Crounse J.D., Roehl C.M., and Wennberg P.O. (2020) Impacts of traffic reductions associated with COVID-19 on Southern California air quality. *Geophysical Research Letters*, 47(23), e2020GL090164. Available at https://agupubs.onlinelibrary.wiley.com/doi/abs/10.1029/2020GL090164.

Pernak R., Alvarado M., Lonsdale C., Mountain M., Hegarty J., and Nehrkorn T. (2019) Forecasting surface $O_3$ in Texas urban areas using random forest and generalized additive models. *Aerosol and Air Quality Research*, 19, 2815-2826, doi: 10.4209/aaqr.2018.12.0464.

Sacramento Metropolitan Air Quality Management District (2011) Exceptional events demonstration for 1-hour ozone exceedances in the Sacramento regional nonattainment area due to 2008 wildfires. Report to the U.S. Environmental Protection Agency, March 30.

Simon H., Baker K.R., and Phillips S. (2012) Compilation and interpretation of photochemical model performance statistics published between 2006 and 2012. *Atmospheric Environment*, 61, 124-139, doi: 10.1016/j.atmosenv.2012.07.012.

Solberg S., Walker S.-E., Schneider P., Guerreiro C., and Colette A. (2018) Discounting the effect of meteorology on trends in surface ozone: development of statistical tools. Technical paper by the European Topic Centre on Air Pollution and Climate Change Mitigation, Bilthoven, the Netherlands, ETC/ACM Technical Paper 2017/15, August. Available at https://www.eionet.europa.eu/etcs/etc-atni/products/etc-atni-reports/etcacm_tp_2017_15_discount_meteo_on_o3_trends.

Solberg S., Walker S.-E., Guerreiro C., and Colette A. (2019) Statistical modelling for long-term trends of pollutants: use of a GAM model for the assessment of measurements of $O_3$, $NO_2$ and PM. Report by the European Topic Centre on Air pollution, transport, noise and industrial pollution, Kjeller, Norway, ETC/ATNI 2019/14, December. Available at https://www.eionet.europa.eu/etcs/etc-atni/products/etc-atni-reports/etc-atni-report-14-2019-statistical-modelling-for-long-term-trends-of-pollutants-use-of-a-gam-model-for-the-assessment-of-measurements-of-o3-no2-and-pm-1.

Texas Commission on Environmental Quality (2021) Dallas-Fort Worth area exceptional event demonstration for ozone on August 16, 17, and 21, 2020. April. Available at https://www.tceq.texas.gov/assets/public/airquality/airmod/docs/ozoneExceptionalEvent/2020-DFW-EE-Ozone.pdf.

U.S. Census Bureau (2010) State & County QuickFacts. Available at http://quickfacts.census.gov/qfd/states/.html.

U.S. Environmental Protection Agency (2015) 40 CFR Part 50, Appendix U: interpretation of the primary and secondary National Ambient Air Quality Standards for ozone. Available at https://www.ecfr.gov/cgi-bin/text-idx?SID=43eb095cc6751633290941788ab4f3bd&mc=true&node=ap40.2.50_119.u.

U.S. Environmental Protection Agency (2016) Guidance on the preparation of exceptional events demonstrations for wildfire events that may influence ozone concentrations. Final report, September. Available at www.epa.gov/sites/production/files/2016-09/documents/exceptional_events_guidance_9-16-16_final.pdf.

U.S. Environmental Protection Agency (2018) Guidance on the preparation of exceptional events demonstrations for stratospheric ozone intrusions. Report by the U.S. Environmental Protection Agency Office of Air Quality Planning and Standards, Air Quality Policy Division, Air Quality Assessment Division, Research Triangle Park, NC, EPA-457/B-18-001, November. Available at https://www.epa.gov/sites/production/files/2018-11/documents/exceptional_events_soi_guidance_11-8-2018.pdf.

U.S. Environmental Protection Agency (2020) Green Book: 8-hour ozone (2015) area information. Available at https://www.epa.gov/green-book/green-book-8-hour-ozone-2015-area-information.

Venter Z.S., Aunan K., Chowdhury S., and Lelieveld J. (2020) COVID-19 lockdowns cause global air pollution declines. *Proceedings of the National Academy of Sciences*, 117(32), 18984-18990, doi: 10.1073/pnas.2006853117. Available at https://www.pnas.org/content/pnas/117/32/18984.full.pdf.

Wood S. (2020) Mixed GAM computation vehicle with automatic smoothness estimation. Available at https://cran.r-project.org/web/packages/mgcv/mgcv.pdf.

Wood S.N. (2017a) *Generalized additive models: an introduction with R*, 2nd edition, CRC Press, Boca Raton, FL.

Wood S.N. (2017b) *Generalized additive models: an introduction with R, second edition*, 2nd Edition, Chapman and Hall/CRC.

Zhang L., Lin M., Langford A.O., Horowitz L.W., Senff C.J., Klovenski E., Wang Y., Alvarez R.J., II, Petropavlovskikh I., Cullis P., Sterling C.W., Peischl J., Ryerson T.B., Brown S.S., Decker Z.C.J., Kirgis G., and Conley S. (2020) Characterizing sources of high surface ozone events in the southwestern US with intensive field measurements and two global models. *Atmospheric Chemistry & Physics*, 20, 10379-10400, doi: 10.5194/acp-20-10379-2020. Available at https://acp.copernicus.org/articles/20/10379/2020/acp-20-10379-2020.pdf.